Synthesis, ^{18}F-labelling and radiopharmacological characterisation of the C-terminal 30mer of Clostridium perfringens enterotoxin as a potential claudin-targeting peptide

Löser, R.; Bader, M.; Kuchar, M.; Wodtke, R.; Lenk, J.; Wodtke, J.; Kuhne, K.; Bergmann, R.; Haase-Kohn, C.; Urbanová, M.; Steinbach, J.; Pietzsch, J.;

Originally published:

February 2019

Amino Acids 51(2019)2, 219-244

DOI: https://doi.org/10.1007/s00726-018-2657-9

Synthesis, ^{18}F-labelling and radiopharmacological characterisation of the C-terminal 30mer of *Clostridium perfringens* enterotoxin as a potential claudin-targeting peptide

Reik Löser[1,2,*], Miriam Bader[1,2,§], Manuela Kuchar[1,2,§], Robert Wodtke[1,2], Jens Lenk[1,2], Johanna Wodtke[1,#], Konstantin Kuhne[1,2], Ralf Bergmann[1], Cathleen Haase-Kohn[1], Marie Urbanová[3], Jörg Steinbach[1,2], Jens Pietzsch[1,2]

Abstract

The cell surface receptor claudin-4 (Cld-4) is upregulated in various tumours and represents an important emerging target for both diagnosis and treatment of solid tumors of epithelial origin. The C-terminal fragment of the *Clostridium perfringens* enterotoxin cCPE$_{290-319}$ appears as a suitable ligand for targeting Cld-4. The synthesis of this 30mer peptide was attempted via several approaches, which has revealed sequential SPPS using three pseudoproline-dipeptide building blocks to be the most efficient one. Labelling with fluorine-18 was achieved on solid phase using *N*-succinimidyl 4-[^{18}F]fluorobenzoate ([^{18}F]SFB) and 4-[^{18}F]fluorobenzoyl chloride as ^{18}F-acylating agents, which was most advantageous when [^{18}F]SFB was reacted with the resin-bound 30mer containing an N-terminal 6-aminohexanoic spacer. Binding to Cld-4 was demonstrated via surface plasmon resonance using a protein construct containing both extracellular loops of Cld-4. In addition, cell binding experiments were performed for ^{18}F-labelled cCPE$_{290-319}$ with the Cld-4 expressing tumour cell lines HT-29 and A431 that were complemented by fluorescence microscopy studies using the corresponding fluorescein isothiocyanate-conjugated peptide. The 30mer peptide proved to be sufficiently stable in blood plasma. Studying the *in vivo* behavior of ^{18}F-labelled cCPE$_{290-319}$ in healthy mice and rats by dynamic PET imaging and radiometabolite analyses has revealed that the peptide is subject to substantial liver uptake and rapid metabolic degradation *in vivo*, which limits its suitability as imaging probe for tumour-associated Cld-4.

Keywords: radiolabelled peptides, ^{18}F-fluorobenzoylation, difficult peptide sequences, claudin family of tight junction proteins, molecular imaging, small animal positron emission tomography

[1] *Helmholtz-Zentrum Dresden Rossendorf, Institute of Radiopharmaceutical Cancer Research, Bautzner Landstraße 400, 01328 Dresden, Germany*
[2] *Faculty of Chemistry and Food Chemistry, School of Science, Technische Universität Dresden, Mommsenstraße 4, 01062 Dresden, Germany*
[3] *Department of Physics and Measurements, University of Chemistry and Technology, 166 28 Prague, Czech Republic*
[*] *Corresponding author, r.loeser@hzdr.de*
[§] *These authors contributed equally to this study*
[#] *J. Wodtke née Pufe*

Abbreviations

Ac	Acetyl
Ahx	6-Aminohexanoyl
BSA	Bovine serum albumin
Cld	Claudin
2-ClTrtCl	2-Chlorotrityl chloride
CPE	*Clostridium perfringens* enterotoxin
cCPE	C-terminal domain of *Clostridium perfringens* enterotoxin
DMEM	Dulbecco's mofified Eagle's medium
DIPEA	*N,N*-diisopropylamine
DMF	*N*,*N*-dimethylformamide
DMSO	Dimethyl sulfoxide
EC	Electron capture
ECD	Electronic circular dichroism
EDTA	N,N,N',N'-Ethylenediamine tetraacetic acids
ESI	Electrospray ionisation
ESM	Electronic supplementary material
Et	Ethyl
FBz	4-Fluorobenzoyl
FITC	Fluorescein-5-isothiocyanate
Fmoc	9*H*-Fluorene-9-ylmethoxycarbonyl
HFIP	Hexafluoroisopropanol
HATU	*O*-(7-Azabenzotriazol-1-yl)-*N*,*N*,*N*',*N*'-tetramethyluronium hexafluorophosphate
HBTU	*O*-(Benzotriazol-1-yl)-*N*,*N*,*N*',*N*'-tetramethyluronium hexafluorophosphate
HOBt	1-Hydroxybenzotriazol
HPLC	High performance liquid chromatography
ID	Injected dose
MBHA	4-Methyl benzhydrylamine
Me	Methyl
MR	Magnetic resonance
MS	Mass spectrometry
PBS	Phosphate-buffered saline
PDA	Photo diode array
PET	Positron emission tomography
PFA	Paraformaldeyde
p.i.	*post injectionem*
RIPA	Radioimmunoprecipitation assay
RP	Reversed phase
SDS-PAGE	Sodium dodecyl sulfate polyacrylamide gel electrophoresis
[^{18}F]SFB	*N*-Succinimidyl 4-[^{18}F]fluorobenzoate
SPECT	Single photon emission computed tomography
SPR	Surface plasmon resonance
SPPS	Solid-phase peptide synthesis
TBS	Tris-buffred saline
*t*Bu	*tert*-Butyl
TFA	Trifluoroacetic acid
TFE	2,2,2-Trifluoroethanol
Trt	Trityl
UPLC	Ultra performance liquid chromatography

Three and single letter codes of amino acids are used according to the guidelines of the IUPAC-IUB commission on biochemical nomenclature (see *Eur. J. Biochem.* **1984**, *138*, 9-37)

Introduction

Claudins are a family of single-chain membrane proteins containing four membrane-spanning helices, which comprises at least 27 distinct members. Together with occludins, junctional adhesion molecules and the zonula occludens proteins, claudins constitute the proteinaceous component of specialised differentiations of epithelial and endothelial cell membranes called tight junctions, which are sites in which close contacts between adjacent cells are formed based on interactions of these membrane proteins (Takahashi et al. 2012; Salvador et al. 2016). Claudins are functioning by engaging in either homophilic interactions with claudins of identical subtypes at the surface of adjacent cells or heterophilic interactions with claudins of different subtypes (Piontek et al. 2017a). Most tumours originate from epithelial and endothelial cells, which implicates the involvement of tight junctions in oncogenic progression. With regards to the role of claudins in cancer, it has been found that their expression can increase or decrease depending on the kind and stage of the tumour (Singh and Dhawan 2015; Osanai et al. 2017). However, Cld-4 and, to a lesser extent, Cld-3, have been shown to be upregulated in various malignancies such as gastrointestinal, breast, pancreatic, prostate, uterine and ovarian cancer (Ding et al. 2013; Kwon 2013). Their aberrant expression seems to impair the structure of tight junctions, which in turn supports tumour progression by enhancing cell migration, invasion and metastasis (Boireau et al. 2007). This renders Cld-4 an interesting target for the diagnosis and differentiation of tumours and potentially also as a target for therapeutics (Kominsky et al. 2007; Neesse et al. 2012).

A vector for targeting Cld-4 has been identified in the C-terminal domain of the enterotoxin of the pathogenic bacterium *Clostridium perfringens*. This 35-kDa single-chain proteotoxin exerts its cytotoxic action via the pore-forming N-terminal domain, while its C-terminal domain is responsible for targeting the surface of intestinal epithelial cells via interaction with Cld-4 and -3 (Mitchell and Koval 2010). The C-terminal domain of CPE comprises the amino acids 171-319 (Hanna et al. 1995). Its X-ray crystal structure has been solved, which has revealed that it exhibits a β-sandwich-type fold consisting of nine largely antiparallel β sheets (Van Itallie et al. 2008) (Fig. 1). Visualisation of tumour-associated Cld-4-has been shown for fluorophore (Neesse et al. 2013), indium-111 (Mosley et al. 2015) and Xe-labelled cCPE (Piontek et al. 2017b) using optical, SPECT and MR imaging, respectively. Due to the large molar mass of 14 kDa, drawbacks such as slow pharmacokinetics and potential immunogenicity (Suzuki et al. 2011) are associated to the use of cCPE as imaging agent. The site within cCPE that is responsible for the interaction with Cld-4 has been demonstrated to be confined to the fragment comprising the C-terminal residues 290 to 319 ($cCPE_{290-319}$; see Fig. 3 for sequence), both on the basis of radioligand binding experiments using ^{125}I-labelled cCPE fragments (Hanna et al. 1991) as well by using surface plasmon resonance (Ling et al. 2008). The 30mer peptide's capability of tumour-targeting *in vivo* has been claimed for fluorescein-conjugated $cCPE_{290-319}$ in a mouse xenograft model of ovarian cancer (Cocco et al. 2010). Residues of cCPE that are critical for its interaction with Cld-4 have been identified by subjecting the 16 C-terminal amino acids of the protein to an alanine scan (Takahashi et al. 2008). This and other studies have revealed that the tyrosines 306, 310 and 312 and Leu 315 are important for receptor binding (Veshnyakova et al. 2010), which are located in a flexible loop between β sheets 8 and 9, i.e., residues Lys 304-Tyr 312, or on β sheet 9, respectively, according to the crystal structure shown in Fig. 1A. Very recently, these findings have been confirmed by solving the X-ray crystal structure of cCPE complexed with lipid bilayer-embedded Cld-4 (Shinoda et al. 2016b).

To the best of our knowledge, neither the chemical synthesis of $cCPE_{290-319}$ nor its labelling with radionuclides has been reported so far. Considering the overexpression of Cld-4 in various kinds of

solid tumours, radiolabelled derivatives of $cCPE_{290-319}$ would be beneficial for diagnosis and, perspectively, also for therapy of such tumours. This can be expected from the successful application of radiolabelled peptides targeting peptide-activated G protein-coupled receptors in nuclear medicine. However, compared to Cld-4, the expression of such receptors is restricted to a minority of tumours such as neuroendocrine tumours, which overexpress somatostatin receptors (Fani and Maecke 2012) (Ullrich et al. 2016). Herein, we envisage the preparation of $cCPE_{290-319}$ by solid-phase peptide synthesis and its labelling with fluorine-18, which represents the most advantageous radionuclide for positron emission tomography (PET) in terms of positron energy (635 keV) and β^+/EC branching ratio (97%) (Hess et al. 2001; van der Born et al. 2017). Labelling of peptides with fluorine-18 can be straightforward achieved via ^{18}F-fluorobenzoylation using *N*-succinimidyl [^{18}F]fluorobenzoate ([^{18}F]SFB) (Kim et al. 2014; Richter and Wuest 2014). Labelling of $cCPE_{290-319}$ by ^{18}F-acylation reactions in solution is potentially challenging due to the presence of two internal lysine residues in the sequence. Therefore, the reaction of the side chain-protected 30mer with [^{18}F]SFB on solid support was envisaged, as this approach has been revealed to be efficient for the site-selective labelling of lysine-containing peptides (Kuchar et al. 2012; Kuchar et al. 2018). Apart from the study presented herein, labelling of claudin-targeting peptides with fluorine-18 has been recently reported for the 17mer $cCPE_{303-319}$ C-terminally extended by three lysine residues and other non-CPE-related peptides using oxime-forming conjugation with 5-[^{18}F]fluoro-5-deoxyribose. However, no results on their radiopharmacological properties were published (Feni et al. 2017).

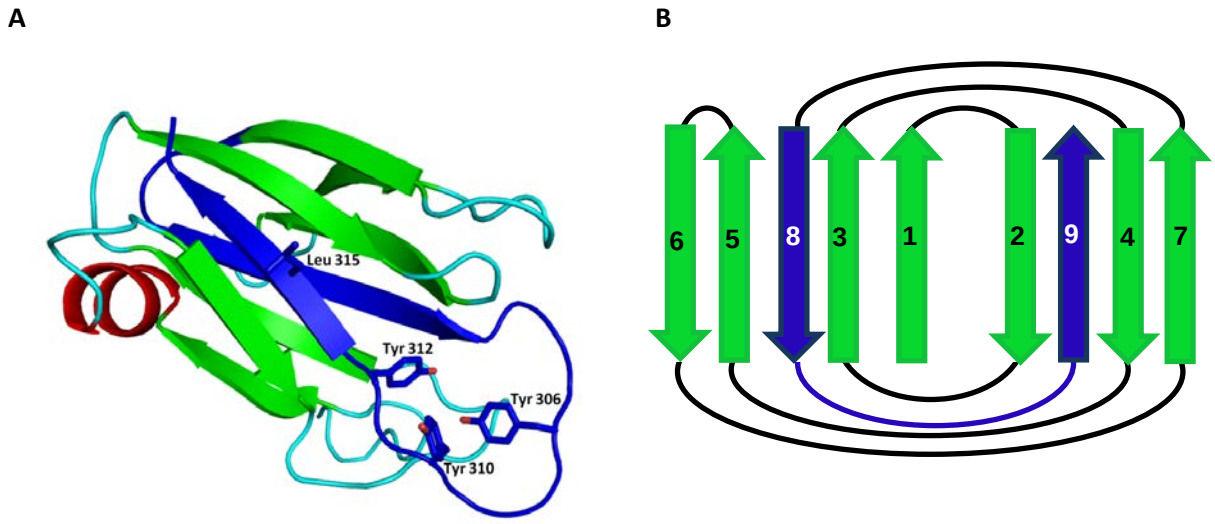

Fig. 1: A) X-ray crystal structure of $cCPE_{194-319}$. The fragment covering the last 30 C-terminal amino acids are highlighted in dark blue, the other parts of the protein are coloured according to secondary structure elements (red: helices, green:β sheets, cyan: loops). Side-chain atoms that are critical for the interaction with Cld-4 are shown in stick representation. PDB entry: 2QUO (Van Itallie et al. 2008) **B**) Topology diagram for the same protein, which shows that all β sheets except 1 and 3 are in antiparallel orientation to each other. For clarity, the short helix between β sheets 1 and 2 is not shown.

Materials and methods

Solid phase peptide synthesis

General remarks

All chemical reagents and solvents were obtained from commercial suppliers and used without further purification. Fmoc-protected amino acids and coupling reagents were purchased from MultiSynTech and Iris Biotech. Fmoc-protected pseudoproline dipeptides were obtained from Aapptec. Linker-functionalised polystyrene resins (Fmoc-Rink-Amide MBHA and Fmoc-Phe-preloaded Wang resin) were purchased from Multisyntech and Merck. HPLC systems used for analysis and purification of the synthesised peptides are documented in detail in ESM. Mass spectra were obtained on a Micromass Quattro/LC (Waters) or a Waters Xevo TQ-S mass spectrometer equipped with an electrospray ionisation source (operated in positive mode), each driven by the Mass Lynx software. ESI-MS spectra for compounds **1**-**3**, **4a**-**g**, **5a**, **b** and **6** are shown in ESM.

Manual manipulation of the polystyrene-based resins was done in polypropylene syringes equipped with a 25 µm polyethylene filter (Multisyntech). The reaction mixtures were shaken on an orbital shaker (600 rpm) at room temperature, if not stated otherwise. Washing of resin was done on a filtration bottle supported by a vacuum pump.

If not described otherwise, peptides were synthesised by microwave-assisted, fully automated solid-phase peptide synthesis using Fmoc-protected L-amino acid with appropriately protected side chain functionalities as building blocks by employing a CEM Liberty Microwave Peptide Synthesizer combined with a CEM Discover microwave reactor as previously reported (Kuchar et al. 2012).

Loading of 2-ClTrtCl resin and manual coupling of the first 3 amino acids

A solution of Fmoc-Phe-OH (116 mg, 0.3 mmol) and DIPEA (0.8 mL, 4.5 mmol, 2.9 eq) in DMF (3.5 mL) were added to 1 g (1.55 mmol) of pre-swollen (30 min in 5 mL DMF) 2-ClTrtCl resin. After shaking the resulting mixture for 5 h, the resin was washed with DMF and CH_2Cl_2 (3×5 mL each). Subsequently, the resin was treated (4×5 min) with a mixture of CH_2Cl_2/MeOH/DIPEA (5 mL; v/v/v=17:1:2), washed (CH_2Cl_2, EtOH, CH_2Cl_2; 3×5 mL each) and dried *in vacuo*. The loading degree was determined as previously described (Wodtke et al. 2015).

The pre-swollen resin (30 min in 5 mL DMF) loaded with the initial amino acid (0.325 mmol) was treated with 20% (v/v) piperidine/DMF (4×5 mL, 10 min each). Washing with DMF (4×5 mL each) was followed by treatment with 5% (v/v) DIPEA in DMF (4×5 mL, 1 min each) and repeated washing with DMF (2×5 mL, 1 min each). The next amino acid (1.3 mmol) was dissolved in DMF (5 mL) and added to the resin. After 10 min, HBTU (493 mg, 1.3 mmol), HOBt (176 mg, 1.3 mmol) and DIPEA (454 µL, 2.6 mmol) were added as neat compounds. After 4 h the resin was rinsed with DMF (4×5 mL each) and CH_2Cl_2 (4×5 mL each) and dried *in vacuo*.

Fragment condensation

The fully protected 15mer peptide $cCPE_{290-304}$ containing a free C-terminus was suspended in 4 mL of solvent and added to the pre-swollen peptidyl resin (5 ml DMF, 30 min) containing N-terminally

deprotected $cCPE_{305-319}$ followed by HATU and DIPEA as neat compounds. The synthesis was carried under the conditions outlined in the table below.

solvent	N-terminal fragment	C-terminal fragment	HATU	DIPEA	Conditions
DMF	0.055 mmol	0.05 mmol	0.075 mmol	0.1 mmol	27.5 h, room temperature
NMP	0.055 mmol	0.05 mmol	0.1 mmol	0.1 mmol	30 min, 55 °C, 70 W (Heinlein et al. 2011)

N-terminal modifications

N-terminal 4-fluorobenzoylation of peptides was carried out as previously published (Kuchar et al. 2012), except that CH_2Cl_2 was used as solvent instead of DMF and the reaction time was extended to 5 h.

N-terminal attachment of the 6-aminohexanoic spacer was performed by adding a solution of Fmoc-6-aminohexanoic acid (85 mg, 0.24 mmol; synthesised according to (Wojczewski et al. 2000)) in DMF (2 mL) to the pre-swollen peptidyl resin (0.06 mmol) containing N-terminally deprotected $cCPE_{290-319}$ followed by HBTU (91 mg, 0.24 mmol) and DIPEA (85 µL, 0.48 mmol) as neat compounds. After 4 h, the resin was washed with DMF (4×5 mL each). The Fmoc group was removed as described above. Finally, the resin was washed with DMF (3×5 mL each) and CH_2Cl_2 (3×5 mL each) and dried *in vacuo*.

For N-terminal conjugation with fluorescein, a solution of FITC (70.1 mg, 0.18 mmol) and triethylamine (25 µL, 0.18 mmol) was added to the pre-swollen peptidyl resin (0.06 mmol) containing $Ahx\text{-}cCPE_{290-319}$. After 5 h, the resin was washed with DMF, EtOH and CH_2Cl_2 (3×5 mL each) and dried *in vacuo*. Cleavage from the resin and purification of the FITC-conjugated peptide by semi-preparative HPLC (Method 3) were carried out as described below.

Cleavage from 2-ClTrtCl resin under conservation of side-chain protecting groups

The pre-swollen (30 min in 5 mL of CH_2Cl_2) peptidyl resin containing the $cCPE_{290-304}$ 15mers was treated with HFIP/CH_2Cl_2 (5 mL; v/v=1:4) for 15 min, which was repeated four times. The combined filtrates were concentrated to 1-2 mL in a N_2 stream, treated with ice-cold diethyl ether (20 mL) and kept on ice for 30 min. The white precipitate was filtered off, washed with ice-cold diethyl ether and dried *in vacuo*.

Resin cleavage under concomitant removal of the side-chain protecting groups

The pre-swollen (30 min in 5 mL of CH_2Cl_2) peptidyl resin was treated with a mixture of TFA/H_2O/triethylsilane 95:2.5:2.5 (v/v/v; 7 mL per 0.1 mmol of peptidyl resin) for 5 h. Cleavage in analytical scale (mini-cleavage) was performed with 10 mg of peptidyl resin in 1 mL of the cleavage cocktail for 1 h. The filtrate was collected and the remaining resin washed with TFA. The combined filtrates were concentrated to 1-2 mL in a N_2 stream, treated with ice-cold diethyl ether (20 mL) and kept on ice for 30 min. The precipitate was filtered off, washed with ice-cold diethyl ether and dried *in vacuo*.

Characterisation of distinct products

cCPE$_{290\text{-}319}$ (1)

Sequence: H-SLDAGQYVLVMKANSSYSGNYPYSILFQKF-OH

Peptide **1** served as starting material for all N-terminal modifications. It was synthesised by MW-assisted SPPS under standard conditions. Only a small amount was cleaved from the resin and purified to provide material for SPR measurements and to establish an HPLC system for radiolabeling.

resin:		Wang resin
loading:		0.37 mmol/g
yield (for peptide-loaded resin, n = 5):		90 ± 7%
yield (for isolated purified peptide):		24 mg, 29%
M (calculated; $C_{154}H_{226}N_{36}O_{46}S$):		3389.66 g/mol
M (found; ESI-MS+):		*m/z* = 1138.6 ($[M+Na+2H]^{3+}$)
		m/z = 1131.2 ($[M+3H]^{3+}$)
		m/z = 848.7 ($[M+4H]^{4+}$)
RP-HPLC	system 1:	t_R = 22.3 min
	system 2:	t_R = 22.4 min
	system 3:	t_R = 25.5 min
	system 4:	t_R = 24.0 min
purity		≥98%

Fmoc-cCPE$_{305\text{-}319}$ (2)

Sequence: H-SYSGNYPYSILFQKF-OH

Compound **2** was solely characterised by mini-cleavage as resin-bound peptide was used for fragment condensation.

resin:		Wang
loading:		0.37 mmol/g
yield (crude product, n = 2):		87 ± 15%
M (calculated; $C_{88}H_{120}N_{18}O_{24}$)		1813.9 g/mol
M (found; ESI-MS+):		*m/z* = 907,6 ($[M+2H]^{2+}$)
RP-HPLC	(system 1):	t_R = 17.8 min

cCPE$_{290\text{-}304}$ (3)

Sequence: Fmoc-SLDAGQYVLVMKANS-OH

Synthesis was carried out at 2-ClTrtCl resin to ensure conservation of protecting groups after cleavage. Full characterisation was only done for the synthesis on the Ser^{tBu}-Asn^{Trt}-Ala-preloaded resin under standard conditions of solid-phase peptide synthesis. Yield refers to the amount of the crude, fully protected peptide. MS analysis was done on the deprotected peptide obtained after mini-cleavage.

resin:	2-ClTrtCl; preloaded with Ser^{tBu}-Asn^{Trt}-Ala
loading degree:	0.41 mmol/g
yield (crude product, n = 3):	54 ± 10%
M (calculated; $C_{84}H_{124}N_{18}O_{25}S$):	1816.9 g/mol
M (found; ESI-MS+):	*m/z* = 1840.0 ($[M+Na]^+$)
	m/z = 1818.0 ($[M+H]^+$)
	m/z = 931.5 ($[M+2Na]^{2+}$)
RP-HPLC system 1:	t_R = 19.8 min

FBz-cCPE$_{290-319}$ × 2 TFA (4a)

Sequence: FBz-SLDAGQYVLVMKANSSYSGNYPYSILFQKF-OH × 2 TFA

The complete amount of resin-bound peptide was subjected to cleavage, purified and characterised after lyophylisation. Peptide **4a** was used for SPR measurements, ECD spectroscopy and served as non-radioactive reference compound for [^{18}F]FBz-cCPE$_{290-319}$. The yields stated below refer to the employed amount of peptide-loaded resin.

yield (n = 2):	8.3-20.9 mg (9-12%)
M (calculated; $C_{164}H_{235}FN_{36}O_{47}S$:	3511.68 g/mol
M (found; ESI-MS+):	*m/z* = 1179.0 ($[M+Na+2H]^{3+}$)
	m/z = 1171.8 ($[M+3H]^{3+}$)
	m/z = 879.1 ($[M+4H]^{4+}$)
RP-HPLC system 1:	t_R = 25.8 min
system 2:	t_R = 26.8 min
system 3:	t_R = 28.2 min
system 4:	t_R = 31.0 min
purity:	≥97%

Ahx-cCPE$_{290-319}$

Sequence: H-Ahx-SLDAGQYVLVMKANSSYSGNYPYSILFQKF-OH

Free peptide was isolated in small amounts obtained by mini-cleavage for characterisation. The remaining resin was used for radiolabelling with [^{18}F]SFB and to synthesise the corresponding non-radioactive reference compound and for conjugation with FITC.

resin:	Wang
loading degree:	0.37 mmol/g
yield (gravimetrical for resin-bound peptide, n = 3):	93 ± 6%
M (calculated; $C_{163}H_{243}N_{37}O_{47}S$):	3502.75 g/mol
M (found; ESI-MS+):	*m/z* = 1183.4 ($[M+2Na+H]^{3+}$)
	m/z = 1176.1 ($[M+Na+2H]^{3+}$)

		m/z = 893.6 ([M+3Na+H]$^{4+}$)
RP-HPLC	system 2:	t_R = 22.3 min
	system 4$_b$:	t_R = 26.6 min

FBz-Ahx-cCPE$_{290-319}$ × 2 TFA (5a)

Sequence: FBz-Ahx-SLDAGQYVLVMKANSSYSGNYPYSILFQKF-OH × 2 TFA

Purified **5a** was used for inhibition in cell binding studies and SPR measurements.

yield:		19.8 mg, 20%
M (calculated; $C_{170}H_{246}FN_{37}O_{48}S$):		3624.77 g/mol
M (found; ESI-MS+):		m/z = 1228.3 ([M+Na+K+H]$^{3+}$)
		m/z = 1209.8 ([M+3H]$^{3+}$)
		m/z = 907.5 ([M+4H]$^{4+}$)
RP-HPLC	system 2:	t_R = 26.2 min
	system 3:	t_R = 28.1 min
	system 4$_b$:	t_R = 32.0 min
purity:		≥94%

FITC-Ahx-cCPE$_{290-319}$ × 2 TFA (6)

Sequence: FITC-Ahx-SLDAGQYVLVMKANSSYSGNYPYSILFQKF-OH × 2 TFA

yield:		55.7 mg, 23%
M (calculated; $C_{184}H_{254}N_{38}O_{52}S_2$):		3891.78 g/mol
M (found; ESI-MS+):		m/z = 1298.3 ([M+3H]$^{3+}$)
		m/z = 974.0 ([M+4H]$^{4+}$)
RP-HPLC	System 1:	t_R = 25.9 min
	System 2:	t_R = 26.8 min
	System 3:	t_R = 28.2 min
purity:		≥95%

Ahx-cCPE$_{290-319}$-amide:

Sequence: H-Ahx-SLDAGQYVLVMKANSSYSGNYPYSILFQKF-NH_2

Synthesised under standard conditions of MW-assisted SPPS using pseudoproline dipeptides. The resin-bound peptide served as reactant for fluorobenzoylation. Only a small amount was cleaved from the resin and purified.

resin:	Rink-Amide-MBHA
	0.55 mmol/g

loading degree:		90%
yield (gravimetrical for resin-bound peptide):		3501.76 g/mol
M (calculated; $C_{163}H_{244}N_{38}O_{46}S$):		*m/z* = 1169.2 ($[M+3H]^{3+}$)
M (found; ESI-MS+):		*m/z* = 877.2 ($[M+4H]^{4+}$)
		t_R = 23.2 min
RP-HPLC	system 1:	t_R = 22.1 min
	system 2:	t_R = 26.6 min
	system 4_b:	

FBz-Ahx-cCPE$_{290-319}$-amide × 2 TFA (5b)

Sequence: FBz-Ahx-SLDAGQYVLVMKANSSYSGNYPYSILFQKF-NH_2 × 2 TFA

Obtained by fluorobenzoylation of resin-bound Ahx-cCPE$_{290-319}$-amide.

yield:		16.6 mg, 14%
M (calculated; $C_{163}H_{244}N_{38}O_{46}S$):		3623.78 g/mol
M (found; ESI-MS+):		*m/z* = 1209.6 ($[M+3H]^{3+}$)
		m/z = 917.1 ($[M+2Na+2H]^{4+}$)
		m/z = 907.8 ($[M+4H]^{4+}$)
RP-HPLC	system 1:	t_R = 25.6 min
	system 2:	t_R = 26.2 min
	system 3:	t_R = 28.1 min
	system 4_b:	t_R = 30.5 min
purity:		≥73%

FBz-cCPE$_{290-319}$-Tyr306Ala × 2 TFA (4b)

Sequence: FBz-SLDAGQYVLVMKANSS**A**SGNYPYSILFQKF-OH × 2 TFA

This peptide was synthesised by N-terminal fluorobenzoylation of the corresponding resin-bound peptide as described for the wild-type peptide **4a**. The yield refers to the used amount of resin-bound peptide.

yield:		3.3 mg, 3%
M (calculated; $C_{160}H_{237}FN_{36}O_{46}S$):		3419.65 g/mol
M (found; ESI-MS+):		*m/z* = 1155.9 ($[M+2Na+H]^{3+}$)
		m/z = 1148.6 ($[M+Na+2H]^{3+}$)
RP-HPLC	system 1:	t_R = 25.1 min
	system 2:	t_R = 25.5 min
	system 3:	t_R = 28.6 min
purity:		≥81%

FBz-cCPE$_{290-319}$-Tyr306Phe × 2 TFA (4c)

Sequence: FBz-SLDAGQYVLVMKANSS**F**SGNYPYSILFQKF-OH × 2 TFA

This peptide was synthesised by N-terminal fluorobenzoylation of the corresponding resin-bound peptide as described for the wild-type peptide **4a**. The yield refers to the used amount of resin-bound peptide.

yield:		29.1 mg, 22%
M (calculated; $C_{161}H_{229}FN_{36}O_{47}S$):		3495.69 g/mol
M (found; ESI-MS+):		*m/z* = 1174.6 ($[M+Na+2H]^{3+}$)
		m/z = 1167.1 ($[M+3H]^{3+}$)
		m/z = 875.7 ($[M+4H]^{4+}$)
RP-HPLC	system 1:	t_R = 28.5 min
	system 2:	t_R = 27.6 min
	system 3:	t_R = 28.7 min
purity:		≥98%

FBz-cCPE$_{290-319}$-Tyr306Trp × 2 TFA (4d)

Sequence: FBz-SLDAGQYVLVMKANSS**W**SGNYPYSILFQKF-OH × 2 TFA

This peptide was synthesised by N-terminal fluorobenzoylation of the corresponding resin-bound peptide as described for the wild-type peptide **4a**. The yield refers to the used amount of resin-bound peptide.

yield:		11.4 mg, 9%
M (calculated; $C_{166}H_{236}FN_{37}O_{46}S$):		3534.70 g/mol
M (found; ESI-MS+):		*m/z* = 1187.0 ($[M+Na+2H]^{3+}$)
		m/z = 894.0 ($[M+2Na+2H]^{4+}$)
RP-HPLC	system 1:	t_R = 25.3 min
	system 3:	t_R = 28.9 min
purity:		≥99%

FBz-cCPE$_{290-319}$-Tyr306pFPhe × 2 TFA (4e)

Sequence: FBz-SLDAGQYVLVMKANSS(**pFF**)SGNYPYSILFQKF-OH × 2 TFA

This peptide was synthesised by N-terminal fluorobenzoylation of the corresponding resin-bound peptide as described for the wild-type peptide **4a**. The yield refers to the used amount of resin-bound peptide.

yield:		34.7 mg, 24%
M (calculated; $C_{164}H_{234}F_2N_{36}O_{46}S$):		3513.68 g/mol
M (found; ESI-MS+):		*m/z* = 1194.7 ($[M+3Na]^{3+}$)
		m/z = 1187.1 ($[M+2Na+H]^{3+}$)
		m/z = 1180.0 ($[M+Na+2H]^{3+}$)
		m/z = 1173.0 ($[M+3H]^{3+}$)
		m/z = 889.2 ($[M+2Na+2H]^{4+}$)
RP-HPLC	system 2:	t_R = 28.0 min
	system 3:	t_R = 29.2 min
purity:		99%

FBz-cCPE$_{290-319}$-Leu315Ala × 2 TFA (4f)

Sequence: FBz-SLDAGQYVLVMKANSSYSGNYPYSI**A**FQKF-OH × 2 TFA

This peptide was synthesised by N-terminal fluorobenzoylation of the corresponding resin-bound peptide as described for the wild-type peptide **4a**. The yield refers to the used amount of resin-bound peptide.

yield:		16.2 mg, 15%
M (calculated; $C_{161}H_{229}FN_{36}O_{47}S$):		3469.63 g/mol
M (found; ESI-MS+):		*m/z* = 1180.2 ($[M+3Na]^{3+}$)
		m/z = 1172.5 ($[M+2Na+H]^{3+}$)
		m/z = 1165.3 ($[M+Na+2H]^{3+}$)
		m/z = 879.5 ($[M+2Na+2H]^{4+}$)
RP-HPLC	system 1:	t_R = 23.5 min
	system 2:	t_R = 23.6 min
	system 3:	t_R = 24.3 min
purity:		98%

FBz-cCPE$_{290-319}$-Tyr306Ala-Leu315Ala × 2 TFA (4g)

Sequence: FBz-SLDAGQYVLVMKANSS**A**SGNYPYSI**A**FQKF-OH × 2 TFA

This peptide was synthesised by N-terminal fluorobenzoylation of the corresponding resin-bound peptide as described for the wild-type peptide **4a**. The yield refers to the used amount of resin-bound peptide.

yield:	15.8 mg, 12%
M (calculated; $C_{155}H_{225}FN_{36}O_{46}S$):	3377.61 g/mol
M (found; ESI-MS+):	*m/z* = 1141.9 ($[M+2Na+H]^{3+}$)
	m/z = 1134.5 ($[M+Na+2H]^{3+}$)

		m/z = 856.9 ($[M+4H]^{4+}$)
RP-HPLC	system 1:	t_R = 23.1 min
	system 2:	t_R = 23.6 min
	system 3:	t_R = 26.5 min
purity:		≥99%

ECD Spectroscopy

Stock solutions of peptide **4a** were prepared at a concentration of 0.5 mg/mL in a mixture of 10 mM sodium phosphate pH 7.4 and CH_3CN (1:1, v/v). The high absorbance at this concentration did not allow measurements below 200 nm. To obtain ECD spectra of **4a** at a concentration of 0.125 mg/mL, the stock solution was diluted with the buffer/CH_3CN mixture. The high absorbance for this solvent mixture did not allow measurements below 200 nm for both concentrations.To measure spectra of peptide **4a** in the presence of 50% TFE, a stock solution was prepared in buffer/CH_3CN/TFE 1:1:2 (v/v/v) at a concentration of 0.5 mg/mL. 1% of TFA was added and the mixture was heated (50 °C) for complete dissolution. Dilution to 0.125 mg/mL was done with the identical solvent mixture. In this case, the ECD scanning was possible bellow 190 nm. The ECD spectra were measured in a quartz cuvette (Starna) with an optical path length of 1 mm using a J-810 spectropolarimeter (Jasco, Japan). The conditions of the measurements were as follows: a spectral region of 200 (180) - 400 nm, a scanning speed of 20 nm/min, a response time of 8 s, a resolution of 1 nm, a bandwidth of 1 nm and a sensitivity of 100 mdeg. The final spectrum was obtained as an average of 5 accumulations. The spectra were corrected for a baseline by subtracting the spectra of the corresponding polypeptide-free solution. The ECD measurements were conducted at room temperature. Molar ellipticities were calculated according to (Urbanova and Maloň 2012).

Labelling with fluorine-18

Synthesis of [^{18}F]SFB

[^{18}F]Fluoride was produced at a cyclotron (Cyclone 18/9, IBA, Belgium) via the $^{18}O(p,n)^{18}F$ nuclear reaction. The automated synthesis of [^{18}F]SFB was performed according to (Mäding et al. 2005) with implemented modifications as published in (Kapty et al. 2011).

Radiolabelling of $cCPE_{290-319}$ with [^{18}F]SFB

^{18}F-labelling of the resin-bound 30mer, which contained a free N-terminal amino group but was otherwise fully protected, was carried out in orientation to (Kuchar et al. 2012). 3-10 mg (0.9-3 µmol) of peptidyl resin were subjected to reaction with [^{18}F]SFB. The major difference lies in the isolation of the cleaved radiolabelled peptide. The resin containing the ^{18}F-labelled peptide was treated with 300 µL of TFA/H_2O/triethylsilane 95:2.5:2.5 (v/v/v) at 50 °C for 15 min. The filtrate was collected and the remaining resin washed with 100 µL of cleavage cocktail. The combined filtrates were diluted with 300 µL of CH_3CN/H_2O (v/v=1:1) and the resulting solution subjected to purification by semi-preparative radio-HPLC. Alternatively, the combined filtrates obtained after cleavage were treated with ice-cold

diethyl ether (1.5 mL) in a 2 mL test tube and centrifuged. The etheric layer was discarded and the pellet dissolved in 700 µL of CH_3CN/H_2O/TFA (v/v/v=8:6:1) and the resulting solution subjected to purification by semi-preparative radio-HPLC.

Radiolabelling of $cCPE_{290\text{-}319}$ with 4-[^{18}F]fluorobenzoyl chloride

To prepare 4-[^{18}F]fluorobenzoyl chloride (in orientation to the procedures published in (Lang et al. 1999; Kiesewetter and Eckelman 2001; Seimbille et al. 2005)), the [^{18}F]SFB radiosynthesis was interrupted at the stage of 4-[^{18}F]fluorobenzoic acid, which was reacted with neat α,α-dichloromethyl methyl ether (1 mL) for 2 min at 90 °C. After cooling to 40 °C, the mixture was again heated to 90 °C for 2 min. The reaction of the resin-bound 30mer with 4-[^{18}F]fluorobenzoyl chloride was performed equally to that with [^{18}F]SFB, with the exceptions of reducing the temperature to 40 °C, applying non-aqueous solvent (300 µL of CH_2Cl_2/DMF 1:1 (v/v)) and the addition of DIPEA equimolar to resin-bound peptide. After the completed reaction, the resin was washed with CH_2Cl_2 (2×2 mL). Cleavage from resin was followed by the precipitation step as described above.

Radiolabelling of Ahx-$cCPE_{290\text{-}319}$ with [^{18}F]SFB

The pre-swollen peptidyl resin was treated with a solution of [^{18}F]SFB and DIPEA (equimolar amounts to peptide-bound resin) in 300 µL of DMF at 50 °C for 30 min under gentle magnetic stirring. After washing with CH_2Cl_2 (2×2 mL) the resin was treated with 300 µL of TFA/H_2O/triethylsilane 95:2.5:2.5 (v/v/v) at 30 °C for 15 min. The filtrate was collected in a 2 mL test tube, the remaining resin was washed with 100 µL of cleavage cocktail and the combined filtrates were treated with ice-cold diethyl ether (1.5 mL) and centrifuged. The etheric layer was discarded and the pellet dissolved in 700 µL of CH_3CN/H_2O/TFA (v/v/v=8:6:1) at 60 °C. The resulting solution containing the ^{18}F-labelled peptide was subjected to semi-preparative HPLC (Method 4_b). The product-containing eluate was collected according to the monitored γ trace of the chromatogram and diluted with H_2O (30 mL). The resulting solution was passed over a pre-conditioned LiChrolut® RP-18 cartridge. The cartridge was washed with H_2O (3 mL) and eluted with ethanol/H_2O (v/v=1:1; 4×500 µL).

Synthesis of [^{18}F]FBz-$cCPE_{290\text{-}319}$ ([^{18}F]4a) with [^{18}F]SFB

Sequence: [^{18}F]FBz-SLDAGQYVLVMKANSSYSGNYPYSILFQKF-OH × 2 TFA

resin:	Wang
loading degree:	0.37 mmol/g
resin-bound activity (n = 7):	7 ± 3%
radiochemical yield (d.c.; n = 3):	1 ± 0,2%
RP-HPLC system 2:	t_R = 26,8 min
system 4:	t_R = 37,0 min
radiochemical purity:	≥98%
time of synthesis:	ca. 140 min

Synthesis of [^{18}F]FBz-$cCPE_{290\text{-}319}$ ([^{18}F]4a) with [^{18}F]FBzCl

Sequence: [^{18}F]FBz-SLDAGQYVLVMKANSSYSGNYPYSILFQKF-OH × 2 TFA

resin:	Wang
loading degree:	0.37 mmol/g
resin-bound activity (n = 4):	24 ± 12%
radiochemical yield (d.c.; n = 2):	2 ± 0,2%
RP-HPLC system 2:	t_R = 26.8 min
system 4:	t_R = 37.0 min
radiochemical purity:	≥98%
time of synthesis:	ca. 150 min

Synthesis of [^{18}F]FBz-Ahx-cCPE$_{290-319}$ ([^{18}F]5a) with [^{18}F]SFB

Sequence: [^{18}F]FBz-Ahx-SLDAGQYVLVMKANSSYSGNYPYSILFQKF-OH × 2 TFA

resin:	Wang
loading degree:	0.37 mmol/g
resin-bound activity (n = 11):	65 ± 4%
radiochemical yield (d.c.; n = 10):	7 ±3%
molar activity (n = 10):	1.5 ± 0.3 GBq/µmol
RP-HPLC system 2:	t_R = 27.0 min
system 4$_b$:	t_R = 31.0 min
radiochemical purity:	≥ 99%
time of synthesis:	ca. 130 min

Surface plasmon resonance

The SPR analyses were performed using a Biacore T100 (GE Healthcare) device. The ligand MKH$_{10}$AS-Cld-4$_{29-81}$-LEVLFQGP-Cld-4$_{139-160}$ (M=10.6 kDa; purchased from Abcam, #ab124320) comprising both extracellular loops of human Cld-4 was immobilised on a CM5 sensor chip using the amine coupling kit (GE Healthcare) and PBS (GE Healthcare) following the protocol published elsewhere (Tondera et al. 2017). After the final coupling step using a solution of Cld-4 at a concentration of 20 µg/mL in 10 mM acetate buffer (pH = 4) and the blocking of the surface using ethanolamine 5,500-6,500 arbitrary response (resonance) units (RU) of Cld-4 were immobilised on the sensor surface. A reference cell was prepared by blank immobilisation. Kinetic data were obtained in the single-cycle mode at 25 °C using the respective cCPE$_{290-319}$ derivatives **1**, **4a**-**g** and **5a** and **b** at concentrations of 2-10 µM. The flow buffer used was PBS containing 1% DMSO. Association and dissociation of all analytes was followed in real-time and measured at 25 °C at a flow rate of 30 µL/min. The surfaces were regenerated by a sequence of glycine (10 mM, pH = 3.0, 5 s) and NaOH (0.05 mM, 5 s) followed by a stabilisation period of 300 s. The rate constants according to a two-state reaction model (see scheme below) were obtained by fitting the data including reference subtraction and blank buffer correction derived from both blank runs using the Biacore T200 Evaluation software 3.0. (Tondera et al. 2017).

$$R + L \underset{k_{d1}}{\overset{k_{a1}}{\rightleftharpoons}} RL \underset{k_{d2}}{\overset{k_{a2}}{\rightleftharpoons}} RL^*$$

The parameters K_D, k_{off} and k_{on} were calculated from the individual rate constants by the following equations (Tummino and Copeland 2008):

$$K_D = \frac{k_{d1}}{k_{a1}(1+\frac{k_{a2}}{k_{d2}})} \qquad \text{(I)}$$

$$k_{off} = \frac{k_{d1}k_{d2}}{k_{a2}+k_{d1}+k_{d2}} \qquad \text{(II)}$$

$$k_{on} = \frac{k_{off}}{K_D} \qquad \text{(III)}$$

Measurements towards thermodynamic analysis for compound **1** were performed in multiple-cycle mode at 15, 20, 25, and 30 °C. The obtained K_D values were analysed by non-linear regression using the van't Hoff equation for changing heat capacity (de Mol et al. 2005) as implemented in the Biacore evaluation software. The reference temperature was defined as 298 K.

Western blot analysis

Preparation of protein extracts from subconfluent cell cultures using RIPA buffer as well as western blot analysis was performed as described elsewhere (Mamat et al. 2012). In brief, 50 µg protein lysate were separated in a 10% v/v sodium dodecyl sulfate polyacrylamide gel electrophoresis (SDS-PAGE) and transferred to a PVDF membrane (Fisher Scientific) using a semi-dry transfer system (Bio-Rad). After blocking with 5% w/v skimmed milk for at least 1 h, PVDF membrane was incubated with polyclonal rabbit anti-human Cld-4 IgG (abcam, ab15104; 1:500) for 2 h at room temperature and afterwards overnight at 4 °C. Membranes were washed 3 times with TBS-T (TBS with 0.05% v/v Tween20) for 20 min and incubated with the appropriate horseradish peroxidase coupled secondary antibodies (goat anti-rabbit IgG, Sigma Aldrich, A0545, 1:5000) for 1 h at room temperature. Protein bands were detected with Super Signal West Dura Chemiluminescent Substrate (Fisher Scientific) and the MF-ChemiBis 3.2 imaging system (Biostep). To verify equal protein loading, membranes were stripped (62.5 mm Tris pH 6.8, 2% SDS, and 0.7% β-mercaptoethanol) and reprobed with rabbit anti-actin IgG (Sigma Aldrich, A5060) and horseradish peroxidase coupled goat anti-rabbit IgG (Sigma Aldrich, A0545).

Immunocytochemistry

HT-29 and A431 cells were seeded in chamber slides (Corning) and cultivated over night. Cells were washed twice with PBS and subsequently fixed with PFA solution (4% (m/V) PFA, 2.5% (m/V) sucrose in PBS) for 30 min. Afterwards, the cells were blocked with blocking solution (10% FCS in PBS with 0.5% Tween 20) for 30 min before being incubated with the rabbit polyclonal anti- Cld-4 antibody (abcam ab15104, 1:50) for 1h. Then, cells were washed 3 times with PBS-T (PBS with 0.5% Tween 20) and incubated with the secondary antibody (donkey anti-rabbit Alexa Fluor 546; Molecular Probes A10039, 1:200) for 1h. Afterwards, they were washed 3 times for 15 min with PBS-T and nuclei were counterstained as described below. Cells were mounted with antifade mounting medium (Dako) and imaged with confocal microscopy (Olympus Fluoview 1200).

Microscopy and flow cytometry with FITC-Ahx-cCPE$_{290-319}$ (6)

HT-29 (12.6×10^4) and A431 (6×10^4) cells were seeded in 8-well chamber slides (ibidi) and cultured overnight. Then, cells were washed with PBS an incubated with 10 µM of **6** (1 mM stock in DMSO) or

fluorescein (1.5 µL of 1 mM stock in water) in DMEM media (150 µL) without supplements. After 0, 1, 3 and 4 h of incubation, cells were washed 3 times with PBS and fixed with PFA solution (4% (m/V) PFA, 2.5% (m/V) sucrose in PBS) for 15 min. Then, they were washed again 3 times with PBS and nuclei were counterstained with Hoechst 33258 (10 µg/mL Sigma-Aldrich) for 5 min and analysed by confocal microscopy (Olympus Fluoview 1200). The experiment was repeated twice. For flow cytometry cells were seeded in 6-well plates (Greiner Bio-One) and the experiment was done analogously to the description above. After incubation with **6** and washing with PBS cells were detached with trypsin/EDTA (0.05%/0.02%) and resuspended in flow buffer (1% (m/V) BSA in PBS) before being analysed with flow cytometry (AttuneNxT, Thermo Fisher). Median fluorescence intensity (MFI) of 3 independent experiments was determined.

Stability of FITC-Ahx-cCPE$_{290-319}$ (6) in human serum

A 10 µM solution of FITC-Ahx-cCPE$_{290-319}$ (**6**) in human serum was prepared in Protein LoBind tubes from a 10 mM stock solution in DMSO. The solution was incubated at 37 °C and 700 rpm. Samples were taken before (T_0) and at various time points during incubation (T_x). Immediately after taking samples, an equal volume of EtOH/CH_3CN 1:1 (v/v) was added (c_{T0} = 50 µM) to inactivate serum proteases and precipitate all serum proteins. Precipitation was performed for at least one hour at -20 °C before centrifugation (3750 g, 4 °C, 5 min). The supernatant was transferred into a 0.22 µm Corning® Costar® Spin-X® centrifuge tube filter and centrifuged (3750 g, 4 °C, 5 min). The discharge was precipitated again for at least one hour at -20 °C before further centrifugation (3750 g, 4 °C, 5 min). For analysis by UPLC, the sample solutions were diluted 1:5 in the appropriate starting gradient (c_{T0} = 10 µM). Separation and analysis was performed by a UPLC-ESI-MS (Waters I-Class UPLC with PDA eλ Detector and coupled to XEVO TQ-S ESI-ToF-MS; Waters Acquity BEH C18 column (2.1x100 mm, 1,7 µm particle size), gradient 25 - 75% 1:1 CH_3CN/MeOH (0.1% AcOH) / H_2O (0.1% AcOH), 5 min). Detection was performed by absorbance measurement at a suitable wavelength (FITC, λ = 485 nm) and ESI-MS coupling. For quantitative comparison of peptide stability, absorbance measurements were analysed and the ratio of the peptide peak area at T_0 to total peak area was defined as 100% stability. All further samples were calculated as percentages to this ratio. All measurements were performed in triplicates.

Radiopharmacological characterisation of [^{18}F]FBz-Ahx-cCPE$_{290-319}$ ([^{18}F]5a) in vitro

Cell binding studies of [^{18}F]FBz-Ahx-cCPE$_{290-319}$ ([^{18}F]**5a**)

Human colorectal adenocarcinoma (HT-29; ATCC HTB-38) and squamous cell/epidermoid carcinoma (A431, ATCC CRL-1555) cell lines were routinely cultivated in DMEM supplemented with 10% (v/v) heat-inactivated fetal calf serum (FCS), penicillin (100 U/mL), streptomycin (100 µg/mL), glutamine (4 mM), 1% HEPES (1 M; A431 cells only) at 37 °C and 5% CO_2 in a humidified incubator. Radiotracer uptake studies were performed in monolayer cultures. Therefore, cells were seeded in 24-well plates at a density of 1.0×10^5 cells/mL and grown to confluence.

Cell binding of [^{18}F]**5a** was studied at temperatures of 4 °C and 37 °C and incubation times of 5, 10, 30 and 60 min in quadruplicate.

15-30 MBq of [^{18}F]**5a** were dissolved in ethanol/H_2O 1:1 (v/v, 2 mL) and diluted into PBS according to the number of wells. After removing the medium, 250 µL of PBS and 250 µL of the radiotracer-

containing solution were added. Optionally, instead of PBS 250 µL of 10 µM FBz-Ahx-cCPE$_{290-319}$ (1% DMSO/PBS) were added 10 min prior to addition of the radiotracer. After the respective incubation time, the supernatants were discarded and the cell washed with ice-cold PBS (3 × 500 µL) and lysed with 500 µL of 1% SDS/0.1 M NaOH. Half of the lysate was used for activity measurement (decay corrected; relative to a mixture of 25 µL of the radiotracer-containing PBS solution and 225 µL of 1% SDS/0.1 M NaOH) with Cobra II gamma counter (Canberra-Packard). Activity measurements were corrected for unspecific tracer binding determined in empty (cell-free) plates using the same experimental conditions. The other half was used for determination of the total protein concentration in duplicate (2 × 25 µL) using the bicinchoninic acid assay (BCA; Pierce) and bovine serum albumin as protein standard. Uptake data for all experiments are expressed as percentage of injected dose per mg protein (%ID/mg protein).

To prove the stability during cellular incubation, the radiotracer-containing supernatant of HT-29 cells was analysed after 60 min at 37 °C by radio-HPLC.

Investigation of stability of [^{18}F]FBz-Ahx-cCPE$_{290-319}$ ([^{18}F]**5a**) in blood plasma

Plasma stability was investigated by incubating [^{18}F]FBz-Ahx-cCPE$_{290-319}$ in blood plasma of a Wistar rat at 37 °C for 1h. Subsequently, the sample was treated with ice-cold methanol for precipitation of plasma proteins, centrifuged, and the supernatant subjected to HPLC analysis using an (Agilent Technologies 1200 LC) using a Zorbax C-18 300SB column (250 mm × 9.4 mm) as stationary phase and a mixture of water (A) and acetonitrile (B) containing 0.1% TFA each as mobile phase. A binary gradient was run at a flow rate of 3 mL/min starting at 25% B to 60% B within 20 min.

Radiopharmacological characterisation of [^{18}F]FBz-Ahx-cCPE$_{290-319}$ ([^{18}F]5a) in vivo

Animal experiments were carried out according to the guidelines of the German Regulations for Animal Welfare. The protocol was approved by the local Ethical Committee for Animal Experiments (reference numbers 24D-9168.11-4/2007-2 and 24-9168.21-4/2004-1).

Investigation of *in vivo* stability of [^{18}F]FBz-Ahx-cCPE$_{290-319}$ ([^{18}F]**5a**)

For the investigation of metabolic stability, 20-30 MBq of [^{18}F]**5a** dissolved in physiological saline (0.5 mL) were injected into the tail vein of male Wistar rats under anesthesia with a gas mixture of 10% desflurane and 30% oxygen/air. At defined time points blood samples were taken from right femoral artery via catheter. The exact volume and activity (decay-corrected according to time of injection) of the blood samples was determined for%ID/mL calculation. The samples were centrifuged at 3 min at 11000 g, the obtained supernatant was removed and treated with ice-cold methanol for precipitation of plasma proteins. The resulting suspension was centrifuged again (11000 g, 3min) and subjected to HPLC analysis on an Agilent 1100 system equipped with UV/Vis DAD and a radiation detector (Canberra-Packard, Radiomatic Flo-one Beta 150TR – with PET flow cell). A Zorbax 300SB-C18 column (250 x 9.4 mm; 5 µm) was used as stationary phase, elution was done in gradient mode at a flow rate of 3 mL/min using the following programme: 0-5 min 95% water/5% acetonitrile/0.1% trifluoroacetic acid, 5-15 min gradient 100% acetonitrile/0.1% trifluoroacetic acid, 15-20 min plateau at 100%

acetonitrile/0.1% trifluoroacetic acid, 20-23 min back to 0-5 min 95% water/5% acetonitrile/0.1% trifluoroacetic acid.

The ratio of area under the curve of original [^{18}F]**5a** to the summed peak areas of all observed ^{18}F-labelled species was calculated for every time point. The obtained fractions were multiplied with the activity concentration (%ID/mL) of the corresponding blood samples for the calculation of total clearance activity concentrations.

PET Experiments

Pilot dynamic small animal PET experiments were then performed in both healthy male Wistar rats and NMRI Foxn1$^{nu/nu}$ mice using 24 MBq and 7 MBq, respectively, of **[^{18}F]5a** following the protocols published elsewhere with some minor modifications (Wolf et al. 2011; Kuchar et al. 2018). In brief, one rat and 2 mice were positioned under anesthesia as described above and immobilised prone with their medial axis parallel to axis of the scanner with thorax and abdominal region (organs of interest: heart, liver, spleen, kidneys, large vessels) in the center of field of view of a dedicated PET/CT scanner for small animals (NanoScan PET/CT scanner, Mediso). PET acquisition was started 20 s before intravenous (i.v.) infusion of the radiotracer through a needle catheter into a lateral tail vein and emission data were acquired continuously for a tracer-dependent duration of 0-60 min p.i. Acquired data were sorted into 28-32 time frames and reconstructed as described elsewhere (Pietzsch et al. 2005). Images were analysed by assigning 3-dimensional regions-of-interest (ROI) over the heart region, the liver, and the kidneys using ROVER software (ABX GmbH). From these ROIs time-activity-curves (TACs) representing the total (decay-corrected) fluorine-18 activity in a defined volume and expressed as radioactivity concentration, percent of maximum were obtained in each rat and mouse.

Results and discussion

Synthesis of cCPE$_{290-319}$ and derivatives

Initial attempts to prepare cCPE$_{290-319}$ (**1**) by sequential solid-phase peptide synthesis using Wang linker-functionalised polystyrene resin led to crude material that contained the desired 30mer peptide in insufficient amounts and that has revealed difficult to purify (Fig. 2A). Hence, the C-terminal fragment of cCPE comprising the amino acid residues 290-319 can be considered as "difficult peptide/sequence" (Tickler and Wade 2007; Paradis-Bas et al. 2016). For this reason, the 30mer sequence was deconstructed into two fragments of equal size. As the serine residue that is present at the C-terminus of the resulting N-terminal fragment can be introduced as C-terminal pseudoproline dipeptide, epimerisation at this position during fragment condensation of both 15mers at solid support should be largely suppressed. This approach of peptide fragment condensation has been successfully applied in the synthesis of the C-terminally thioester-functionalised, N-glycosylated 1-39 fragment of RNase C (Heinlein et al. 2011). The C-terminal fragment 305-319 (**2**) of cCPE$_{290-319}$ was assembled by MW-assisted SPPS under standard conditions. The gravimetrically determined yield of the resin-bound peptide was in the range of 76-95%. For the synthesis of the N-terminal fragment Fmoc-cCPE$_{290-304}$ (**3**), the 2-ClTrtCl linker was chosen as anchor group for resin attachment, as this should enable the efficient release of the 15mer under conservation of all side-chain protecting groups under mildly acidic conditions (Bollhagen et al. 1994). To avoid cleavage of the resin-attached pseudoproline dipeptide consisting of Asn and Ser by diketopiperazine formation, removal of the Fmoc group was carried out under the optimised conditions identified by Heinlein et al., i.e. DBU/HOBt/DMF 2.1:1.7:69.2 (v/w/v) (Heinlein et al. 2011). The following amino acid was attached by non-automated manual coupling to enable determination of resin-loading at the tripeptide stage. All subsequent steps were carried out under standard conditions of MW-assisted automated SPPS. After cleavage from the resin with HFIP/CH_2Cl_2 1:3 (v/v) the desired protected 15mer bearing Asn^{Trt}-Ser($\psi^{Me,Me}$pro)-OH at the C-terminus was isolated in a yield of only 6%. It was hypothesised that this might be due to diketopiperazine formation at later stages of peptide chain assembly by nucleophilic attack of the amidic N_α nitrogen atom at the C-terminal carbonyl carbon (Goodman and Stueben 1962). Therefore, the N-terminal 15mer was synthesised with the *t*Bu-protected C-terminal serine residue under otherwise identical conditions, which resulted in yields ranging from 43-59% (n=3) for the isolated peptide. Under the chosen conditions, Fmoc deprotection is carried out with 20% piperidine/DMF containing 0.1 M HOBt, which might lead to partial cleavage of the peptide from the resin due to repeated exposure to the slightly acidic medium. For this reason, the synthesis of the pseudoproline-free N-terminal 15mer was attempted under modified conditions suggested by (Friligou et al. 2011), which, however, did not result in higher yields. Fragment condensation was carried out with HATU as coupling reagent to minimise epimerisation and DIPEA as base in DMF at room temperature. The N-terminal fragment has revealed to be incompletely soluble in that solvent. Analysis by mass spectrometry and HPLC after 22 h indicated the presence of a mixture of the desired 30mer peptide and unreacted C-terminal 15mer, which were difficult to separate from each other. Performing the coupling of the two fragments under MW irradiation (55 °C, 70 W, 30 min according to (Heinlein et al. 2011)) and changing the solvent from DMF to NMP did not result in a more complete reaction progress. In contrast, the N-terminal fragment was still detectable in the crude mixture despite its improved solubility in NMP compared to DMF, which might be due to aggregate formation with the peptidyl resin under these conditions. Parameters and results for all synthetic trials are summarised in

Table 1.

As the fragment condensation was not superior over the sequential SPPS of the 30mer, the latter approach was reconsidered. As there are three additional internal serine residues in the sequence, the introduction of serines 304, 307 and 313 using the pseudoproline dipeptides Fmoc-Asn^{Trt}-Ser($\psi^{Me,Me}$pro)-OH (Ser 304) and Fmoc-Tyr^{tBu}-Ser($\psi^{Me,Me}$pro)-OH (Ser 307 and 313) was envisaged. This resulted in a gravimetrically determined yield of 90±7% (n=5) for the resin-bound peptide, compared to 60% for conventional serine introduction. The composition of the crude product was reproducible and significantly more favourable than for the sequential synthesis without pseudoproline dipeptides (Fig. 2B). The use of pseudoproline dipeptides as building blocks for introducing β-hydroxyamino acids was found to be beneficial for the synthesis of several other long peptides (White et al. 2004; Harris et al. 2012; Šebestik et al. 2012; Vernieri et al. 2014; Winkler and Tian 2015) and has been mainly attributed to the disruption of β-structures because of the unique conformational properties imparted by the five-membered oxazolidine ring and masking of the amide proton, which in consequence prevents peptide aggregation and self-association (Tuchscherer and Mutter 2003; Mutter 2013). To investigate the influence of the resin anchor group, the synthesis was also performed at the 2-ClTrtCl resin, which resulted in a considerably lower gravimetric yield of resin-bound peptide of 43%. This result can be explained by partial loss of the resin-bound peptide during MW irradiation. This finding is in agreement with another study, which has revealed that peptide chlorotrityl esters are not stable during MW-assisted SPPS. This has been attributed to displacement of the peptidyl moiety by other nucleophiles that are present in the coupling mixture via a S_N1-type mechanism (Echalier et al. 2013).

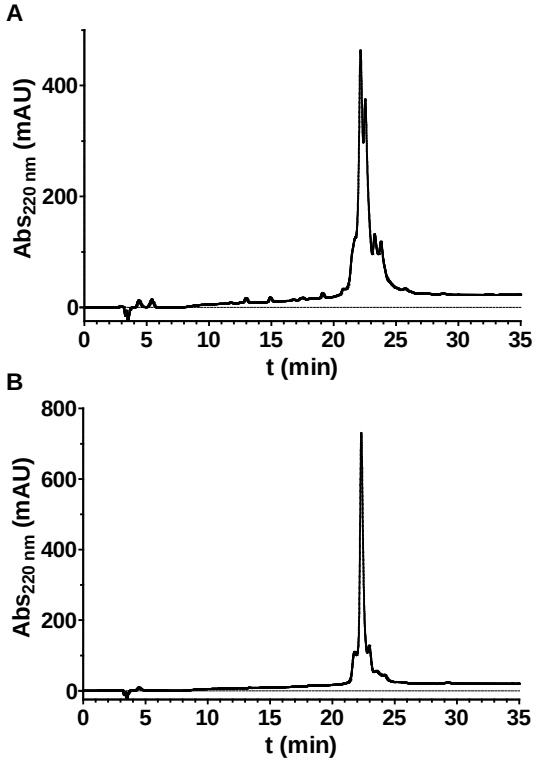

Fig. 2: HPLC chromatograms of crude products of cCPE$_{290-319}$ (**1**) obtained by sequential SPPS at Wang linker-functionalised resin. A) without pseudoproline dipeptides, B) synthesis using three pseudoproline dipeptide building blocks for introducing Ser 304, 307 and 313. Chromatograms for all synthetic strategies are shown in Fig. S1 in ESM.

The successfully established sequential SPPS of $cCPE_{290-319}$ enabled the synthesis of analogues, which are summarised in Fig. 3. Structural variations involved modifications at the N-terminus such as 4-fluorobenzoylation and conjugation of FITC via a 6-aminohexanoic spacer (Jullian et al. 2009), which will serve as reference compounds for the ^{18}F-labelled peptides or probes for fluorescence-based experiments, respectively. The 4-fluorobenzoyl group was introduced either by direct attachment to the amino group of the N-terminal Ser residue or via the 6-aminohexanoic spacer. For the directly 4-fluorobenzoylated $cCPE_{290-319}$, analogues in which amino acid residues that were suggested to be critical for the interaction with Cld-4 were exchanged by other amino acids, such as alanine or related non-proteinogenic amino acids.

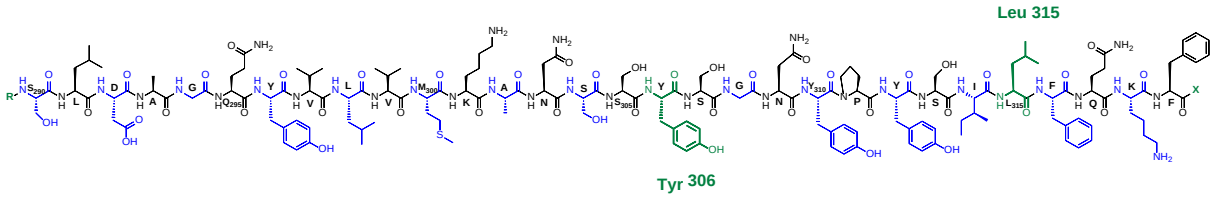

cpd	name	R	Tyr306	Leu315	X
1	$cCPE_{290-319}$	H	+	+	OH
2	$cCPE_{305-319}$	H	+	+	OH
3	Fmoc-$cCPE_{290-304}$	Fmoc	+	+	OH
4a	FBz-$cCPE_{290-319}$	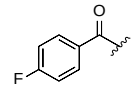 FBz	+	+	OH
4b	FBz-$cCPE_{290-319}$-Y306A		Y306A	+	
4c	FBz-$cCPE_{290-319}$-Y306F		Y306F	+	
4d	FBz-$cCPE_{290-319}$-Y306W		Y306W	+	
4e	FBz-$cCPE_{290-319}$-Y306pFF		Y306pFF	+	
4f	FBz-$cCPE_{290-319}$-L315A		+	L315A	
4g	FBz-$cCPE_{290-319}$-Y306A-L315A		Y306A	L315A	
5a	FBz-Ahx-$cCPE_{290-319}$	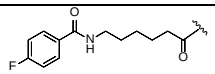 FBz-Ahx	+	+	OH
5b	FBz-Ahx-$cCPE_{290-319}$-amide		+	+	NH_2
6	FITC-Ahx-$cCPE_{290-319}$	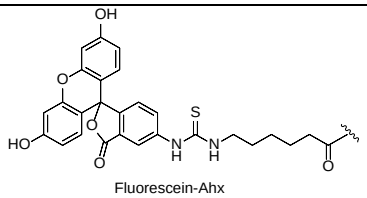 Fluorescein-Ahx	+	+	OH

Fig. 3: Structural variations for peptides derived from $cCPE_{290-319}$ (pFF: 4-fluorophenylalanine).

Table 1: Summary of parameters and results for synthesis of $cCPE_{290-319}$ and its 15mer fragments

peptide	linker	loading degree (mmol/g)	preloading	HOBt	PPD	yield (%)
$cCPE_{305-319}$ (**2**)	Wang	0.37	F	+	-	87 ± 15 (*n*=2)[c]
$cCPE_{290-304}$ (**3**)	2-ClTrtCl	0.51	S^{tBu}	+	-	20[a]
$cCPE_{290-304}$ (**3**)	2-ClTrtCl	0.51	S^{tBu}	-	-	39[a]
$cCPE_{290-304}$ (**3**)	2-ClTrtCl	0.41	S^{tBu}-N^{Trt}-A	+	-	54 ± 10 (*n*=3)[a,c]
$cCPE_{290-304}$ (**3**)	2-ClTrtCl	0.31	$S^{\psi Me,MePro}$-N^{Trt}-A	+	+	6[a]
$cCPE_{290-304}$ (**3**)	2-ClTrtCl	0.41	S^{tBu}-N^{Trt}-A	+	-	59[a,b]
$cCPE_{290-319}$ (**1**)	Wang	0.37	F	+	+	90 ± 7 (*n*=5)[c]
$cCPE_{290-319}$ (**1**)	Wang	0.37	F	+	-	60
$cCPE_{290-319}$ (**1**)	2-ClTrtCl	0.28	F	+	+	43
$cCPE_{290-319}$ (**1**)	2-ClTrtCl	0.22	F-K^{Boc}-Q^{Trt}	+	+	35

[a]yields refer to the isolated peptides, all other yields were gravimetrically determined for the resin-bound peptides

[b]modified microwave conditions according to (Friligou et al. 2011)

[c]mean ± standard deviation

Radiolabelling via ^{18}F-fluorobenzoylation

Initially, labelling of $cCPE_{290-319}$ with fluorine-18 was attempted by reacting resin-bound, fully side-chain protected **1** with [^{18}F]SFB (Scheme 1A) in orientation to the previously published procedure (Kuchar et al. 2012). This method has been demonstrated to be highly suitable for the site-selective labelling of lysine-including peptides and was therefore selected for radiolabelling of this 30mer peptide, which contains a lysine residue at the second-last C-terminal position (Fig. 2). Progress of the reaction was evaluated by determining the decay-corrected resin-associated radioactivity after filtration and washing in relation to initial activity of [^{18}F]SFB as well as the radiochemical yields for the crude and purified product. In contrast to the conditions reported in (Kuchar et al. 2012) that were optimised for peptides of less than 15 amino acids in length attached to Rink-amide resin, two major modifications proved to be crucial for the successful preparation of 30mer [^{18}F]**4a**. First, prior to acidolytic cleavage of the ^{18}F-labelled peptide, the resin had to be carefully washed with dichloromethane. This step was necessary to remove DMF present from the labelling mixture, which acts as competing proton acceptor, because the Wang linker is considerably less acid-sensitive than the Rink anchor group. Second, the crude ^{18}F-labelled peptide had to be precipitated with ice-cold ether and redissolved in CH_3CN/H_2O/TFA=8:6:1 prior to purification by semi-preparative HPLC as immediate subjection of the [^{18}F]**4a**-containing cleavage cocktail to HPLC impeded the separation process. Despite these methodological adjustments, the radiochemical yields for the isolated radiolabelled peptide did not exceed 1%, which was attributed to the insufficient reaction between [^{18}F]SFB and the N-terminus of protected, resin-bound **1** as obvious from the low retention of the [^{18}F]SFB activity on the solid support.

Therefore, [^{18}F]SFB was substituted by the more reactive 4-[^{18}F]fluorobenzoyl chloride. This reagent was prepared by modifying the automated synthesis of [^{18}F]SFB in the way that intermediate [^{18}F]fluorobenzoic acid was reacted with α,α-dichloromethyl methyl ether in orientation to procedures

reported in the literature (Lang et al. 1999; Kiesewetter and Eckelman 2001; Seimbille et al. 2005). In contrast to labelling with [^{18}F]SFB, the addition of buffered aqueous solution was avoided. Even though the retention of ^{18}F activity was approximately as twice as high compared to [^{18}F]SFB, only 4.5 MBq of purified [^{18}F]**4a** were obtained when using 1.9 GBq of 4-[^{18}F]fluorobenzoyl chloride. As higher activities of this reagent would have been difficult to handle due to its volatility, further attempts to obtain [^{18}F]**4a** in higher amounts by this approach were not undertaken.

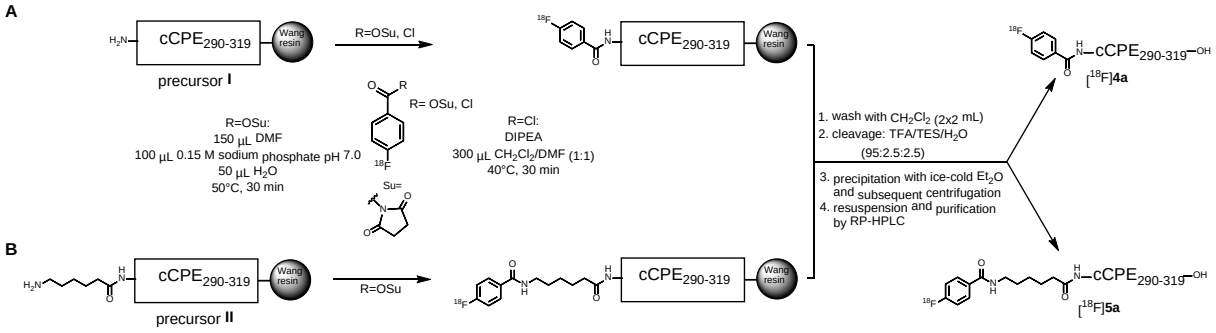

Scheme 1: Radiolabelling of cCPE$_{290\text{-}319}$ by ^{18}F-fluorobenzoylation directly at the N-terminus (**A**) and via a 6-aminohexanoic spacer (**B**). The frame around the 30mer sequence refers to the resin-bound, fully side-chain protected peptide including Ser residues 304, 307 and 313 as acetone-derived pseudoprolines.

As the reaction of both ^{18}F-fluorobenzoylating agents with protected, resin-bound **1** resulted in insufficient radiochemical yields, an N-terminal 6-aminohexanoic spacer was introduced, which should improve the nucleophilicity of the resin-bound amino group for both steric as well as electronic reasons. [^{18}F]SFB was reacted with the corresponding resin-bound precursor under non-aqueous conditions in the presence of DIPEA as base in equimolar amounts to the peptidic precursor, which resulted in considerably increased activity retention on solid phase compared to the radiolabelling in the absence of the spacer. When 2500 MBq of [^{18}F]SFB were used, about 700-1000 MBq of the precipitated crude product were obtained. Purification by semi-preparative HPLC (Fig. 3) was accompanied by significant activity loss. The radiochemical yield of the isolated product was further diminished when the pooled fractions were concentrated under reduced pressure. Therefore, [^{18}F]**5a** was alternatively isolated by solid-phase extraction of the HPLC fractions with a LiChrolut®RP-18 cartridge. Elution with ethanol as biocompatible solvent provided [^{18}F]**5a** in amounts ranging from 83-102 MBq, corresponding to decay-corrected radiochemical yields of 7-12%. Using non-radioactive **5a** as calibration standard, a molar activity of 1.45±0.3 GBq/µmol (n=10) was determined for [^{18}F]**5a**.

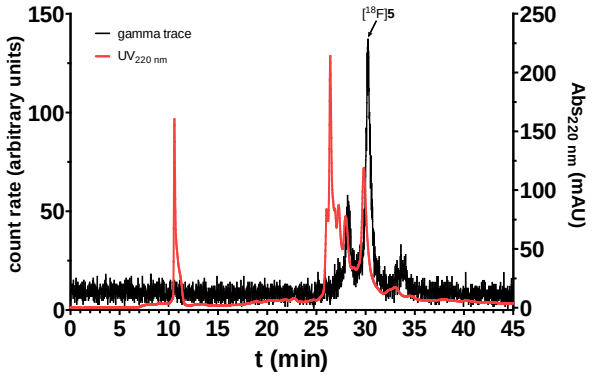

Fig. 4 (radio-)HPLC chromatogram for purification of [^{18}F]FBz-Ahx-cCPE$_{290\text{-}319}$ ([^{18}F]**5a**)

With the optimised approach for radiolabelling of $cCPE_{290-319}$ in hand, sufficient activities of [^{18}F]**5a** were available for radiopharmacological experiments *in cellulo* and *in vivo*, which will be discussed in the sections below. The radiotracer [^{18}F]**5a** was obtained in excellent radiochemical and chemical purities and sufficient molar activity in average synthesis times of ca. 130 min.

Interaction with $(His)_{10}$-Cld-4_{29-81}-LEVLFQGP-Cld-$4_{139-160}$ as Cld-4 mimicking construct

The kinetics and affinity of the interaction of $cCPE_{290-319}$ and its derivatives shown in Fig. 3 with Cld-4 was studied by surface plasmon resonance (SPR). For this purpose, a commercially available protein construct that is composed of both extracellular loops of Cld-4 which are connected by an artificial octapeptide linker (construct **III** in Fig. 5A) was immobilised on the sensor chip. Another SPR study investigating cCPE-Cld-4 interactions has used Cld-4 mimicking constructs that only contained the small extracellular loop of Cld-4 (constructs **I** and **II** in Fig. 5A) (Ling et al. 2008). A very recently published work has employed an immobilised complex of a detergent-stabilised phospholipid bilayer and C-terminally truncated Cld-4 containing all four transmembrane helices for that purpose (Shinoda et al. 2016b).

A representative sensorgram recorded in multiple cycle mode is shown for peptide 4 in Fig. 5B. The obtained binding curves were analysed according to a two-step model as implemented in the machine software. The derived rate constants and dissociation constants are shown in Table 2.

Very recently, a dissociation constant of 3.4 nM has been determined for immobilised full-length cCPE and the detergent-solubilised full-length Cld-4-phospholipid bilayer complex (Shinoda et al. 2016a). Compared to this value, the affinities determined for cCPE (**1**) are lower by approximately three orders of magnitude. This difference can be mainly attributed to the dramatically increased conformational flexibility of the binding partners in the present system compared to the full-length proteins. Even though the Cld-4 interaction site of cCPE is mainly localised in the 30mer region 290-319, the remaining parts of the protein molecule restrain its spatial orientation. Furthermore, both extracellular loops of Cld-4 are highly flexible in the artificial construct whereas in the full-length protein their attachment to the transmembrane helices results in conformational restriction that will partially preorganise the amino acid residues for interaction with cCPE. Experimental evidence for increased flexibility of the truncated binding partners was obtained from analysing the temperature dependence of the binding of **1** to the claudin-mimicking construct. The dissociation constants were determined in the range of 15 to 30 °C and analysed according to the van't Hoff equation, which has revealed a value of -51 kJ/mol for ΔH and 22 kJ/mol for $-T\Delta S$ (Fig. 5D). This indicates that the interaction of 30mer **1** with the Cld-4-derived construct is associated with an entropic penalty because complex formation requires the conformational restriction of both highly flexible binding partners. Opposing enthalpic and entropic contributions are commonly observed during the interaction of linear peptides with protein binding partners (London et al. 2010). The negative binding entropy suggests that the affinity of 1 and the derived 30mer peptides would be stronger towards membrane-embedded full-length Cld-4 compared to construct **III** because of the conformational restriction of the small extracellular loop imparted by the adjacent transmembrane helices in the native protein.

Obviously, removing the N-terminal positive charge **1** by acylation increases the binding affinity, as FBz-$cCPE_{290-319}$ (**4a**) and FBz-Ahx-$cCPE_{290-319}$ (**5a**) show lower K_D values. The improved affinity seems to be mainly due to increased values for the second-order rate constants k_{a1}, which suggests reduced electrostatic repulsion for the N-terminally acylated derivatives during complex formation. This

repulsive force might arise from a local positive charge at the small extracellular loop that is imparted by the residues Lys 157 and Arg 158 of Cld-4 (Piontek et al. 2017a). Apart from removing the positive charge from the N-terminus, N-terminal acylation changes the overall charge state of the 30mer peptide from +1 to 0 at pH 7.4.

As Leu 315 and Tyr 306 were identified as most crucial residues of cCPE with regards to the interaction with Cld-4, we decided to exchange these amino acids against alanine for validation of Cld-4 targeting of **4a** (Harada et al. 2007; Takahashi et al. 2008; Kimura et al. 2010). Furthermore, analogues of diminished affinity to Cld-4 could potentially serve as negative control agents in imaging experiments. The K_D values determined for **4a** and **4f** indicate that exchange of either Tyr 306 or Leu 315 against alanine results in only slight affinity reduction. Notably, exchange of both residues against alanine (**4g**) leads to a drop in the K_D value by approximately one order of magnitude. Based on molecular modelling studies, Tyr 306, Tyr 310, and 312 were proposed to constitute a hydrophobic pit that can adopt Leu 151 of Cld-4, whereas Leu 315 can form contacts with Ala 153 (Protze et al. 2015). This model was recently confirmed by the co-crystal structure of the Cld-4-cCPE complex (Shinoda et al. 2016b). Substitution of each single residue of this triple-tyrosine motif to alanine in full-length cCPE was shown to attenuate binding to Cld-4 (Harada et al. 2007). In line with these results, replacement of Tyr 306 in the fluorobenzoylated 30mer by Ala resulted in slightly diminished binding affinity, even though the loss of affinity is smaller than that observed for the full-length protein. To investigate the influence of hydroxyl group at Tyr 306, this residue was substituted by other aromatic amino acids such as phenylalanine (**4c**), tryptophan (**4d**), and 4-fluorophenylalanine (**4e**), which resulted in only slightly reduced binding affinities. This result is in agreement with the co-crystal structure, which has revealed that the hydroxy groups of all three clustered tyrosines do not directly participate in polar interactions (Shinoda et al. 2016b). Compared to the replacement of Tyr 306, mutation of Leu 315 by Ala was more effective in attenuating the binding affinity. The similar K_D ratios of **4g**/**4f** and **4b**/**4a** indicate a similar change in the free binding enthalpies upon exchange of Tyr 306 to Ala in both 30mer peptides **4f** and **4a**.

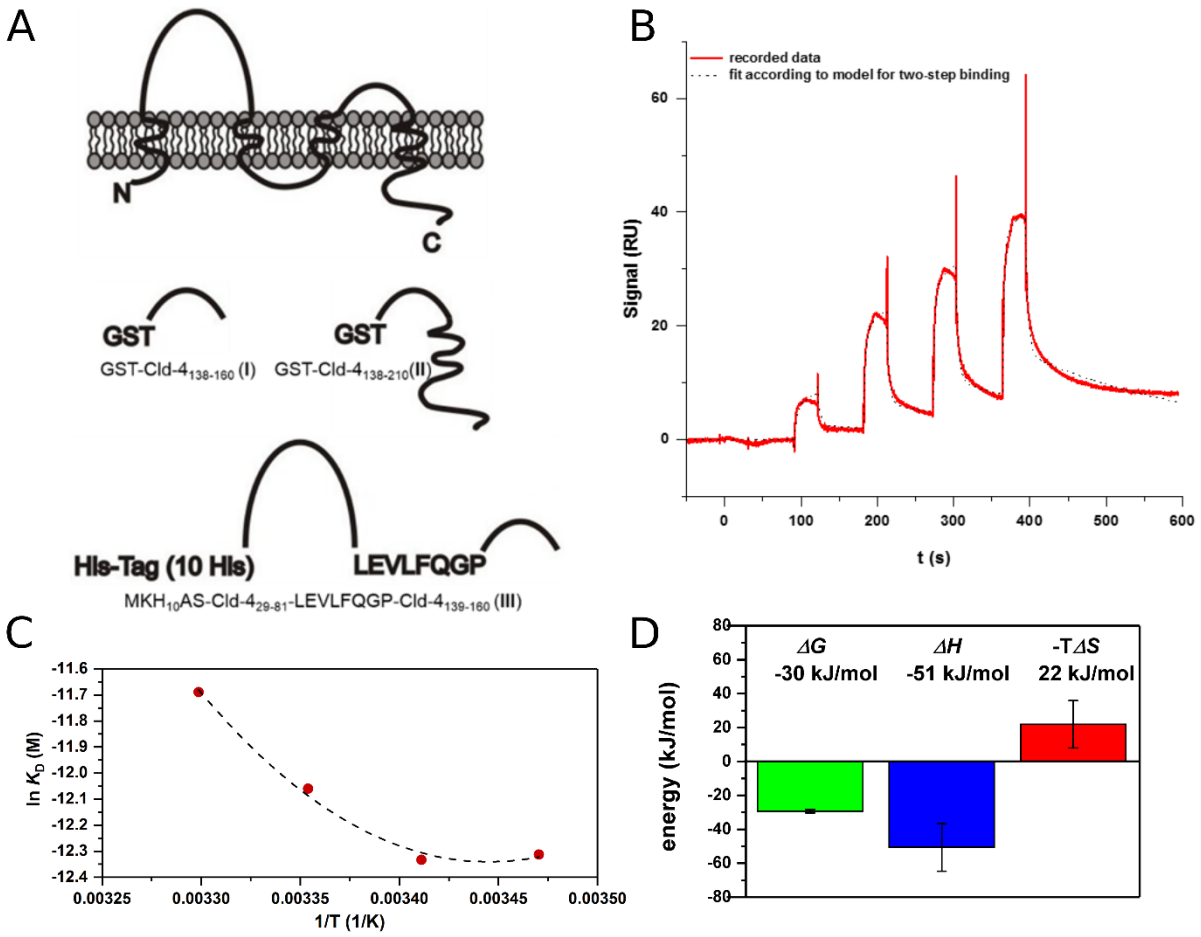

Fig. 5: Investigation of the interaction between cCPE$_{290-319}$ and derivatives and Cld-4 by SPR. **A**) Schematic representation of Cld-4 and derived artificial soluble constructs described in the literature (**I** and **II**, (Ling et al. 2008)) and used in this work (**III**). **B**) Representative sensorgram of FBz-Ahx-cCPE$_{290-319}$ (**5a**). Shown are the sequential measurements (single-cycle mode) for immobilised construct **III** and solutions of **5a** in the concentrations of 2 µM, 4 µM, 6 µM and 10 µM. Sensorgrams for all compounds are included in ESM. **C** and **D**) Thermodynamic analysis for the interaction of compound **1** with immobilised construct **III**. Van't Hoff plot (**C**) and thermodynamic parameters derived thereof (**D**).

Table 2: Dissociation and global rate constants for interaction of cCPE$_{290-319}$ (**1**) and its derivatives with the artificial Cld-4 mimicking protein construct III (seeFig. 5A). Individual rate constants are shown in Table S5 in ESM.

compd	K_D (µM)	k_{on} ($M^{-1}s^{-1}$)	k_{off} (s^{-1})	n
1	10.3	586.4	6.04×10^{-3}	7
4a	1.27	3456.7	4.39×10^{-3}	6
5a	4.44	1391.9	6.18×10^{-3}	8
5b	1.68	7142.9	1.20×10^{-2}	9
4b	1.53	452.3	6.92×10^{-4}	8
4c	2.35	2034.0	4.78×10^{-3}	7
4d	2.49	1718.9	4.28×10^{-3}	7
4e	2.18	2298.2	5.01×10^{-3}	8
4f	6.69	304.9	2.04×10^{-3}	6
4g	9.78	293.5	2.87×10^{-3}	7

In vitro stability and ECD spectra

Considering the peptidic structure of [^{18}F]**5a**, the radiotracer is potentially vulnerable towards degradation by proteolytic enzymes that are present in biological media or associated to cell surfaces. Therefore, the stability of [^{18}F]**5a** in the presence of HT-29 cells and in blood plasma of Wistar rats was investigated by radio-HPLC. Furthermore, the stability of the FITC-conjugated analogue 6 in human serum was investigated by UPLC-DAD-MS. The results are shown in Fig. 6. [^{18}F]**5a** proved to be stable in the presence of HT-29 cells as well as in blood plasma over 60 min. HT-29 is one of the Cld-4 positive cell lines that were selected for radiotracer binding studies reported below. In agreement with these findings, peptide **6** revealed to be virtually stable over 4 h in human serum. After 6 h a degradation product was detectable, with 84.9% of original peptide remaining (Fig. 6C and D). UPLC-MS data indicate that metabolite formation occurs by proteolytic cleavage after Asn 303 (see ESM).

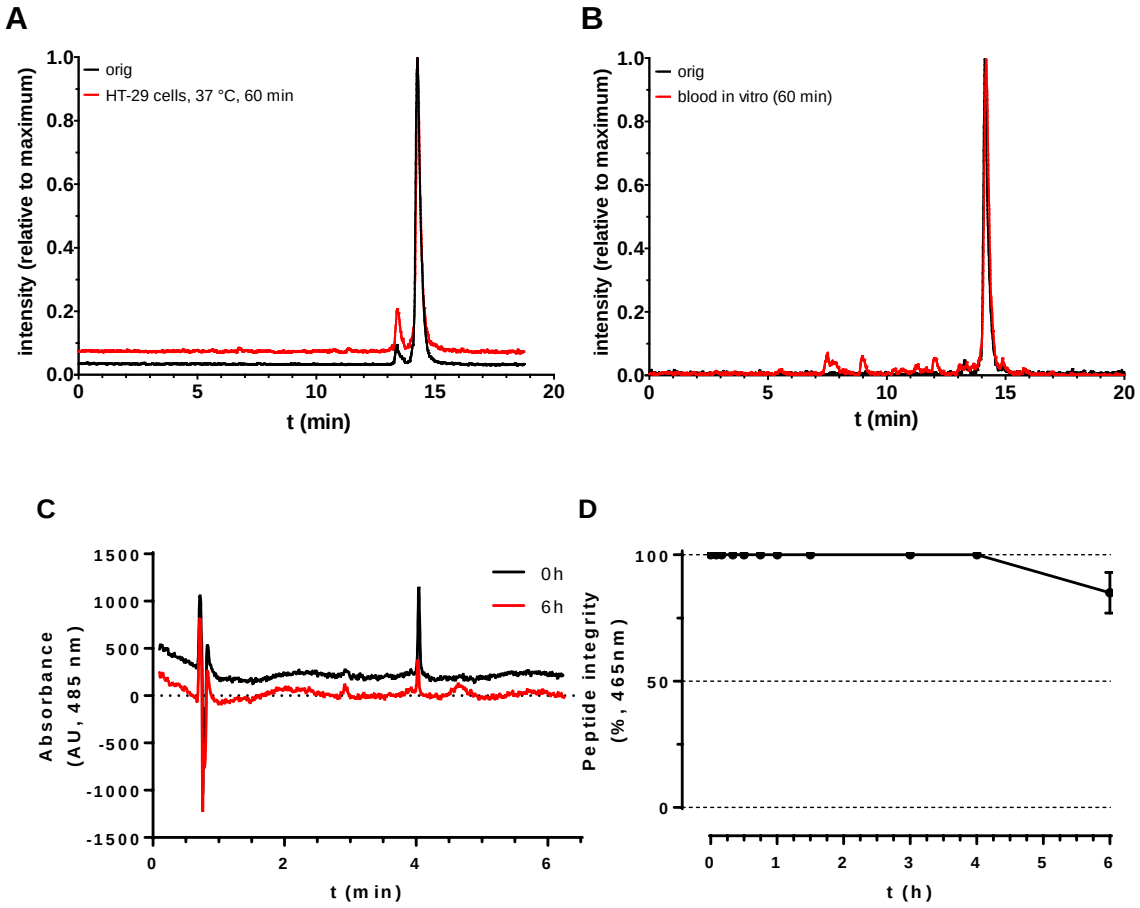

Fig. 6: radio-HPLC and UPLC investigation the stability of [^{18}F]**5a** and **6**, respectively, in biological media *in vitro*. **A**) radio-HPLC chromatograms for [^{18}F]**5a** in HT-29 cell suspension, **B**) radio-HPLC chromatograms for [^{18}F]**5a** in rat blood, **C**) UPLC chromatograms for **6** in human blood plasma, each at 37 °C **D**) time course of integrity of **6** in human blood plasma

The obtained results proved the radiotracer [^{18}F]**5a** to be sufficiently stable for radiopharmacological investigations *in cellulo* and *in vivo*.

Considering the presence of proteases of diverse substrate specificity in blood plasma, the stability of the 30mer peptides [^{18}F]**5a** and **6** in this body fluid is remarkable (Seitz et al. 2006). This might indicate

a stabilised secondary structure of the cCPE-derived 30mer peptide (Tyndall et al. 2005). To support this assumption, ECD spectra of the fluorobenzoylated 30mer **4a** were recorded in a mixture of water and acetonitrile in the absence and presence of TFE (Fig. 7). Interestingly, the shape of the ECD spectrum in the absence of TFE resembles that of a β-sheet structure, as it is characterised by a negative Cotton effect (single minimum) at 219 nm. Therefore, it can be concluded that **4a** might adopt a β-hairpin conformation (Maynard et al. 1998; Woody 2002), which would explain its proteolytic stability (Madala et al. 2010). In the presence of 50% TFE the appearance of the ECD spectrum is changing as two negative Cotton effects at 220 and 208 nm of reduced absolute molar elipticity can be observed, which is indicative of an α-helical conformation. Considering the linear structure of **4a**, conformational changes induced by high concentration of TFE are not surprising. The induction of the β-sheet-α-helix transition upon addition of TFE has been observed for other peptides (Reiersen and Rees 2000) and even for conformationally highly constrained polypeptides of high β-sheet content (Jayaraman et al. 1996). Notably, the shape of the ECD spectra and the molar elipticities are largely independent of the concentration both in the absence and the presence of TFE. This finding indicates that the conformational behaviour of the fluorobenzoylated 30mer **4a** is not influenced by aggregation under the chosen conditions.

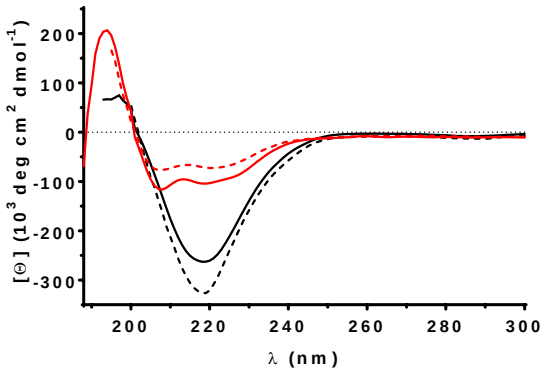

Fig. 7: Electronic circular dichroism (ECD) spectra of FBz-cCPE$_{290-319}$ (**4a**) dissolved in CH_3CN/H_2O 1:1 (v/v) at different concentrations (solid lines: 0.125 mg/mL, dashed lines: 0.5 mg/mL in the absence (black lines) and presence (red lines) of TFE (50% v/v).

Cell binding of [^{18}F]FBz-Ahx-cCPE$_{290-319}$-OH ([^{18}F]5a) and FITC-conjugated analogue 6

To prove targeting of the radiolabelled cCPE$_{290-319}$ [^{18}F]**5a** of Cld-4, radiotracer cell binding experiments have been performed with target-expressing cell lines. Expression of Cld-4 in the epithelial carcinoma cell lines A431 and HT-29 was confirmed by Western blot analysis and microscopic immune fluorescence staining of the viable cells (Fig. 8A+D).

Cell binding studies were performed by incubating [^{18}F]**5a** in an activity concentration range that corresponded to a molar concentration of 0.55 µM for the no-carrier added radiotracer. For both Cld-4 positive cell lines binding of [^{18}F]**5a** steadily increased over the considered time range, while the amount of cell-bound radiotracer after 60 min was higher for the A431 cells (Fig. 8B). Preincubation for 10 min with non-radioactive **5a** at a concentration of 10 µM resulted only in insignificant attenuation of radiotracer binding.

To obtain information towards Cld-4 targeting of $cCPE_{290-319}$ independent of radiotracer binding experiments, microscopic imaging with fluorescently labelled **6** was performed, which differs from **5a** only in the replacement of the fluorobenzoyl group by the FITC-derived moiety. The microscopic images show that cell-associated fluorescence was observable for both cell lines and was stronger after 4 h compared to 1 h of incubation. Cell-associated fluorescence was significantly lower when fluorescein was used instead of **6** (Fig. 8C+D)). Quantification of the fluorescence signal by flow cytometry has revealed that binding of **6** is more intense towards the A431 cells compared to the HT-29 cells, which is in accordance with the results obtained in the radiotracer binding studies with [^{18}F]**5a**.

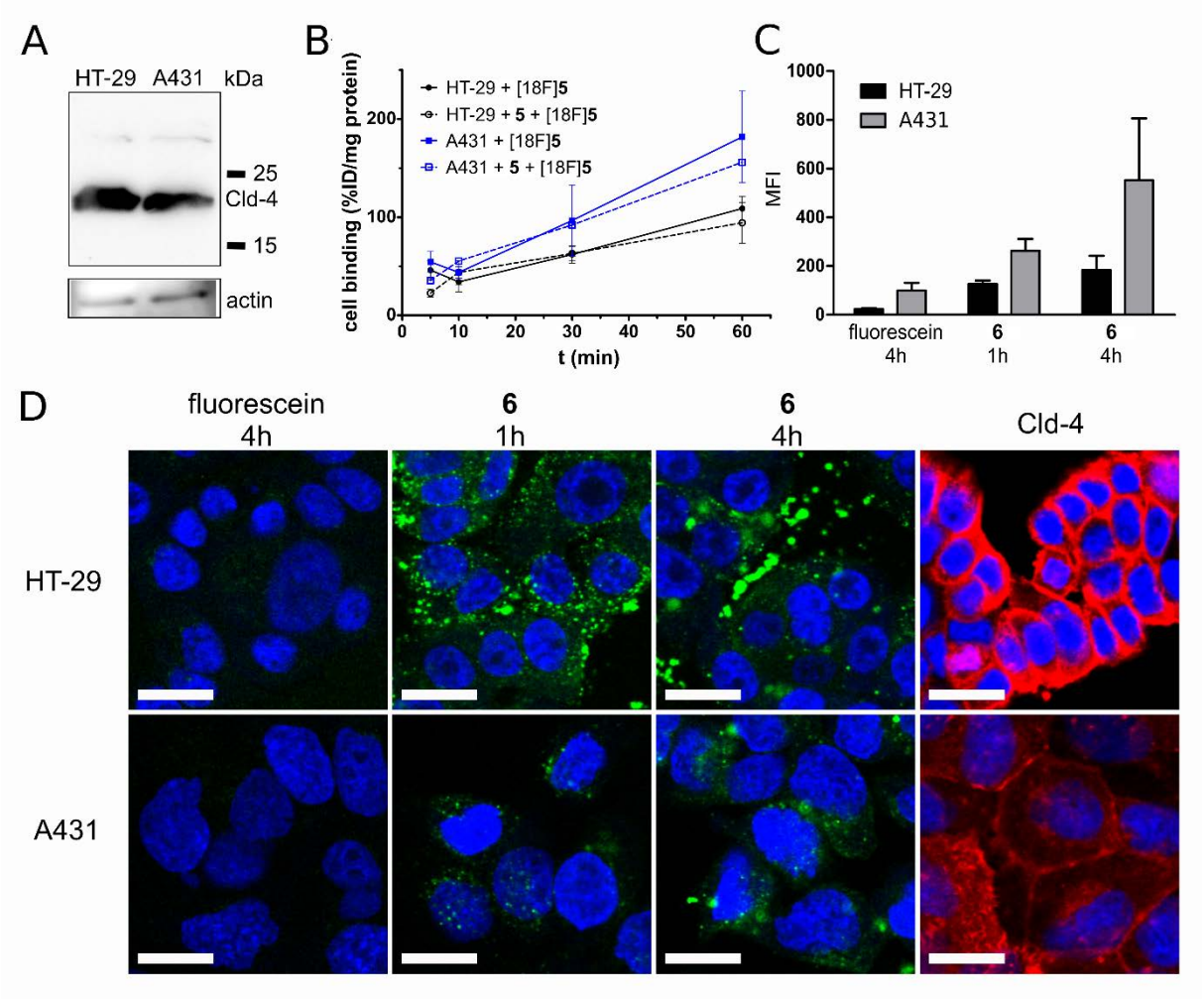

Fig. 8: Cell binding of [^{18}F]**5a** and its FITC-conjugated analogue **6**. **A**) Western blot detection of Cld-4 and actin (HT-29, A431). **B**) Comparison of cell binding of [^{18}F]FBz-Ahx-$cCPE_{290-319}$ ([^{18}F]**5a**) for different tumour cell lines. **C**) Quantification of cell-associated median fluorescence intensity (MFI) of **6** by flow cytometry. MFI expressed as means of three experiments with standard deviation (SD). Histograms are shown in ESM. **D**) Fluorescence microscopic images of FITC-Ahx-$cCPE_{290-319}$ (**6**) and Cld 4-specific monoclonal antibody (rightmost images) to different tumour cell lines; the scale bares represent 20 µm in reality.

PET studies and in vivo stability

The favourable *in vitro* stability of [^{18}F]**5a** encouraged its first orienting *in vivo* evaluation by dynamic PET imaging. Dynamic PET experiments were performed with healthy NMRI nude mice and rats. As shown in Fig. 9A, after 5 min p.i. the majority of the ^{18}F activity in the mouse is located in the liver, while the kidneys are also visible and some activity is concentrated in the urinary bladder. At 30 min

p.i., the ^{18}F activity has mainly accumulated in the gall bladder, the intestines and the urinary bladder. The time-activity curves for the mouse (Fig. 9C) indicate that the gall bladder activity significantly increased at later time points, as reflected by the PET image for 60 min p.i. (Fig. 9A).

When Fig. 9A and B are compared, it becomes obvious that the PET images of [^{18}F]**5a** in healthy Wistar rats largely resemble those obtained in mice, as extensive liver uptake can be discerned at 5 min p.i. Differently to mice, spleen uptake can be observed in rats at 5 min p.i., the kidney uptake is less obvious for the early phase and no gall bladder uptake can be observed because of the lack of that organ in this species. After 60 min p.i. the kidneys appear with more contrast and accumulation of activity is visible in intestine, while [^{18}F]**5a** and potential metabolites derived thereof have been largely cleared from the liver. Of note, the rat urine bladder is out of the field of view in the PET images.

The PET images in Fig. 9 indicate that the elimination of [^{18}F]**5a** occurs via both the hepatobiliary and renal pathways and that the clearance from the blood is very rapid in both rodent species. This statement is supported by the time-activity curve for the large abdominal blood vessels (vena cava, aorta) as region of interest (Fig. 9C+D). The blood activity decreases to approximately 20% of maximum within the first 2 min after injection. At later time points the blood activity slightly increases in both species to reach a local maximum at 25 min p.i. in the mouse, which is probably due to re-extraction of hydrophilic metabolites into the blood. In accordance with the noted rapid blood clearance, the time-activity curve for liver shows that maximum activity is reached within 2 min. The temporal complementarity between the blood and liver time-activity curves suggests that the majority of [^{18}F]**5a** is directly extracted from the blood into the liver.

Such a pronounced liver uptake of a peptidic radiotracer is rather unusual, as elimination of peptides occurs predominantly by renal filtration even though the suppression of hepatic uptake is considered as a common challenge in the development of radiolabelled peptides for molecular imaging (Hosseinimehr et al. 2012). However, the branched peptide insulin, which is composed of 51 amino acids and with regards to its molar mass still comparable to **5a** (3.6 *vs* 5.7 kDa), also undergoes rapid hepatic uptake (Kim et al. 2014), which was proven to be mediated by the insulin receptor (Sodoyez et al. 1983; Sodoyez et al. 1985). Moreover, experiments with rat hepatocytes *in vitro* have been shown that insulin undergoes proteolytic degradation within endosomal compartments after the internalisation of the peptide-receptor complex (Juul et al. 1986). Reflecting the situation for the insulin receptor, claudin-4 has been shown to undergo clathrin-mediated endocytosis (Ivanov et al. 2004). Therefore, involvement of a receptor-mediated uptake could be assumed. It has been found that Cld-1, -2, -3, -5, -7, -8, -12, and -14 are expressed in normal human liver tissue while Cld-4 is absent in hepatocytes (Tsujiwaki et al. 2015). Besides Cld-4, full-length cCPE can bind to Cld-3 with similar affinity and lower affinity to Cld-6, -7, -8, and -14 (Fujita et al. 2000). Whether the observed liver uptake is claudin-mediated or involves other receptors such as scavenger receptors (expressed on liver- and spleen-residing macrophages) remains to be clarified within further studies.

Due to the extremely rapid elimination from the bloodstream, particularly in NMRI nude mice, the animal experiments were not extended to tumour-bearing xenograft mice.

Wistar rats were also employed to evaluate the metabolic stability of [^{18}F]**5a** *ex vivo*. As shown in Fig. 10, the compound undergoes rapid degradation *in vivo*. As this finding is in contrast to the stability observed for [^{18}F]**5a** in rat blood *in vitro*, the degradation is interpreted by liver uptake-induced metabolisation. PET images in mice indicate renal filtration as substantial route for excretion and radio-

HPLC analysis of rat urine 60 min p.i. suggests the elimination of one hydrophilic radiolabelled main metabolite (Fig. 10C). Noteworthy, no original radiotracer is detectable in the urine. Therefore, proteolytic degradation seems to be mainly taking place in the liver and is probably followed by re-transfer of hydrophilic metabolites into the blood that undergo there further processing to a final radiometabolite that is excreted into the urine. This assumption is supported by the PET-derived time-activity curves discussed above. Excretion of hydrophilic catabolites from hepatocytes into the blood or bile canaliculi is a fundamental process in drug metabolism and is mainly achieved by secondary and primary active transport mediated by carriers located in the basolateral and apical membranes, respectively (Hosseinimehr et al. 2012).

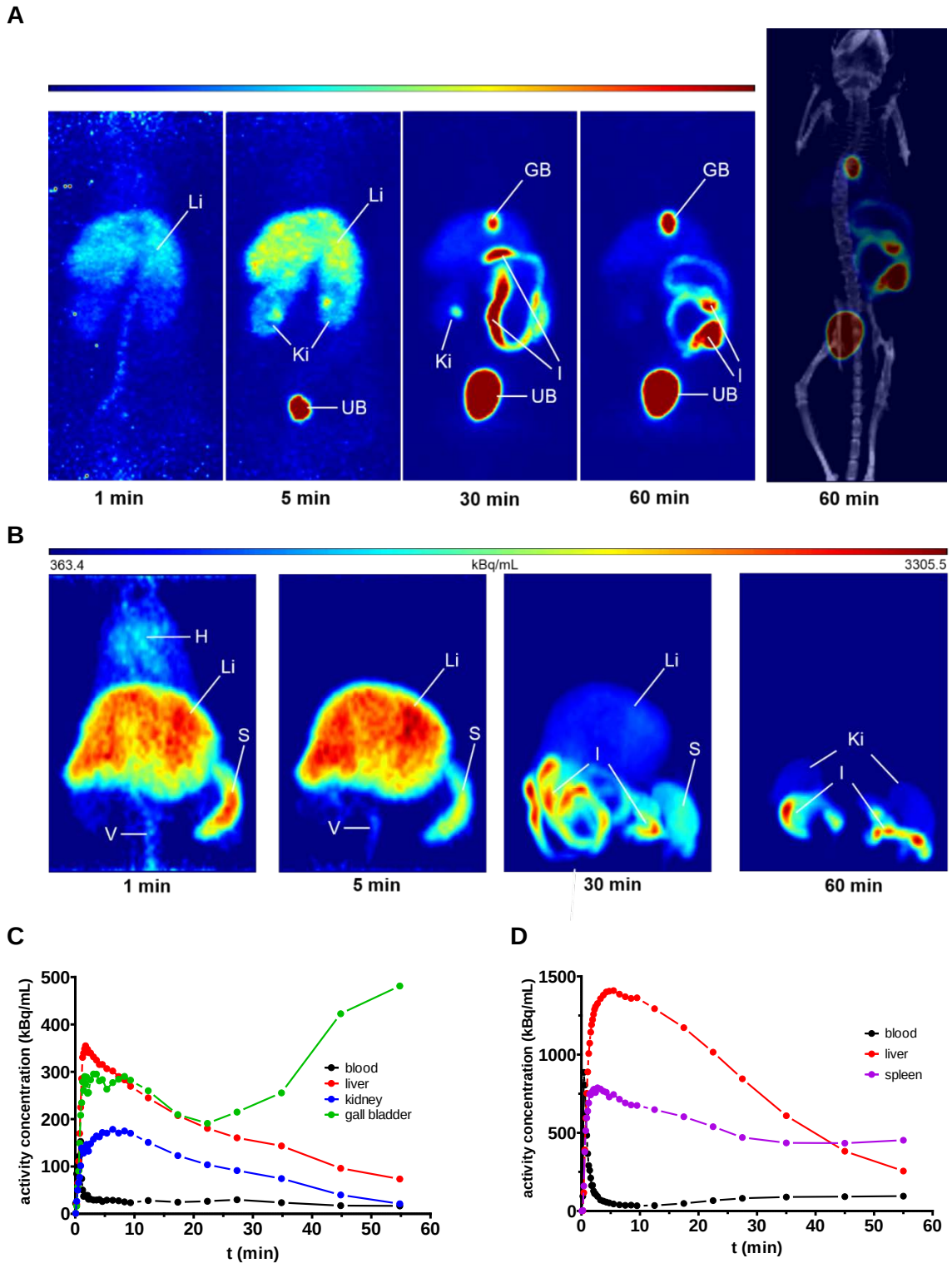

Fig. 9: PET investigation of [^{18}F]**5a** in mouse and rat. **A** and **B**) Representative coronal images of a mouse (**A**) and a rat (**B**) obtained from small animal PET study, showing ^{18}F-activity distribution *in vivo* as maximum intensity projection (0-60 min) after intravenous injection of [^{18}F]**5a**. GB, gall bladder; H, heart; Lu, lung; Li, liver; Ki, kidney; UB, urinary bladder; V, blood vessel (abdominal aorta and vena cava); S, spleen. Yellow-red colors show highest activity concentration (Bq/mL). For anatomical orientation, the PET-CT image at 60 min p.i. is shown in **A**. **C** and **D**) Corresponding time-activity-curves showing kinetics of the ^{18}F-activity concentration during the entire study period of 60 min after injection of [^{18}F]**5a** in mouse (**C**) and rat (**D**) as calculated from ROI analysis of dynamic small animal PET scans over the large abdominal vessel region (aorta, vena cava) representing the blood pool as well as liver and kidneys.

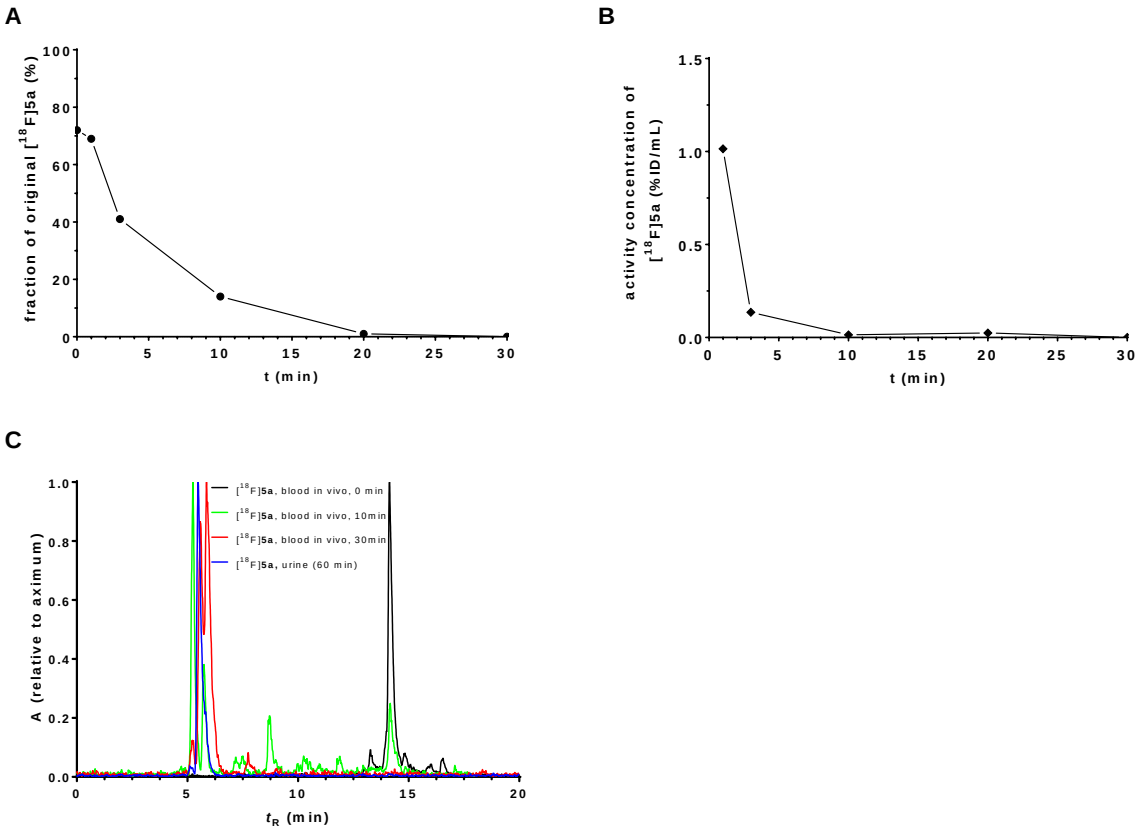

Fig. 10: Investigation of metabolic stability and arterial blood clearance of [^{18}F]**5a** in healthy male Wistar rats. **A**) Time course of metabolic transformation as derived from radio- HPLC analysis of withdrawn blood samples. **B**) Time course of arterial blood clearance as calculated from activity measurements of blood samples and fractions of original peptide. **C**) radio-HPLC chromatograms of blood and urine samples taken at different time points

Conclusions

The efficient preparation of $cCPE_{290-310}$ via step-wise SPPS by incorporating three pseudoproline dipeptides has been established within this study. Its labelling with fluorine-18 was achieved via ^{18}F-fluorobenzoylation on solid phase, which was dependent on the introduction of an N-terminal 6-aminohexanoyl linker for efficient reaction with [^{18}F]SFB. The elaborated method for ^{18}F-labelling on the Wang linker-functionalised polymeric support should be applicable for other peptides of longer sequence and accounted for the initial pharmacokinetic characterisation of $cCPE_{290-310}$ *in vitro* and *in vivo*. Binding experiments for [^{18}F]**5a** and its FITC-conjugated analogue **6** with Cld-4-expressing tumour cell lines indicate the potential of $cCPE_{290-310}$-derived peptides for tumour targeting. However, the high liver uptake of [^{18}F]**5a** and its rapid degradation *in vivo* limits its suitability for imaging of tumour-associated Cld-4.

Therefore, the binding affinity and pharmacokinetic properties of $cCPE_{290-319}$ should be improved for the future development of PET tracers derived from this peptide. This could be achieved by constraining the 30mer in a structure that resembles the one in the full-length protein. This in turn could be realised by designing bicyclic peptides (Rhodes and Pei 2017) based on the crystal structure of the full-length cCPE, for example.

Acknowledgements

We wish to thank Peggy Nehring and Uta Lenkeit for assisting in peptide and radiochemical synthesis and Stefan Preusche and the cyclotron team for providing [^{18}F]fluoride. We highly appreciate the support of Catharina Knöfel, Aline Morgenegg and Mareike Barth in the cell-based and immunohistochemical experiments. Furthermore, we are grateful to Andrea Suhr and Regina Herrlich for skilful assistance in the animal experiments. RL is grateful for partial financial support by the Fonds der Chemischen Industrie. The authors thank the Helmholtz Association for funding a part of this work through the Helmholtz Cross-Programme Initiative “Technology and Medicine – Adaptive Systems”.

Compliance with ethical standards

Conflict of interest

The authors have no conflict of interest to declare.

Ethical approval

The animal experiments were performed in accordance to the guidelines of the German Regulations of Animal Welfare. The protocol was approved by the local Ethical Committee for Animal Experiments (Reference Numbers 24D-9168.11-4/2007-2 and 24-9168.21-4/2004-1).

References

Boireau S, Buchert M, Samuel MS, Pannequin J, Ryan JL, Choquet A, Chapuis H, Rebillard X, Avances C, Ernst M, Joubert D, Mottet N, Hollande F (2007) DNA-methylation-dependent alterations of claudin-4 expression in human bladder carcinoma. Carcinogenesis 28:246-258. doi:10.1093/carcin/bgl120

Bollhagen R, Schmiedberger M, Barlos K, Grell E (1994) A New Reagent for the Cleavage of Fully Protected Peptides Synthesized on 2-Chlorotrityl Chloride Resin. J Chem Soc Chem Commun:2559-2560. doi:10.1039/c39940002559

Cocco E, Casagrande F, Bellone S, Richter CE, Bellone M, Todeschini P, Holmberg JC, Fu HH, Montagna MK, Mor G, Schwartz PE, Arin-Silasi D, Azoudi M, Rutherford TJ, Abu-Khalaf M, Pecorelli S, Santin AD (2010) Clostridium perfringens enterotoxin carboxy-terminal fragment is a novel tumor-homing peptide for human ovarian cancer. BMC cancer 10:349. doi:10.1186/1471-2407-10-349

de Mol NJ, Dekker FJ, Broutin I, Fischer MJE, Liskamp RMJ (2005) Surface Plasmon Resonance Thermodynamic and Kinetic Analysis as a Strategic Tool in Drug Design. Distinct Ways for Phosphopeptides to Plug into Src- and Grb2 SH2 Domains. J Med Chem 48:753-763. doi:10.1021/jm049359e

Ding L, Lu Z, Lu Q, Chen YH (2013) The claudin family of proteins in human malignancy: a clinical perspective. Cancer management and research 5:367-375. doi:10.2147/CMAR.S38294

Echalier C, Al-Halifa S, Kreiter A, Enjalbal C, Sanchez P, Ronga L, Puget K, Verdie P, Amblard M, Martinez J, Subra G (2013) Heating and microwave assisted SPPS of C-terminal acid peptides on trityl resin: the truth behind the yield. Amino Acids 45:1395-1403. doi:10.1007/s00726-013-1604-z

Fani M, Maecke HR (2012) Radiopharmaceutical development of radiolabelled peptides. Eur J Nucl Med Mol Imaging 39 Suppl 1:S11-30. doi:10.1007/s00259-011-2001-z

Feni L, Omrane MA, Fischer M, Zlatopolskiy BD, Neumaier B, Neundorf I (2017) Convenient Preparation of ^{18}F-Labeled Peptide Probes for Potential Claudin-4 PET Imaging. Pharmaceuticals 10:99. doi:10.3390/ph10040099

Friligou I, Papadimitriou E, Gatos D, Matsoukas J, Tselios T (2011) Microwave-assisted solid-phase peptide synthesis of the 60-110 domain of human pleiotrophin on 2-chlorotrityl resin. Amino Acids 40:1431-1440. doi:10.1007/s00726-010-0753-6

Fujita K, Katahira J, Horiguchi Y, Sonoda N, Furuse M, Tsukita S (2000) Clostridium perfringens enterotoxin binds to the second extracellular loop of claudin-3, a tight junction integral membrane protein. FEBS Lett 476:258-261. doi:10.1016/S0014-5793(00)01744-0

Goodman M, Stueben KC (1962) Peptide Synthesis via Amino Acid Active Esters. II. Some Abnormal Reactions during Peptide Synthesis. J Am Chem Soc 84:1279-1283. doi:10.1021/ja00866a044

Hanna PC, Mietzner TA, Schoolnik GK, McClane BA (1991) Localization of the Receptor-binding Region of Clostridium perfringens Enterotoxin Utilizing Cloned Toxin Fragments and Synthetic Peptides. The 30 C-terminal amino acids define a functional binding region. J Biol Chem 266:11037-11043

Hanna PC, Wnek AP, McClane B (1995) Molecular cloning of the 3' half of the Clostridium perfringens enterotoxin gene and demonstration that this region encodes receptor-binding activity. J Bacteriol 171:6815-6820

Harada M, Kondoh M, Ebihara C, Takahashi A, Komiya E, Fujii M, Mizuguchi H, Tsunoda S, Horiguchi Y, Yagi K, Watanabe Y (2007) Role of tyrosine residues in modulation of claudin-4 by the C-terminal fragment of Clostridium perfringens enterotoxin. Biochem Pharmacol 73:206-214. doi:10.1016/j.bcp.2006.10.002

Harris PWR, Kowalczyk R, Hay DL, Brimble MA (2012) A Single Pseudoproline and Microwave Solid Phase Peptide Synthesis Facilitates an Efficient Synthesis of Human Amylin 1–37. Int J Pept Res Ther 19:147-155. doi:10.1007/s10989-012-9325-9

Heinlein C, Varon Silva D, Troster A, Schmidt J, Gross A, Unverzagt C (2011) Fragment condensation of C-terminal pseudoproline peptides without racemization on the solid phase. Angew Chem Int Ed Engl 50:6406-6410. doi:10.1002/anie.201101270

Hess E, Takacs S, Scholten B, Tarkanyi F, Coenen HH, Qaim SM (2001) Excitation function of the $^{18}O(p,n)^{18}F$ nuclear reaction from threshold up to 30 MeV. Radiochim Acta 89:357–362. doi:10.1524/ract.2001.89.6.357

Hosseinimehr SJ, Tolmachev V, Orlova A (2012) Liver uptake of radiolabeled targeting proteins and peptides: considerations for targeting peptide conjugate design. Drug Discov Today 17:1224-1232. doi:10.1016/j.drudis.2012.07.002

Ivanov AI, Nusrat A, Parkos CA (2004) Endocytosis of epithelial apical junctional proteins by a clathrin-mediated pathway into a unique storage compartment. Mol Biol Cell 15:176-188. doi:10.1091/mbc.e03-05-0319

Jayaraman G, Kumar TKS, Arunkumar AI, Yu C (1996) 2,2,2-Trifluoroethanol Induces Helical Conformation in an All β-Sheet Protein. Biochem Biophys Res Commun 222:33-37

Jullian M, Hernandez A, Maurras A, Puget K, Amblard M, Martinez J, Subra G (2009) N-terminus FITC labeling of peptides on solid support: the truth behind the spacer. Tetrahedron Letters 50:260-263. doi:10.1016/j.tetlet.2008.10.141

Juul SM, Jones RH, Evans JL, Neffe J, Sönksen PH, Brandenburg D (1986) Evidence for an early degradative event to the insulin molecule following binding to hepatocyte receptors. Biochim Biophys Acta 856:310-319. doi:10.1016/0005-2736(86)90041-6

Kapty J, Kniess T, Wuest F, Mercer JR (2011) Radiolabeling of phosphatidylserine-binding peptides with prosthetic groups N-[6-(4-[^{18}F]fluorobenzylidene)aminooxyhexyl]maleimide ([^{18}F]FBAM) and N-succinimidyl-4-[^{18}F]fluorobenzoate ([^{18}F]SFB). Appl Radiat Isot 69:1218-1225. doi:10.1016/j.apradiso.2011.05.012

Kiesewetter DO, Eckelman WC (2001) Radiochemical Synthesis of [^{18}F]Fluoropaclitexel ([^{18}F]FPAC). J Label Compd Radiopharm 44:S903-S905

Kim DH, Blacker M, Valliant JF (2014) Preparation and evaluation of fluorine-18-labeled insulin as a molecular imaging probe for studying insulin receptor expression in tumors. J Med Chem 57:3678-3686. doi:10.1021/jm401020c

Kimura J, Abe H, Kamitani S, Toshima H, Fukui A, Miyake M, Kamata Y, Sugita-Konishi Y, Yamamoto S, Horiguchi Y (2010) Clostridium perfringens enterotoxin interacts with claudins via electrostatic attraction. J Biol Chem 285:401-408. doi:10.1074/jbc.M109.051417

Kominsky SL, Tyler B, Sosnowski J, Brady K, Doucet M, Nell D, Smedley JG, 3rd, McClane B, Brem H, Sukumar S (2007) Clostridium perfringens enterotoxin as a novel-targeted therapeutic for brain metastasis. Cancer research 67:7977-7982. doi:10.1158/0008-5472.CAN-07-1314

Kuchar M, Neuber C, Belter B, Bergmann R, Lenk J, Wodtke R, Kniess T, Steinbach J, Pietzsch J, Löser R (2018) Evaluation of fluorine-18-labelled α1(I)-N-telopeptide analogs as substrate-based radiotracers for PET imaging of melanoma-associated lysyl oxidase. Front Chem 6. doi:10.3389/fchem.2018.00121

Kuchar M, Pretze M, Kniess T, Steinbach J, Pietzsch J, Löser R (2012) Site-selective radiolabeling of peptides by ^{18}F-fluorobenzoylation with [^{18}F]SFB in solution and on solid phase: a comparative study. Amino Acids 43:1431-1443. doi:10.1007/s00726-012-1216-z

Kwon MJ (2013) Emerging roles of claudins in human cancer. Int J Mol Sci 14:18148-18180. doi:10.3390/ijms140918148

Lang L, Jagoda E, Schmall B, Vuong B-K, Adams HR, Nelson DL, Carson RE, Eckelman WC (1999) Development of Fluorine-18-Labeled 5-HT1A Antagonists. J Med Chem 42:1576-1586. doi:10.1021/jm980456f

Ling J, Liao H, Clark R, Wong MS, Lo DD (2008) Structural constraints for the binding of short peptides to claudin-4 revealed by surface plasmon resonance. J Biol Chem 283:30585-30595. doi:10.1074/jbc.M803548200

London N, Movshovitz-Attias D, Schueler-Furman O (2010) The structural basis of peptide-protein binding strategies. Structure 18:188-199. doi:10.1016/j.str.2009.11.012

Madala PK, Tyndall JD, Nall T, Fairlie DP (2010) Update 1 of: Proteases universally recognize beta strands in their active sites. Chem Rev 110:PR1-31. doi:10.1021/cr900368a

Mäding P, Füchtner F, Wüst F (2005) Module-assisted synthesis of the bifunctional labelling agent *N*-succinimidyl 4-[^{18}F]fluorobenzoate ([^{18}F]SFB). Appl Radiat Isot 63:329-332. doi:10.1016/j.apradiso.2005.03.005

Mamat C, Mosch B, Neuber C, Köckerling M, Bergmann R, Pietzsch J (2012) Fluorine-18 radiolabeling and radiopharmacological characterization of a benzodioxolylpyrimidine-based radiotracer targeting the receptor tyrosine kinase EphB4. ChemMedChem 7:1991-2003. doi:10.1002/cmdc.201200264

Maynard AJ, Sharman GJ, Searle MS (1998) Origin of β-Hairpin Stability in Solution: Structural and Thermodynamic Analysis of the Folding of a Model Peptide Supports Hydrophobic Stabilization in Water. J Am Chem Soc 120:1996-2007

Mitchell LA, Koval M (2010) Specificity of interaction between clostridium perfringens enterotoxin and claudin-family tight junction proteins. Toxins 2:1595-1611. doi:10.3390/toxins2071595

Mosley M, Knight J, Neesse A, Michl P, Iezzi M, Kersemans V, Cornelissen B (2015) Claudin-4 SPECT Imaging Allows Detection of Aplastic Lesions in a Mouse Model of Breast Cancer. J Nucl Med 56:745-751. doi:10.2967/jnumed.114.152496

Mutter M (2013) Four decades, four places and four concepts. Chimia (Aarau) 67:868-873. doi:10.2533/chimia.2013.868

Neesse A, Griesmann H, Gress TM, Michl P (2012) Claudin-4 as therapeutic target in cancer. Arch Biochem Biophys 524:64-70. doi:10.1016/j.abb.2012.01.009

Neesse A, Hahnenkamp A, Griesmann H, Buchholz M, Hahn SA, Maghnouj A, Fendrich V, Ring J, Sipos B, Tuveson DA, Bremer C, Gress TM, Michl P (2013) Claudin-4-targeted optical imaging detects pancreatic cancer and its precursor lesions. Gut 62:1034-1043. doi:10.1136/gutjnl-2012-302577

Osanai M, Takasawa A, Murata M, Sawada N (2017) Claudins in cancer: bench to bedside. Pflügers Arch Eur J Physiol 469:55-67. doi:10.1007/s00424-016-1877-7

Paradis-Bas M, Tulla-Puche J, Albericio F (2016) The road to the synthesis of "difficult peptides". Chem Soc Rev 45:631-654. doi:10.1039/c5cs00680e

Pietzsch J, Bergmann R, Wuest F, Pawelke B, Hultsch C, van den Hoff J (2005) Catabolism of native and oxidized low density lipoproteins: in vivo insights from small animal positron emission tomography studies. Amino Acids 29:389-404. doi:10.1007/s00726-005-0203-z

Piontek A, Rossa J, Protze J, Wolburg H, Hempel C, Gunzel D, Krause G, Piontek J (2017a) Polar and charged extracellular residues conserved among barrier-forming claudins contribute to tight junction strand formation. Ann N Y Acad Sci 1397:143-156. doi:10.1111/nyas.13341

Piontek A, Witte C, May Rose H, Eichner M, Protze J, Krause G, Piontek J, Schröder L (2017b) A cCPE-based xenon biosensor for magnetic resonance imaging of claudin-expressing cells. Ann N Y Acad Sci 1397:195-208. doi:10.1111/nyas.13363

Protze J, Eichner M, Piontek A, Dinter S, Rossa J, Blecharz KG, Vajkoczy P, Piontek J, Krause G (2015) Directed structural modification of Clostridium perfringens enterotoxin to enhance binding to claudin-5. Cell Mol Life Sci 72:1417-1432. doi:10.1007/s00018-014-1761-6

Reiersen H, Rees AR (2000) Trifluoroethanol may form a solvent matrix for assisted hydrophobic interactions between peptide side chains. Protein Engineering 13:739-743. doi:10.1093/protein/13.11.739

Rhodes CA, Pei D (2017) Bicyclic Peptides as Next-Generation Therapeutics. Chem Eur J 23:12690-12703. doi:10.1002/chem.201702117

Richter S, Wuest F (2014) ^{18}F-Labeled Peptides: The Future Is Bright. Molecules 19:20536-20556. doi:10.3390/molecules191220536

Salvador E, Burek M, Forster CY (2016) Tight Junctions and the Tumor Microenvironment. Curr Pathobiol Rep 4:135-145. doi:10.1007/s40139-016-0106-6

Šebestik J, Zawada Z, Šafařik M, Hlavaček J (2012) Comparative syntheses of peptides and peptide thioesters derived from mouse and human prion proteins. Amino Acids 43:1297-1309. doi:10.1007/s00726-011-1203-9

Seimbille Y, Czernin J, Phelps ME, Silverman DHS (2005) Synthesis of an18F-fluorobenzoate idarubicin derivative as new potential PET radiotracer to predict chemotherapy resistance. J Label Compd Radiopharm 48:819-827. doi:10.1002/jlcr.990

Seitz R, König H, Dodt J (2006) Blood. In: Ullmann's Encyclopedia of Industrial Chemistry. Wiley-VCH, Weinheim. doi:10.1002/14356007.a04_201.pub2

Shinoda T, Shinya N, Ito K, Ishizuka-Katsura Y, Ohsawa N, Terada T, Hirata K, Kawano Y, Yamamoto M, Tomita T, Ishibashi Y, Hirabayashi Y, Kimura-Someya T, Shirouzu M, Yokoyama S (2016a) Cell-free methods to produce structurally intact mammalian membrane proteins. Sci Rep 6:30442. doi:10.1038/srep30442

Shinoda T, Shinya N, Ito K, Ohsawa N, Terada T, Hirata K, Kawano Y, Yamamoto M, Kimura-Someya T, Yokoyama S, Shirouzu M (2016b) Structural basis for disruption of claudin assembly in tight junctions by an enterotoxin. Sci Rep 6:33632. doi:10.1038/srep33632

Singh AB, Dhawan P (2015) Claudins and cancer: Fall of the soldiers entrusted to protect the gate and keep the barrier intact. Semin Cell Dev Biol 42:58-65. doi:10.1016/j.semcdb.2015.05.001

Sodoyez J, Sodoyez-Goffaux F, Guillaume M, Merchie G (1983) [1231]Insulin Metabolism in Normal Rats and Humans: External Detection by a Scintillation Camera. Science 219:865-867. doi:10.1126/science.6337399

Sodoyez JC, Sodoyez Goffaux F, von Frenckell R, De Vos CJ, Treves S, Kahn CR (1985) Differing effects of antiinsulin serum and antiinsulin receptor serum on 123I-insulin metabolism in rats. J Clin Invest 75:1455-1462. doi:10.1172/JCI111848

Suzuki H, Kondoh M, Li X, Takahashi A, Matsuhisa K, Matsushita K, Kakamu Y, Yamane S, Kodaka M, Isoda K, Yagi K (2011) A toxicological evaluation of a claudin modulator, the C-terminal fragment of Clostridium perfringens enterotoxin, in mice. Pharmazie 66:543–546. doi:10.1691/ph.2011.0365

Takahashi A, Komiya E, Kakutani H, Yoshida T, Fujii M, Horiguchi Y, Mizuguchi H, Tsutsumi Y, Tsunoda S, Koizumi N, Isoda K, Yagi K, Watanabe Y, Kondoh M (2008) Domain mapping of a claudin-4 modulator, the C-terminal region of C-terminal fragment of Clostridium perfringens enterotoxin, by site-directed mutagenesis. Biochem Pharmacol 75:1639-1648. doi:10.1016/j.bcp.2007.12.016

Takahashi A, Kondoh M, Suzuki H, Watari A, Yagi K (2012) Pathological changes in tight junctions and potential applications into therapies. Drug Discov Today 17:727-732. doi:10.1016/j.drudis.2012.02.014

Tickler AK, Wade JD (2007) Overview of solid phase synthesis of "difficult peptide" sequences. Curr Protoc Protein Sci Chapter 18:Unit 18 18. doi:10.1002/0471140864.ps1808s50

Tondera C, Laube M, Pietzsch J (2017) Insights into binding of S100 proteins to scavenger receptors: class B scavenger receptor CD36 binds S100A12 with high affinity. Amino Acids 49:183-191. doi:10.1007/s00726-016-2349-2

Tsujiwaki M, Murata M, Takasawa A, Hiratsuka Y, Fukuda R, Sugimoto K, Ono Y, Nojima M, Tanaka S, Hirata K, Kojima T, Sawada N (2015) Aberrant expression of claudin-4 and -7 in hepatocytes in the cirrhotic human liver. Med Mol Morphol 48:33-43. doi:10.1007/s00795-014-0074-z

Tuchscherer G, Mutter M (2003) Template-Assembled Synthetic Proteins. In: Goodman M, Felix A, Moroder L, Toniolo C (eds) Houben-Weyl Methods of Organic Chemistry, vol E22d. G. Thieme, Stuttgart, pp 6-64

Tummino PJ, Copeland RA (2008) Residence Time of Receptor-Ligand Complexes and Its Effect on Biological Function. Biochemistry 47:5481-5492. doi:10.1021/bi8002023

Tyndall JD, Nall T, Fairlie DP (2005) Proteases universally recognize beta strands in their active sites. Chem Rev 105:973-999. doi:10.1021/cr040669e

Ullrich M, Bergmann R, Peitzsch M, Zenker EF, Cartellieri M, Bachmann M, Ehrhart-Bornstein M, Block NL, Schally AV, Eisenhofer G, Bornstein SR, Pietzsch J, Ziegler CG (2016) Multimodal

Somatostatin Receptor Theranostics Using [^{64}Cu]Cu-/[^{177}Lu]Lu-DOTA-(Tyr(3))octreotate and AN-238 in a Mouse Pheochromocytoma Model. Theranostics 6:650-665. doi:10.7150/thno.14479

Urbanova M, Maloň P (2012) Circular Dichroism Spectroscopy. In: Schalley C (ed) Analytical Methods in Supramolecular Chemistry. 2 edn. Wiley-VCH, Weinheim, pp 337-369

van der Born D, Pees A, Poot AJ, Orru RVA, Windhorst AD, Vugts DJ (2017) Fluorine-18 labelled building blocks for PET tracer synthesis. Chem Soc Rev 46:4709-4773. doi:10.1039/c6cs00492j

Van Itallie CM, Betts L, Smedley JG, 3rd, McClane BA, Anderson JM (2008) Structure of the claudin-binding domain of Clostridium perfringens enterotoxin. J Biol Chem 283:268-274. doi:10.1074/jbc.M708066200

Vernieri E, Valle J, Andreu D, de la Torre BG (2014) An optimized Fmoc synthesis of human defensin 5. Amino Acids 46:395-400. doi:10.1007/s00726-013-1629-3

Veshnyakova A, Protze J, Rossa J, Blasig IE, Krause G, Piontek J (2010) On the interaction of Clostridium perfringens enterotoxin with claudins. Toxins 2:1336-1356. doi:10.3390/toxins2061336

White P, Keyte JW, Bailey K, Bloomberg G (2004) Expediting the Fmoc solid phase synthesis of long peptides through the application of dimethyloxazolidine dipeptides. J Pept Sci 10:18-26. doi:10.1002/psc.484

Winkler DFH, Tian K (2015) Investigation of the automated solid-phase synthesis of a 38mer peptide with difficult sequence pattern under different synthesis strategies. Amino Acids 47:787-794. doi:10.1007/s00726-014-1909-6

Wodtke R, Ruiz-Gomez G, Kuchar M, Pisabarro MT, Novotna P, Urbanova M, Steinbach J, Pietzsch J, Löser R (2015) Cyclopeptides containing the DEKS motif as conformationally restricted collagen telopeptide analogues: synthesis and conformational analysis. Org Biomol Chem 13:1878-1896. doi:10.1039/c4ob02348j

Wojczewski C, Schwarzer K, Engels JW (2000) Synthesis of 3'-Thioamido-Modified 3'-Deoxythymidine 5'-Triphosphates by Regioselective Thionation and Their Use as Chain Terminators in DNA Sequencing. Helv Chim Acta 83:1268-1277

Wolf S, Haase-Kohn C, Lenk J, Hoppmann S, Bergmann R, Steinbach J, Pietzsch J (2011) Expression, purification and fluorine-18 radiolabeling of recombinant S100A4: a potential probe for molecular imaging of receptor for advanced glycation endproducts in vivo? Amino Acids 41:809-820. doi:10.1007/s00726-010-0822-x

Woody R (2002) Circular Dichroism. In: Goodman M, Felix A, Moroder L, Toniolo C (eds) Houben-Weyl Methods of Organic Chemistry, vol E22b Synthesis of Peptides. Georg Thieme Verlag, Stuttgart,

Supplementary Material

Synthesis, ^{18}F-labelling and radiopharmacological characterisation of the C-terminal 30mer of the *Clostridium perfringens* enterotoxin as a potential claudin-targeting peptide

Reik Löser[2,2,*], Miriam Bader[1,2,§], Manuela Kuchar[1,2,§], Robert Wodtke[1,2], Jens Lenk[1,2], Johanna Wodtke[1,#], Konstantin Kuhne[1,2], Ralf Bergmann[1], Cathleen Haase-Kohn[1], Marie Urbanová[3], Jörg Steinbach[1,2], Jens Pietzsch[1,2]

CONTENTS

[2] *Helmholtz-Zentrum Dresden Rossendorf, Institute of Radiopharmaceutical Cancer Research, Bautzner Landstraße 400, 01328 Dresden, Germany*
[2] *Faculty of Chemistry and Food Chemistry, School of Science, Technische Universität Dresden, Mommsenstraße 4, 01062 Dresden, Germany*
[3] *Department of Physics and Measurements, University of Chemistry and Technology, 166 28 Prague, Czech Republic*
[*] *Corresponding author, r.loeser@hzdr.de*
[§] *These authors contributed equally to this study*
[#] *J. Wodtke née Pufe*

Analytical and semi-preparative HPLC-Systems

Analytical HPLC system: ***System 1***

- Binary pump: Varian PrepStar 218 Solvent Delivery Module
- Detector (UV/Vis): Varian, ProStar 325
- Detection wavelength: 220 nm
- Stationary phase: Varian 250 × 4.6 mm, Microsorb 60-8 C-18
- Eluent: A: 0.1% TFA in Water, B: 0.1% TFA in acetonitrile
- Flow rate: 1 mL/min
- Elution programme: see Table S1

Table S1: Elution programme for HPLC System 1

time (min)	A (%)	B (%)
0-3	90	10
3-18	50	50
18-35	40	60
35-36	5	95
36-45	5	95
45-46	90	10
46-50	10	10

Analytical HPLC system: ***System 2 –*** used for calibration curve of reference compound FBz-cCPE$_{290-319}$ (**5**) and analysis of radiolabeled [^{18}F]FBz-cCPE$_{290-319}$ ([^{18}F]**5**)

- Pump: Agilent Technologies, 1200 Series
- Detector (DAD): Agilent Technologies, 1200 Series
- Detection wavelength: 220 nm
- Detector (γ radiation): Raytest Gabi
- Autosampler: Agilent Technologies, 1200 Series
- Interface: Agilent Interface 35900E
- Degasser: Agilent Technologies, 1200 Series
- Column switch: Besta
- Stationary Phase: Macherey-Nagel EC 250 × 4.6 mm, Nucleosil Standard 100-7 C-18 with precolumn (4 × 4 mm)
- Eluent: A: 0.1% TFA in Water, B: 0.1% TFA in acetonitrile
- Flow rate: 1 mL/min
- Elution programme: see Table S2

Table S2: Elution programme for HPLC System 2

time (min)	A (%)	B (%)
0-3	90	10
3-18	60	40
18-35	50	50
35-36	5	95
36-45	5	95
46-46	90	10
46-50	90	10

Semi-preparative HPLC system: ***System 3 –*** used for purification of the synthesised non-radioactive peptides; identical to system 1 except for the stationary phase and flow rate, which were Varian Dynamax 250 × 21.4 mm and 10 mL/min, respectively. The elution programme is detailed in Table S3

Table S3: Elution programme for System 3

time (min)	A (%)	B (%)
0-3	90	10
3-30	40	60
30-32	10	90
32-38	10	90
38-40	90	10
40-42	90	10

Semi-preparative HPLC system: ***System 4 –*** used for purification of radiolabeled [^{18}F]FBz-cCPE$_{290-319}$ ([^{18}F]**5**)

- Pump: Jasco, PU-2080 Intelligent HPLC Pump
- Detector (DAD): Jasco, RS-232C
- Detection wavelength: 220 nm
- Detector (γ radiation): Raytest Gabi
- Interface: Jasco, LC-Net II/ADC
- Degasser: Jasco, DG-2080-53
- Stationary Phase: Macherey-Nagel, 250 × 16 mm Nucleosil 100-7 C-18
- Eluent: A: 0.1% TFA in Water, B: 0.1% TFA in acetonitrile
- Flow rate: 4 mL/min
- Elution programme: see Table S4
-

Table S4: Elution programme for System 4

time (min)	A (%)	B (%)
0	90	10
0-15	52	48
15-45	52	48
45-50	0	100
50-55	0	100
60	90	10
70	90	10

Semi-preparative HPLC system: ***System 4$_b$ –*** alternatively used for purification of radiolabeled [^{18}F]FBz-cCPE$_{290-319}$ ([^{18}F]**5**); stationary phase, flow rate and elution programme were identical to HPLC system 4

- Pump: Jasco, PU-1580
- Detector (UV/Vis): Jasco, UV-1575
- Detection wavelength: 220 nm
- Detector (γ radiation): Raytest Gabi
- Degasser: Jasco, DG-2080-53

- Gradient mixer Jasco, LG-2080-02

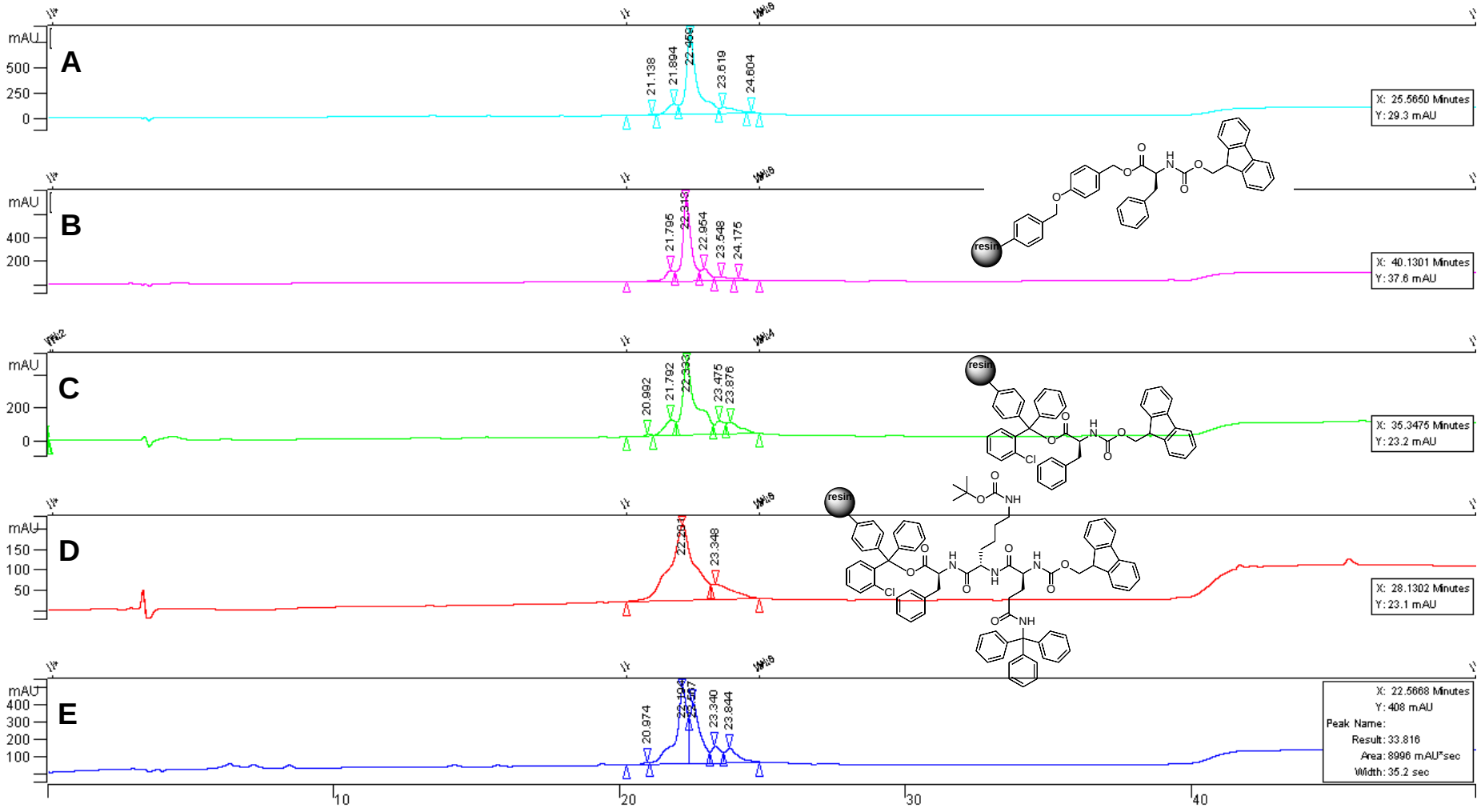

Fig. S11: **HPLC chromatograms of crude peptide 1 obtained by different synthetic strategies. A) Wang linker, loading 0.37 mmol/g, with pseudoproline dipeptides, yield 80 %; B) Wang linker, loading 0.37 mmol/g, with pseudoproline dipeptides, yield 93 %; C) chlorotrityl linker, loading 0.28 mmol/g, with pseudoproline dipeptides, yield 43 %; D) chlorotrityl linker,**

loading 0.28 mmol/g, with pseudoproline dipeptides, preloaded with F-K^{Boc}-Q^{Trt}, with pseudoproline dipeptides, yield 35%; E) Wang linker, loading 0.37 mmol/g, without pseudoproline dipeptides, yield 60 %. Chromatograms B and E are identical to the ones shown in Fig. 2 in the main text.

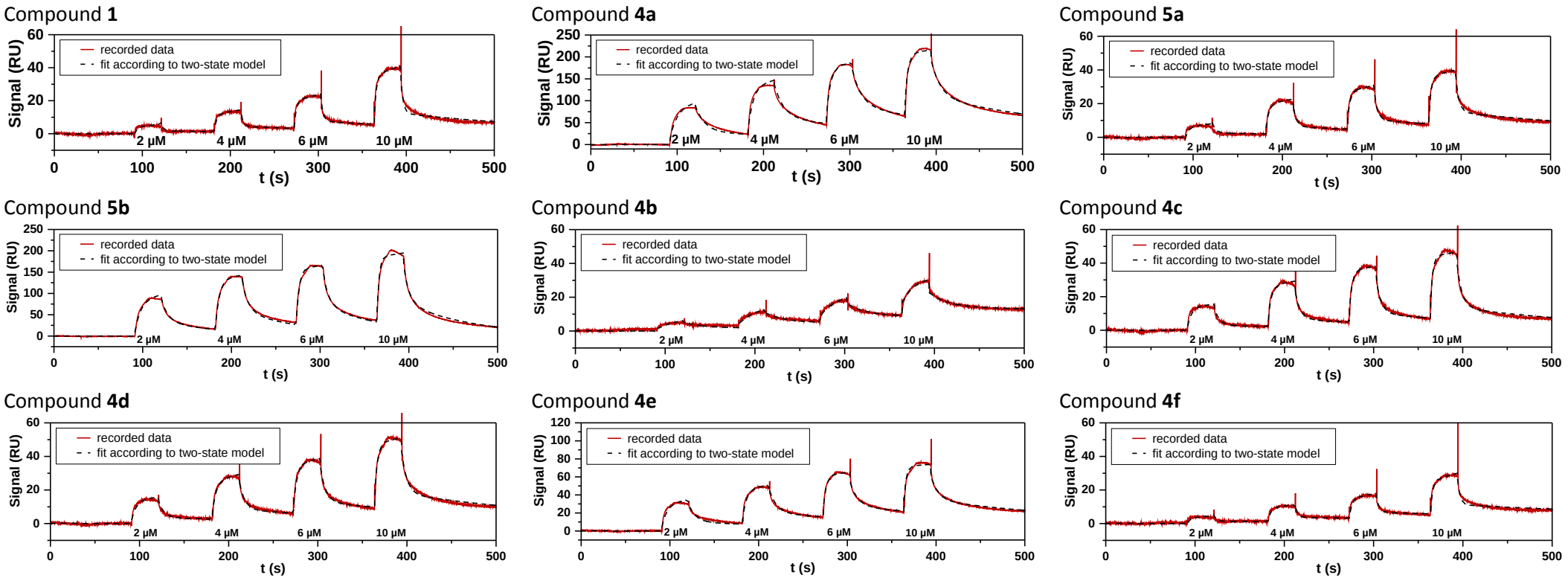

Fig. S12: SPR Sensorgrams for the interaction of cCPE$_{290-319}$-derived peptides **1**, **4a**-**g**, **5a** and **b** with the immobilized claudin-4 mimicking construct MKH$_{10}$AS-Cld-4$_{29-81}$-LEVLFQGP-Cld-4$_{139-160}$ as immobilised ligand measured in the single-cycle mode.

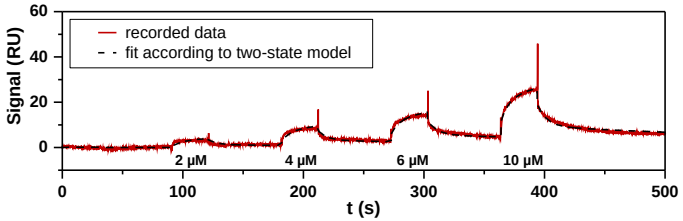
recorded data
fit according to two-state model
Signal (RU)
t (s)
2 µM
4 µM
6 µM
10 µM
0
20
40
60
0
100
200
300
400
500

Table S5: Individual rate constants for interaction of $cCPE_{290-319}$ (**1**) and its derivatives with the artificial claudin-4 mimicking protein construct **III** (see Fig. 5A).

compd	k_{a1} ($M^{-1}s^{-1}$)	k_{a2} (s^{-1})	k_{d1} (s^{-1})	k_{d2} (s^{-1})	*n*
1	$(6.74\pm3.32)\times10^{3}$	$(1.63\pm0.49)\times10^{-2}$	$(2.41\pm0.74)\times10^{-1}$	$(6.61\pm1.07)\times10^{-3}$	7
4a	$(2.34\pm0.32)\times10^{4}$	$(1.04\pm0.11)\times10^{-2}$	$(8.97\pm2.70)\times10^{-2}$	$(5.15\pm1.72)\times10^{-3}$	6
5a	$(1.48\pm0.74)\times10^{4}$	$(1.50\pm1.12)\times10^{-2}$	$(2.10\pm1.14)\times10^{-1}$	$(6.82\pm2.87)\times10^{-3}$	8
5b	$(8.31\pm0.01)\times10^{4}$	$(3.07\pm3.51)\times10^{-1}$	$(1.57\pm0.51)\times10^{-2}$	$(1.31\pm0.54)\times10^{-2}$	9
4b	$(2.14\pm2.06)\times10^{3}$	$(1.22\pm0.34)\times10^{-2}$	$(4.85\pm1.82)\times10^{-2}$	$(8.78\pm3.89)\times10^{-4}$	8
4c	$(2.65\pm0.65)\times10^{4}$	$(9.24\pm1.42)\times10^{-3}$	$(1.73\pm0.34)\times10^{-1}$	$(5.17\pm0.55)\times10^{-3}$	7
4d	$(1.85\pm0.30)\times10^{4}$	$(1.06\pm0.10)\times10^{-2}$	$(1.50\pm0.24)\times10^{-1}$	$(4.71\pm0.31)\times10^{-3}$	7
4e	$(2.85\pm0.60)\times10^{4}$	$(9.93\pm1.42)\times10^{-3}$	$(1.76\pm0.43)\times10^{-1}$	$(5.45\pm1.08)\times10^{-3}$	8
4f	$(6.26\pm3.26)\times10^{3}$	$(1.06\pm0.20)\times10^{-2}$	$(2.48\pm1.44)\times10^{-1}$	$(2.15\pm1.40)\times10^{-3}$	6
4g	$(2.09\pm0.86)\times10^{3}$	$(1.26\pm0.24)\times10^{-2}$	$(9.78\pm4.73)\times10^{-2}$	$(3.34\pm0.84)\times10^{-3}$	7

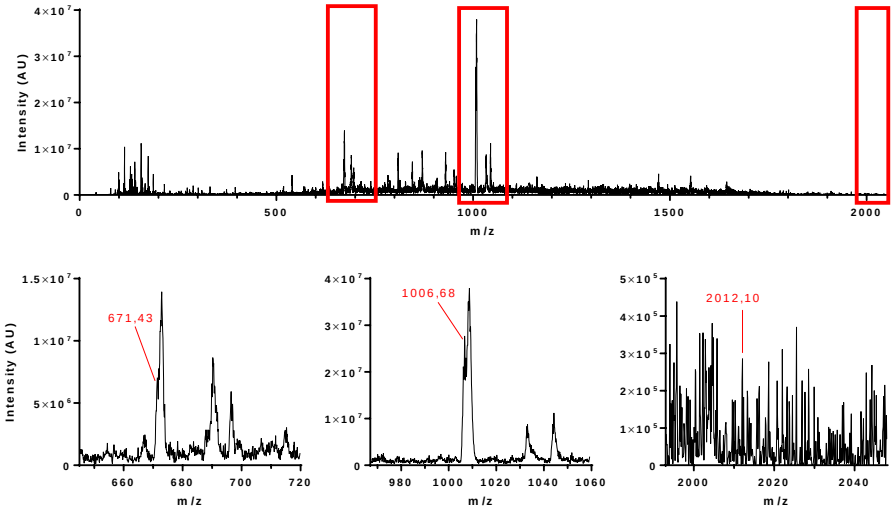

Fig. S13: ESI-MS spectra of the metabolite formed by incubation compound **6** in human serum. The observed peaks can be assigned to the positive ions of FITC-Ahx-$cCPE_{290-303}$ ($[M+3H]^{3+}$, $[M+2H]^{2+}$, $[M+H]^{+}$), which indicates proteolytic cleavage after Asn 303.

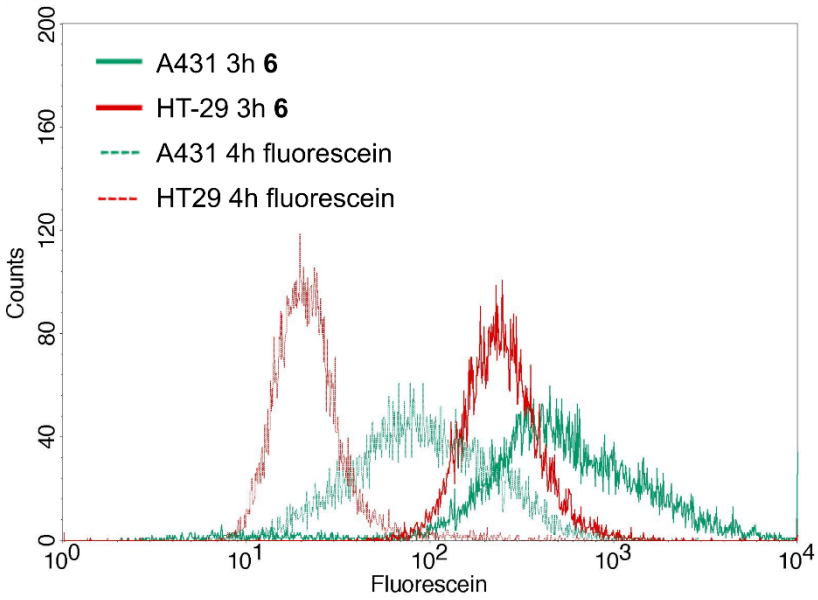

Fig. S14: Flow cytometry histograms of FITC-conjugated peptide 6 and free fluorescein for A431 and HT29 tumour cells.

ESI-MS spectra for compounds 1-13

Compound **1**

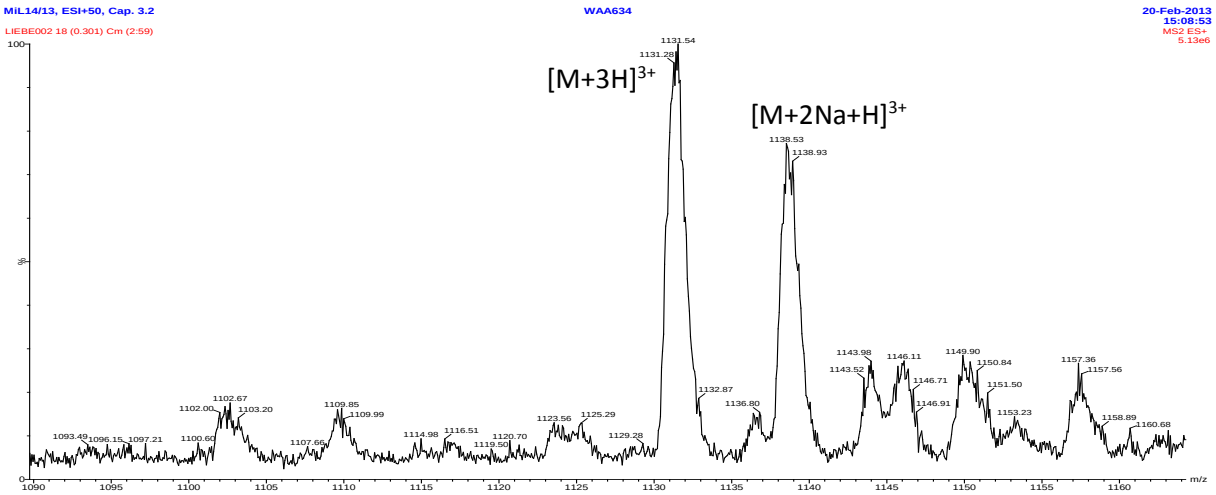

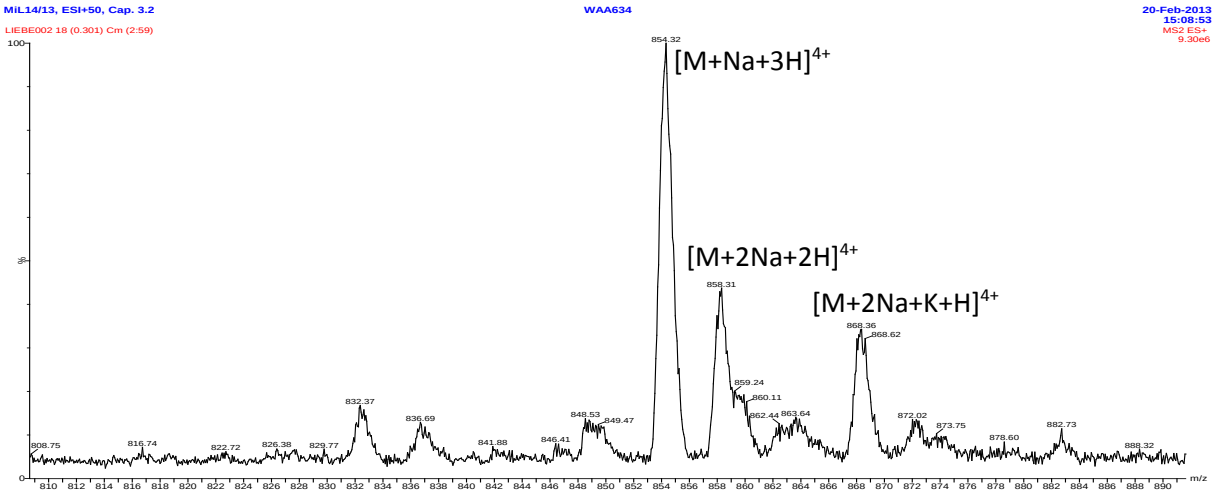

Compound **2**

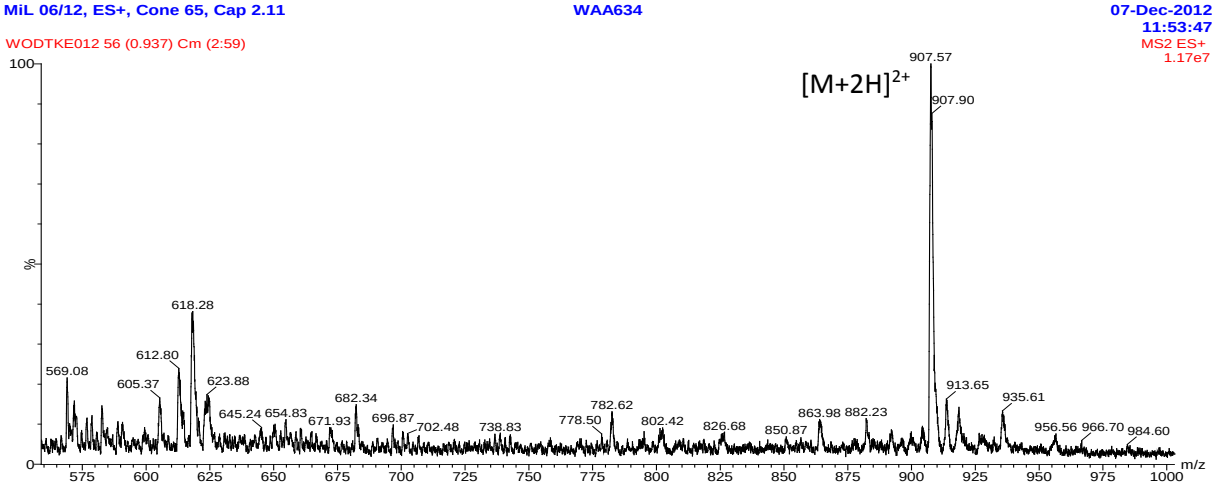
MiL 06/12, ES+, Cone 65, Cap 2.11
WAA634
07-Dec-2012
11:53:47
WODTKE012 56 (0.937) Cm (2:59)
MS2 ES+
1.17e7
100
%
0
[M+2H]2+
907.57
907.90
618.28
612.80
569.08
605.37
623.88
645.24
654.83
671.93
682.34
696.87
702.48
738.83
778.50
782.62
802.42
826.68
850.87
863.98
882.23
913.65
935.61
956.56
966.70
984.60
575
600
625
650
675
700
725
750
775
800
825
850
875
900
925
950
975
1000
m/z

Compound **3**

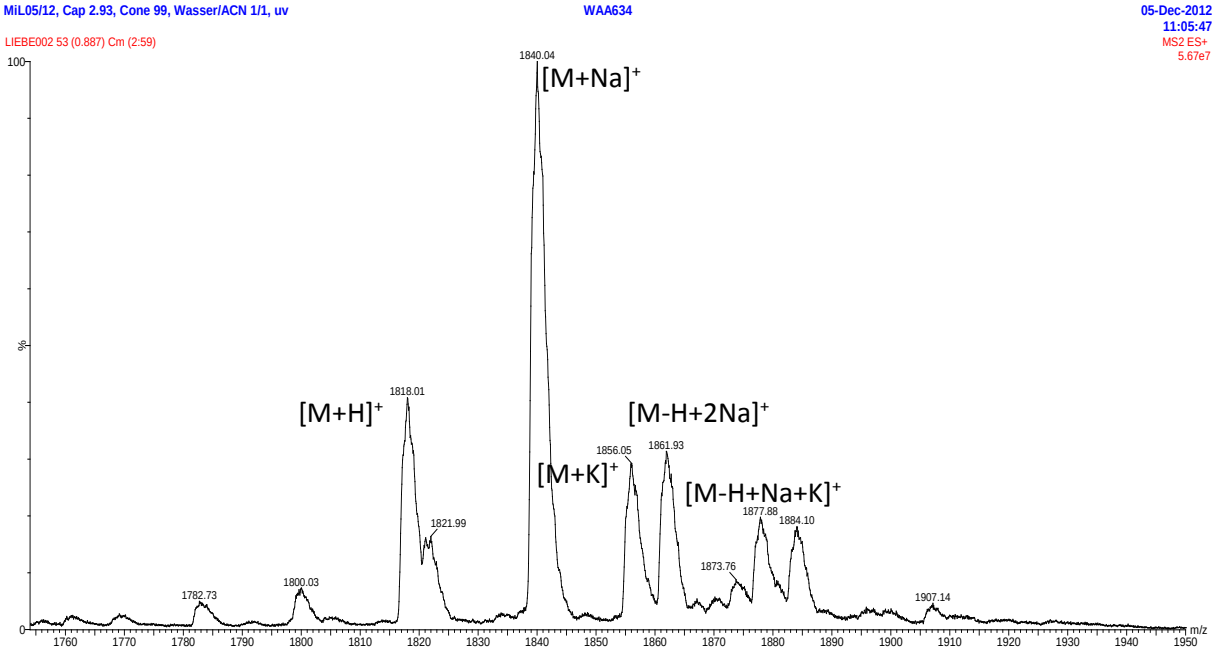
MiL05/12, Cap 2.93, Cone 99, Wasser/ACN 1/1, uv
WAA634
05-Dec-2012
11:05:47
LIEBE002 53 (0.887) Cm (2:59)
MS2 ES+
5.67e7
[M+Na]+
[M+H]+
[M-H+2Na]+
[M+K]+
[M-H+Na+K]+
1840.04
1818.01
1861.93
1856.05
1821.99
1877.88
1884.10
1873.76
1800.03
1782.73
1907.14
m/z

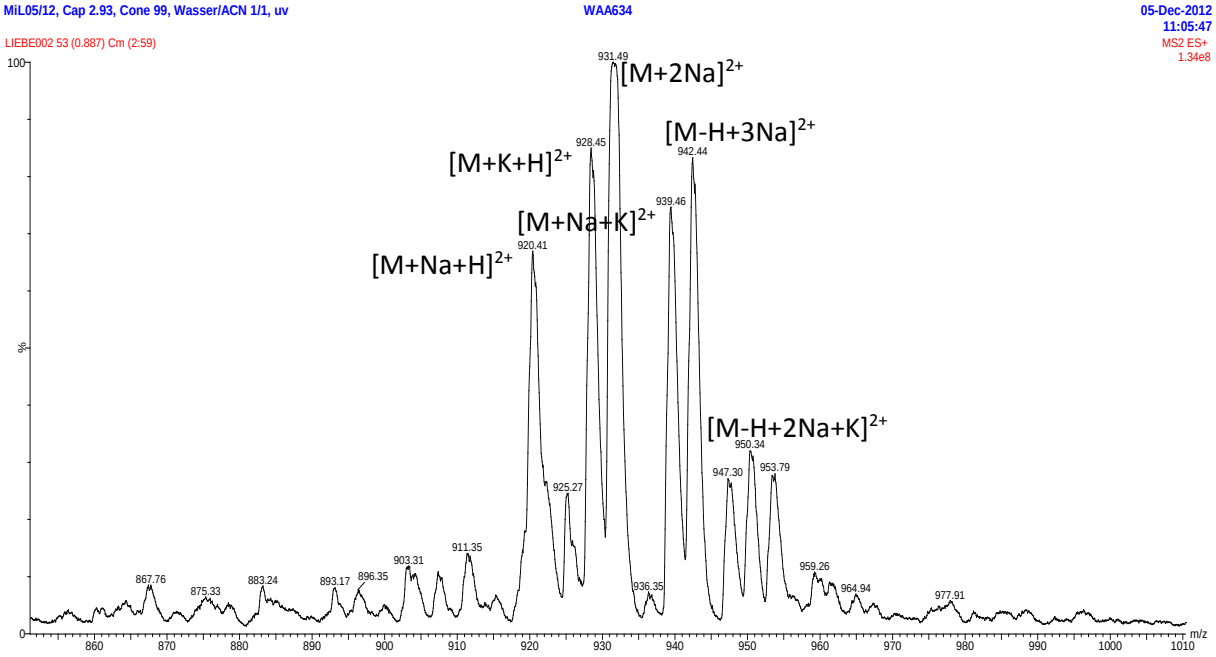
MiL05/12, Cap 2.93, Cone 99, Wasser/ACN 1/1, uv
WAA634
05-Dec-2012
11:05:47
LIEBE002 53 (0.887) Cm (2:59)
MS2 ES+
1.34e8
[M+2Na]2+
[M-H+3Na]2+
[M+K+H]2+
[M+Na+K]2+
[M+Na+H]2+
[M-H+2Na+K]2+
931.49
928.45
942.44
939.46
920.41
950.34
947.30
953.79
925.27
911.35
903.31
896.35
893.17
883.24
875.33
867.76
936.35
959.26
964.94
977.91
m/z

Compound **4a**

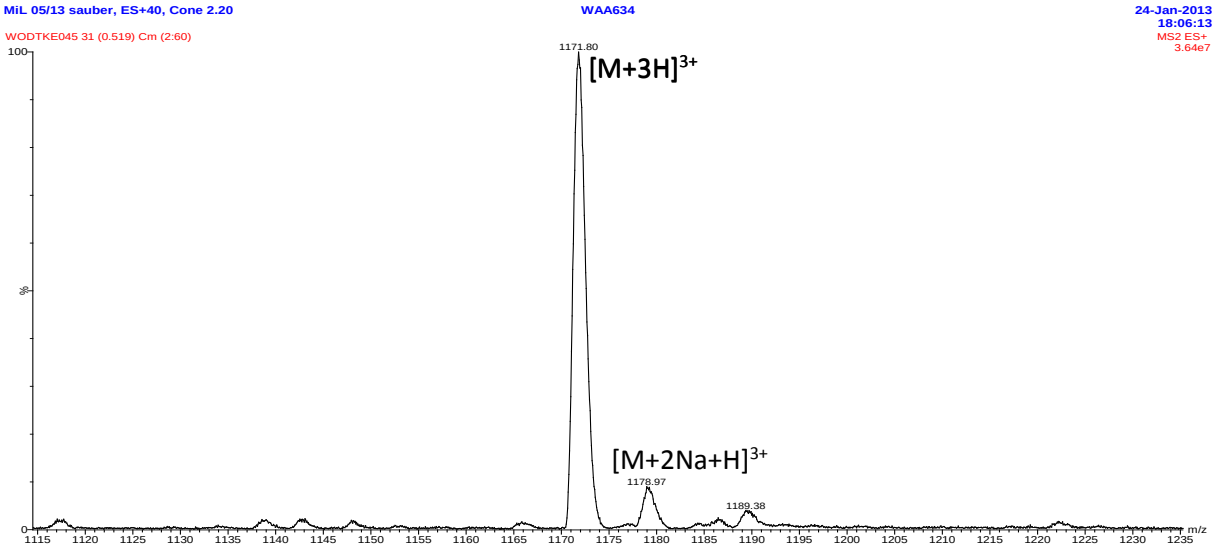
MiL 05/13 sauber, ES+40, Cone 2.20
WAA634
24-Jan-2013
18:06:13
WODTKE045 31 (0.519) Cm (2:60)
MS2 ES+
3.64e7
100
%
0
1171.80
[M+3H]3+
[M+2Na+H]3+
1178.97
1189.38
1115 1120 1125 1130 1135 1140 1145 1150 1155 1160 1165 1170 1175 1180 1185 1190 1195 1200 1205 1210 1215 1220 1225 1230 1235
m/z

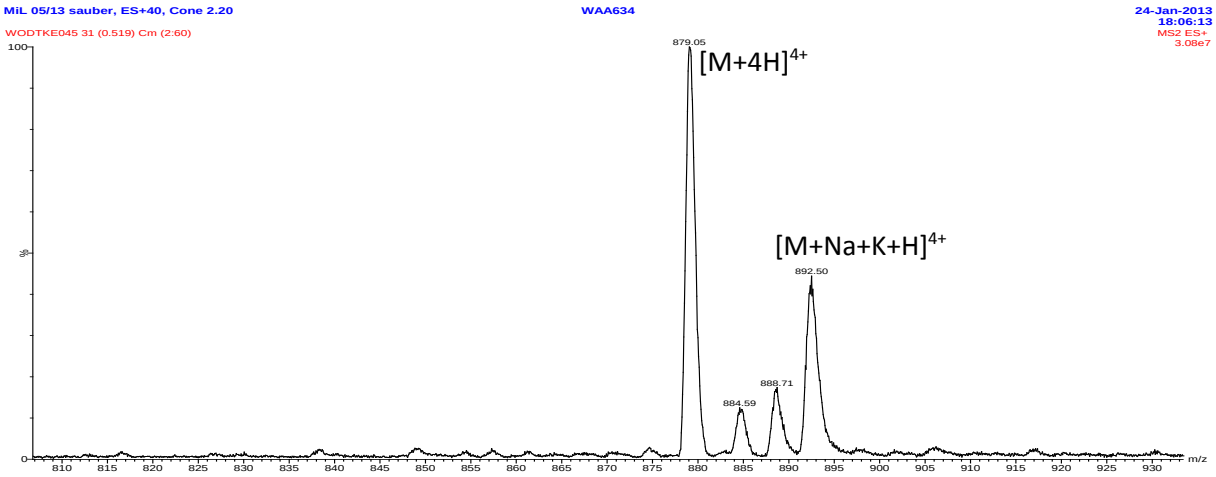
MiL 05/13 sauber, ES+40, Cone 2.20
WAA634
24-Jan-2013
18:06:13
WODTKE045 31 (0.519) Cm (2:60)
MS2 ES+
3.08e7
100
%
0
879.05
[M+4H]4+
[M+Na+K+H]4+
892.50
888.71
884.59
810 815 820 825 830 835 840 845 850 855 860 865 870 875 880 885 890 895 900 905 910 915 920 925 930
m/z

Compound **5a**

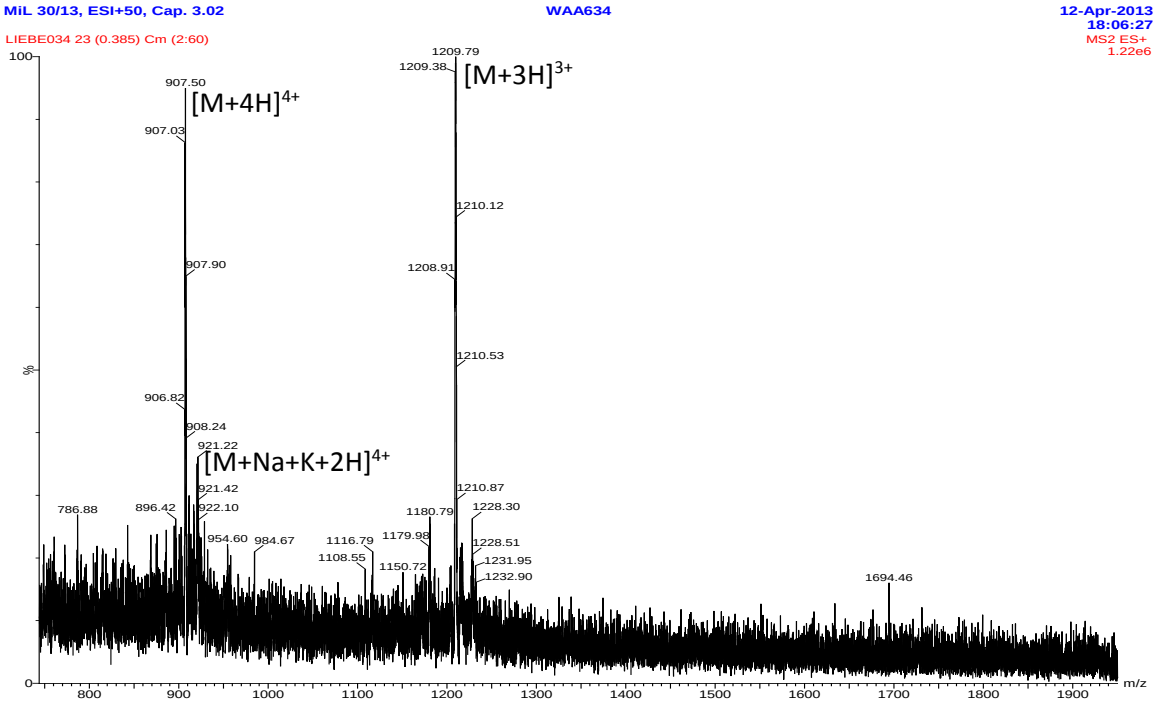
MiL 30/13, ESI+50, Cap. 3.02
WAA634
12-Apr-2013
18:06:27
LIEBE034 23 (0.385) Cm (2:60)
MS2 ES+
1.22e6
100
%
0
[M+4H]4+
[M+3H]3+
[M+Na+K+2H]4+
907.50
907.03
907.90
906.82
908.24
921.22
921.42
922.10
786.88
896.42
954.60
984.67
1209.79
1209.38
1210.12
1208.91
1210.53
1210.87
1180.79
1179.98
1116.79
1108.55
1150.72
1228.30
1228.51
1231.95
1232.90
1694.46
800
900
1000
1100
1200
1300
1400
1500
1600
1700
1800
1900
m/z

Compound **6**

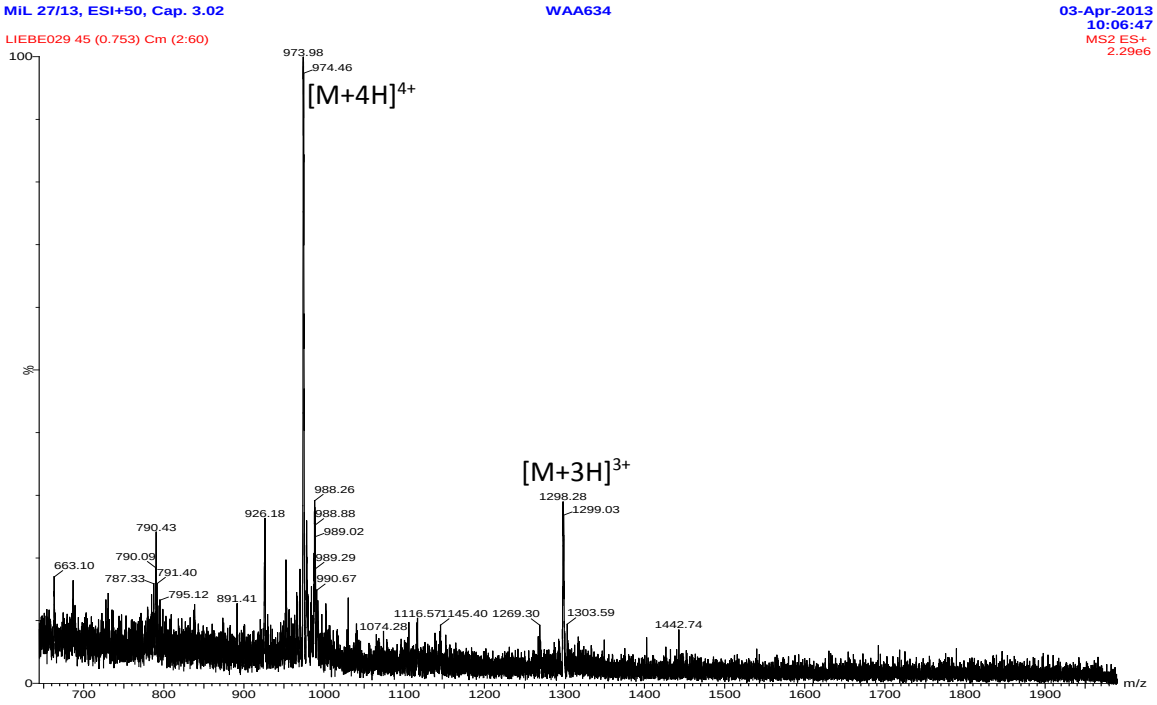
MiL 27/13, ESI+50, Cap. 3.02
WAA634
03-Apr-2013
10:06:47
LIEBE029 45 (0.753) Cm (2:60)
MS2 ES+
2.29e6
100
%
0
973.98
974.46
[M+4H]4+
[M+3H]3+
1298.28
1299.03
988.26
988.88
989.02
989.29
990.67
926.18
790.43
790.09
791.40
787.33
795.12
663.10
891.41
1074.28
1116.57
1145.40
1269.30
1303.59
1442.74
700
800
900
1000
1100
1200
1300
1400
1500
1600
1700
1800
1900
m/z

Compound **5b**

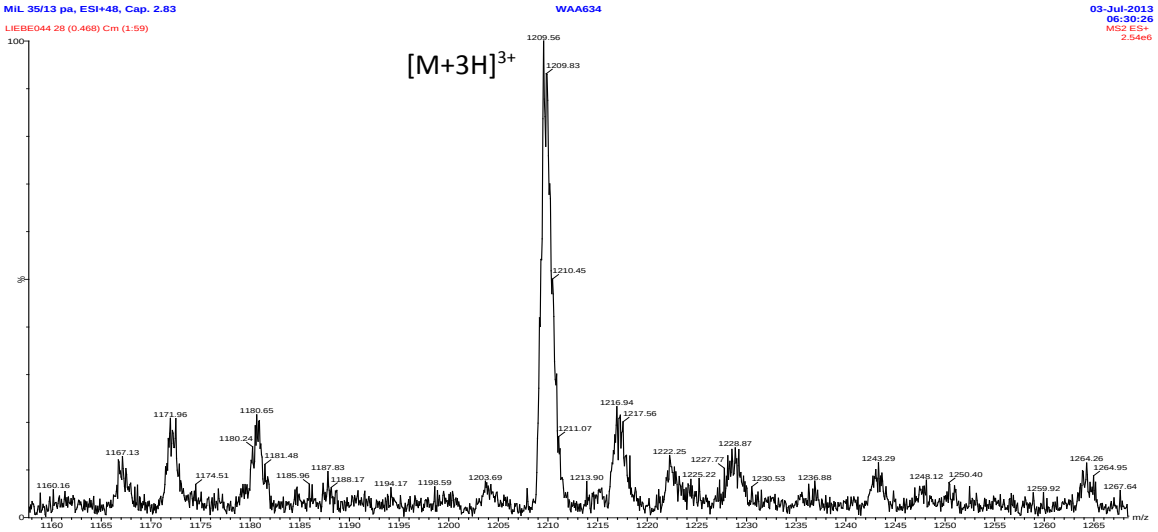
MiL 35/13 pa, ESI+48, Cap. 2.83
LIEBE044 28 (0.468) Cm (1:59)
WAA634
03-Jul-2013
06:30:26
MS2 ES+
2.54e6
[M+3H]3+
1209.56
1209.83
1210.45
1211.07
1216.94
1217.56
1171.96
1180.65
1180.24
1167.13
1181.48
1174.51
1185.96
1187.83
1188.17
1160.16
1194.17
1198.59
1203.69
1213.90
1222.25
1225.22
1227.77
1228.87
1230.53
1236.88
1243.29
1248.12
1250.40
1259.92
1264.26
1264.95
1267.64
%
m/z

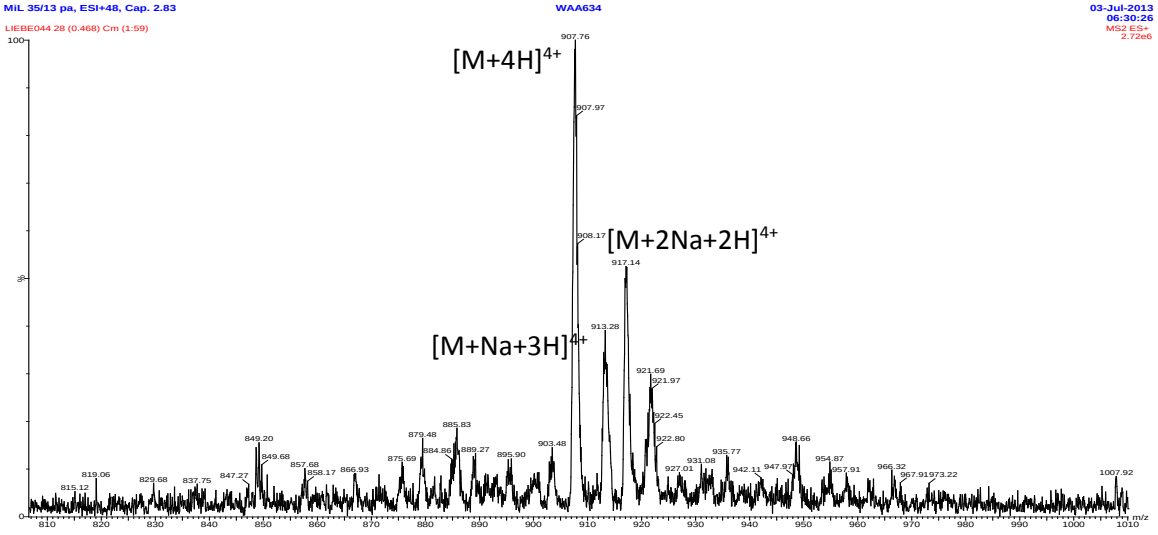
MiL 35/13 pa, ESI+48, Cap. 2.83
LIEBE044 28 (0.468) Cm (1:59)
WAA634
03-Jul-2013
06:30:26
MS2 ES+
2.72e6
[M+4H]4+
907.76
907.97
[M+2Na+2H]4+
908.17
917.14
[M+Na+3H]4+
913.28
921.69
921.97
922.45
922.80
885.83
879.48
884.88
889.27
875.69
895.90
903.48
849.20
849.68
857.68
858.17
866.93
847.27
819.06
815.12
829.68
837.75
931.08
935.77
942.11
947.97
948.66
954.87
957.91
966.32
967.91
973.22
1007.92
%
m/z

Compound **4b**

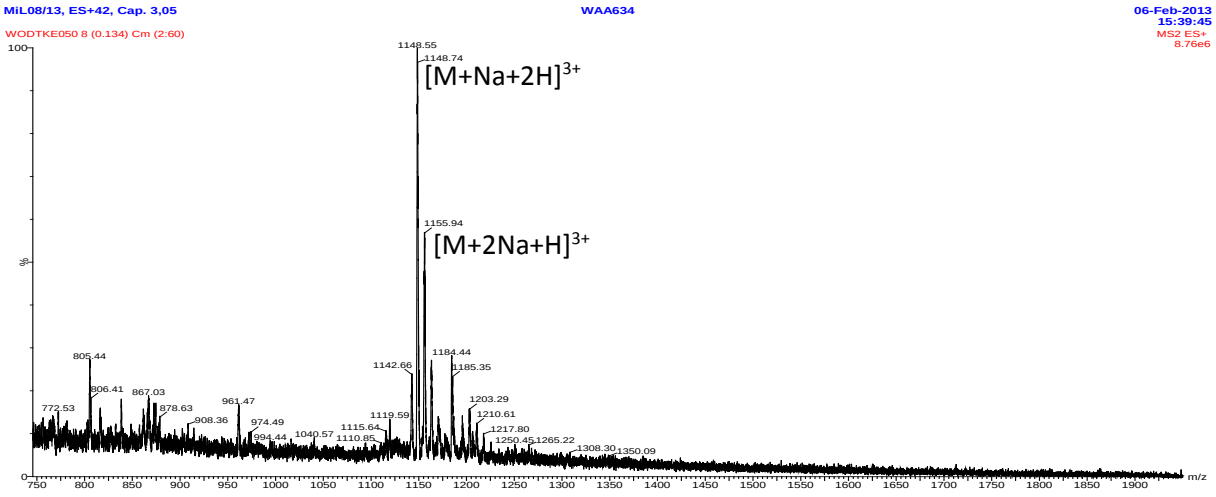
MiL08/13, ES+42, Cap. 3,05
WAA634
06-Feb-2013
15:39:45
WODTKE050 8 (0.134) Cm (2:60)
MS2 ES+
8.76e6
100
%
0
1148.55
1148.74
[M+Na+2H]3+
1155.94
[M+2Na+H]3+
805.44
806.41
867.03
878.63
772.53
908.36
961.47
974.49
894.44
1040.57
1115.64
1110.85
1119.59
1142.66
1184.44
1185.35
1203.29
1210.61
1217.80
1250.45
1265.22
1308.30
1350.09
750
800
850
900
950
1000
1050
1100
1150
1200
1250
1300
1350
1400
1450
1500
1550
1600
1650
1700
1750
1800
1850
1900
m/z

Compound **4c**

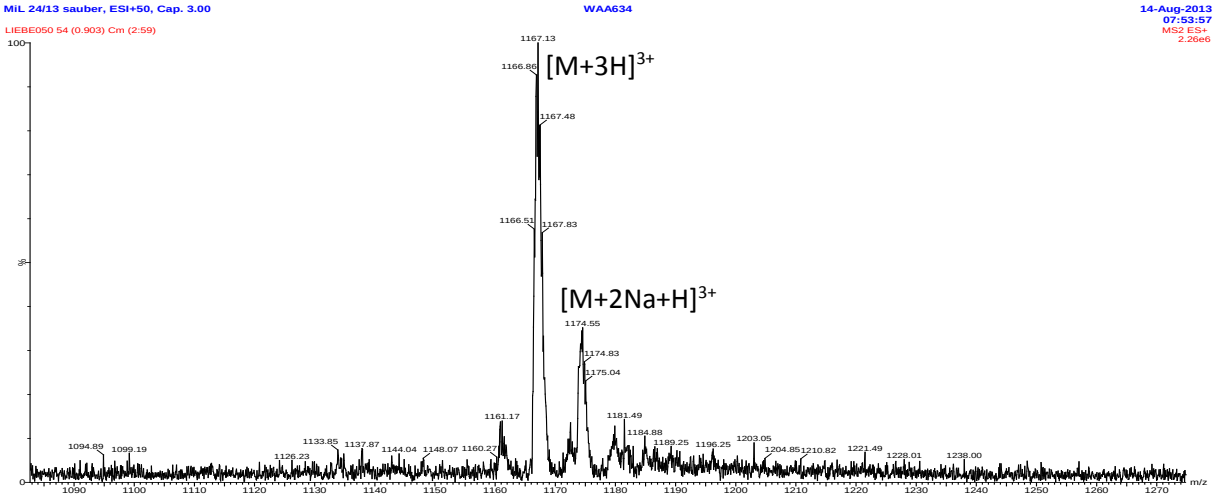
MiL 24/13 sauber, ESI+50, Cap. 3.00
WAA634
14-Aug-2013
07:53:57
MS2 ES+
2.26e6
LIEBE050 54 (0.903) Cm (2:59)
[M+3H]3+
[M+2Na+H]3+
m/z

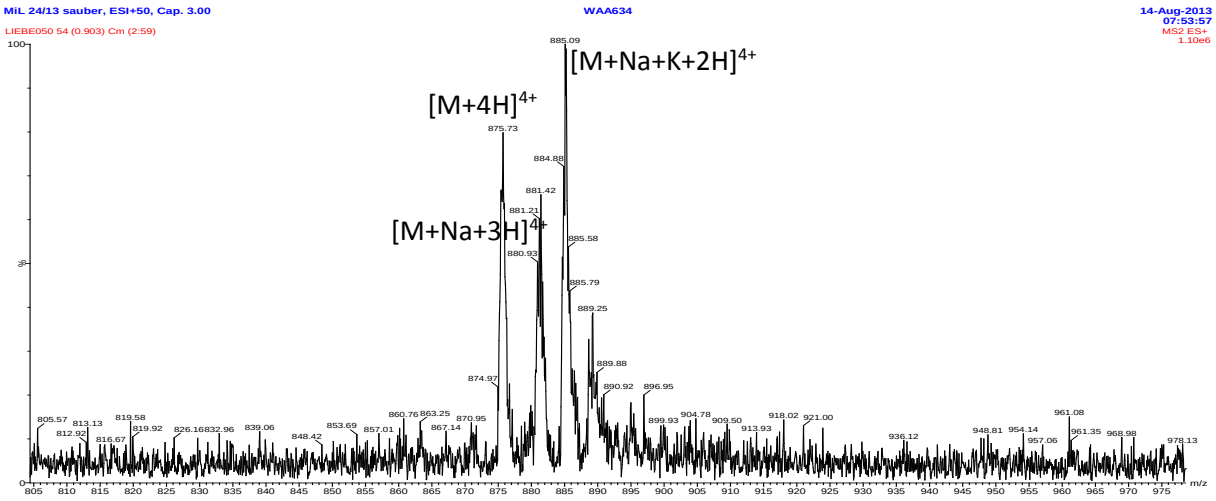
MiL 24/13 sauber, ESI+50, Cap. 3.00
WAA634
14-Aug-2013
07:53:57
MS2 ES+
1.10e6
LIEBE050 54 (0.903) Cm (2:59)
[M+Na+K+2H]4+
[M+4H]4+
[M+Na+3H]4+
m/z

Compound **4d**

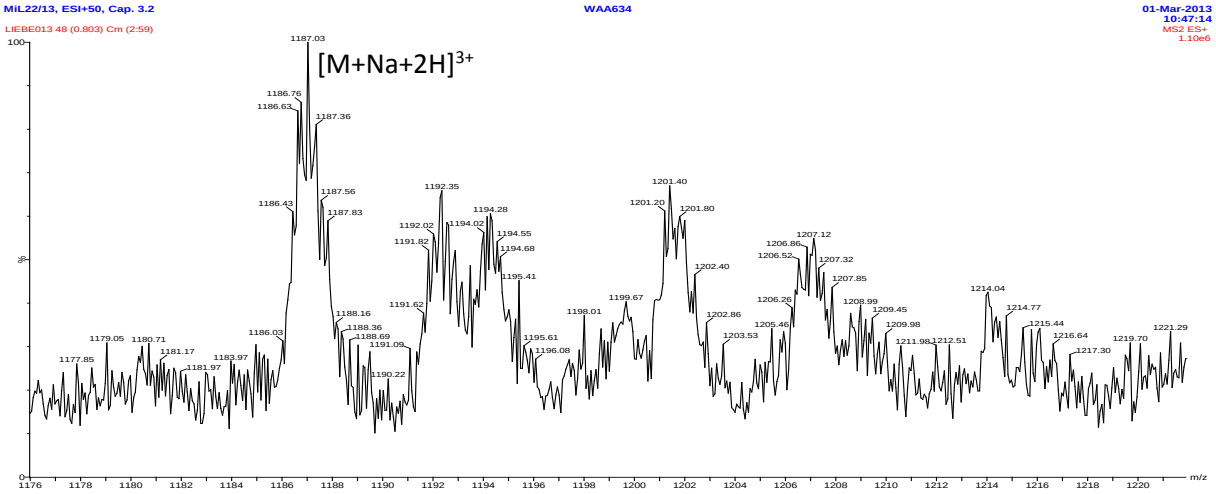
MiL22/13, ESI+50, Cap. 3.2
LIEBE013 48 (0.803) Cm (2:59)
WAA634
01-Mar-2013
10:47:14
MS2 ES+
1.10e6
[M+Na+2H]3+
m/z

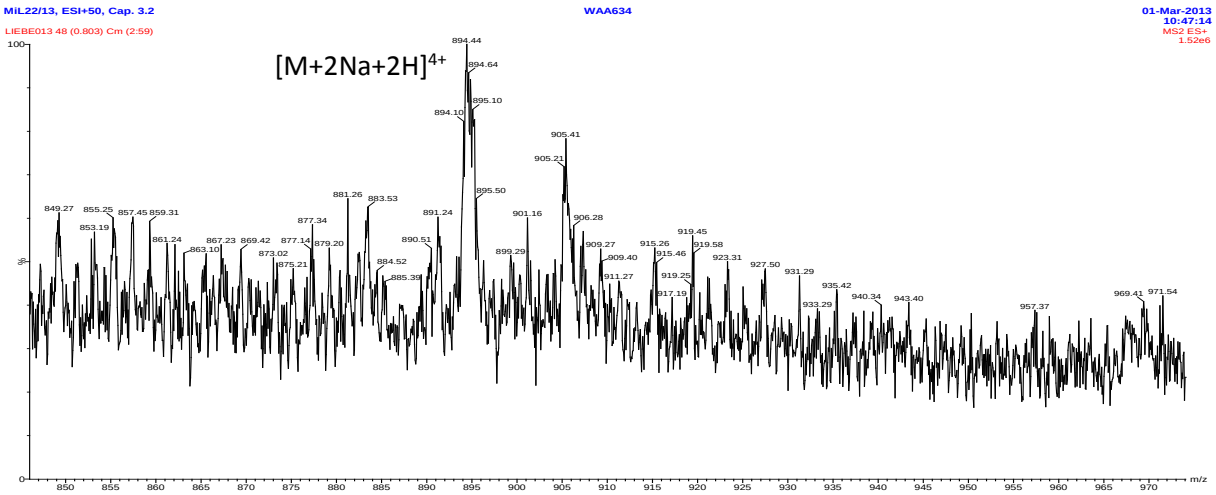
MiL22/13, ESI+50, Cap. 3.2
LIEBE013 48 (0.803) Cm (2:59)
WAA634
01-Mar-2013
10:47:14
MS2 ES+
1.52e6
[M+2Na+2H]4+
m/z

Compound **4e**

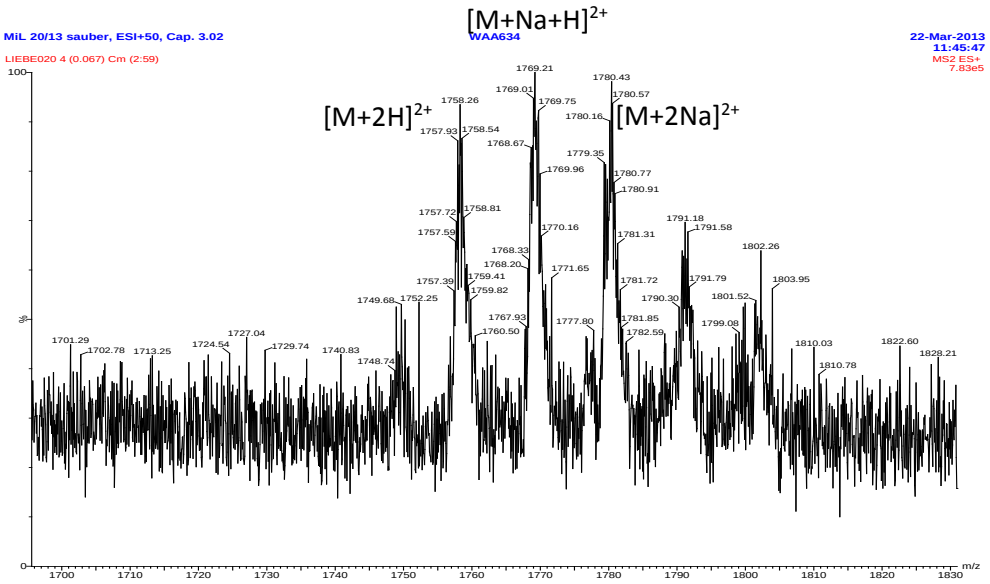
MiL 20/13 sauber, ESI+50, Cap. 3.02
WAA634
22-Mar-2013
11:45:47
LIEBE020 4 (0.067) Cm (2:59)
MS2 ES+
7.83e5
[M+Na+H]2+
[M+2H]2+
[M+2Na]2+
m/z

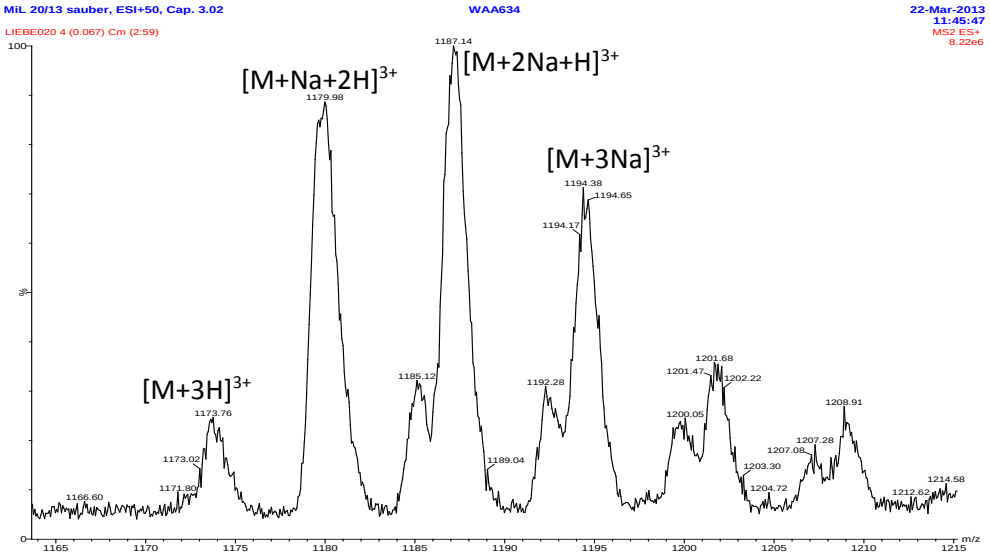
MiL 20/13 sauber, ESI+50, Cap. 3.02
WAA634
22-Mar-2013
11:45:47
LIEBE020 4 (0.067) Cm (2:59)
MS2 ES+
8.22e6
[M+Na+2H]3+
[M+2Na+H]3+
[M+3Na]3+
[M+3H]3+
m/z

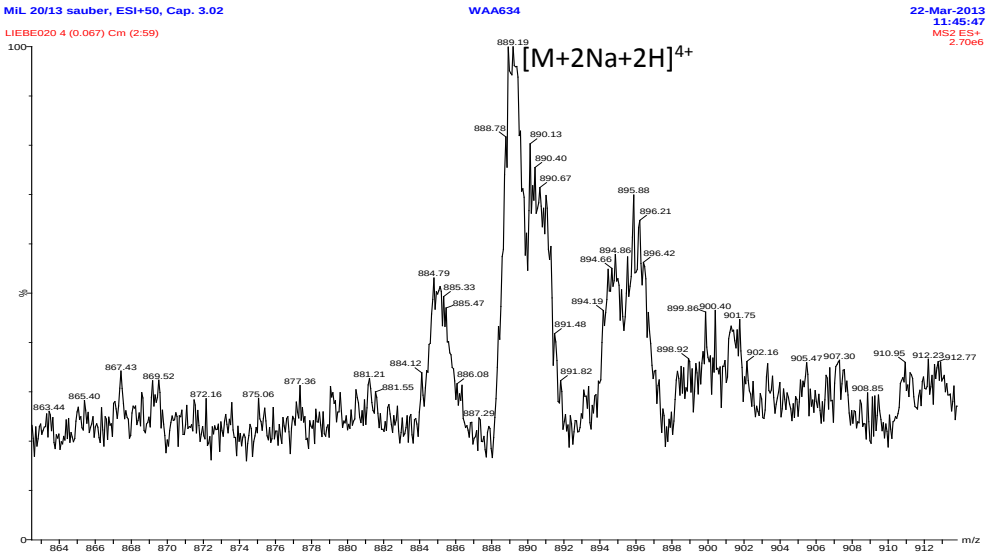
MiL 20/13 sauber, ESI+50, Cap. 3.02
WAA634
22-Mar-2013
11:45:47
LIEBE020 4 (0.067) Cm (2:59)
MS2 ES+
2.70e6
[M+2Na+2H]4+
100
%
0
m/z
889.19
888.78
890.13
890.40
890.67
895.88
896.21
894.66
894.86
896.42
884.79
885.33
885.47
894.19
899.86
900.40
901.75
891.48
898.92
902.16
905.47
907.30
910.95
912.23
912.77
884.12
881.21
881.55
886.08
887.29
867.43
869.52
865.40
863.44
872.16
875.06
877.36
908.85
864
866
868
870
872
874
876
878
880
882
884
886
888
890
892
894
896
898
900
902
904
906
908
910
912

Compound **4f**

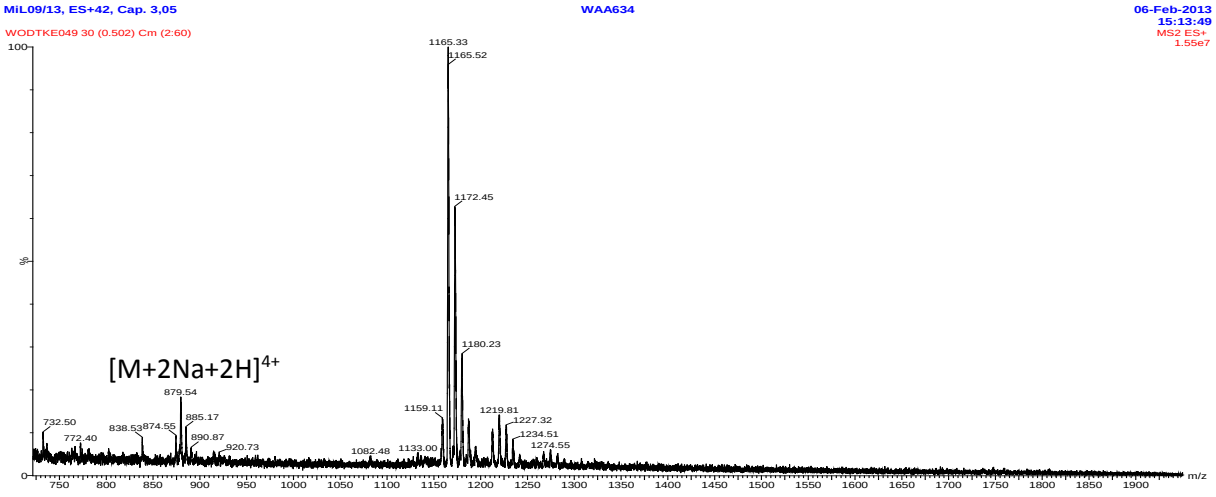
MiL09/13, ES+42, Cap. 3,05
WAA634
06-Feb-2013
15:13:49
MS2 ES+
1.55e7
WODTKE049 30 (0.502) Cm (2:60)
[M+2Na+2H]4+
m/z

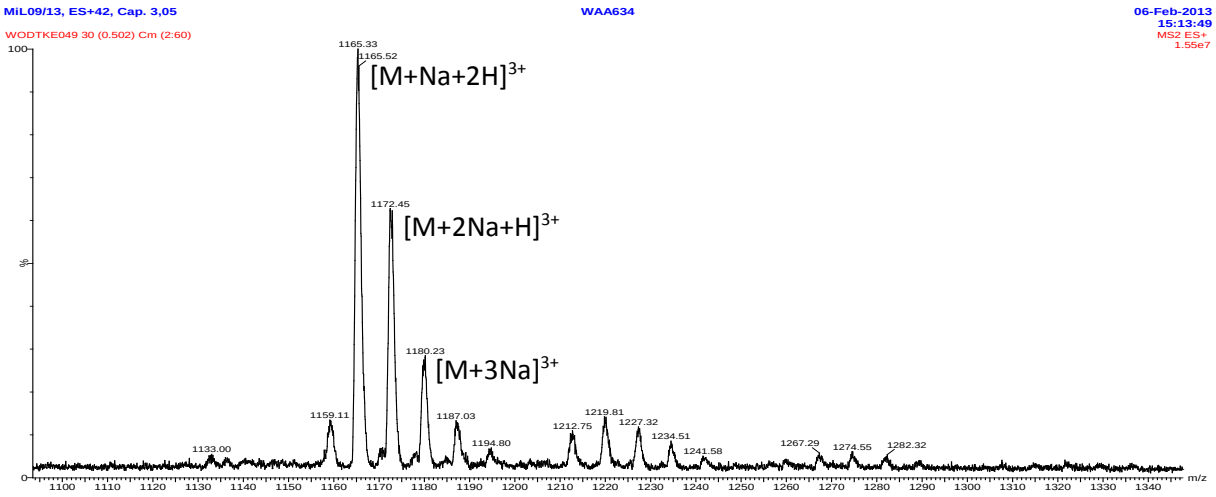
MiL09/13, ES+42, Cap. 3,05
WAA634
06-Feb-2013
15:13:49
MS2 ES+
1.55e7
WODTKE049 30 (0.502) Cm (2:60)
[M+Na+2H]3+
[M+2Na+H]3+
[M+3Na]3+
m/z

Compound **4g**

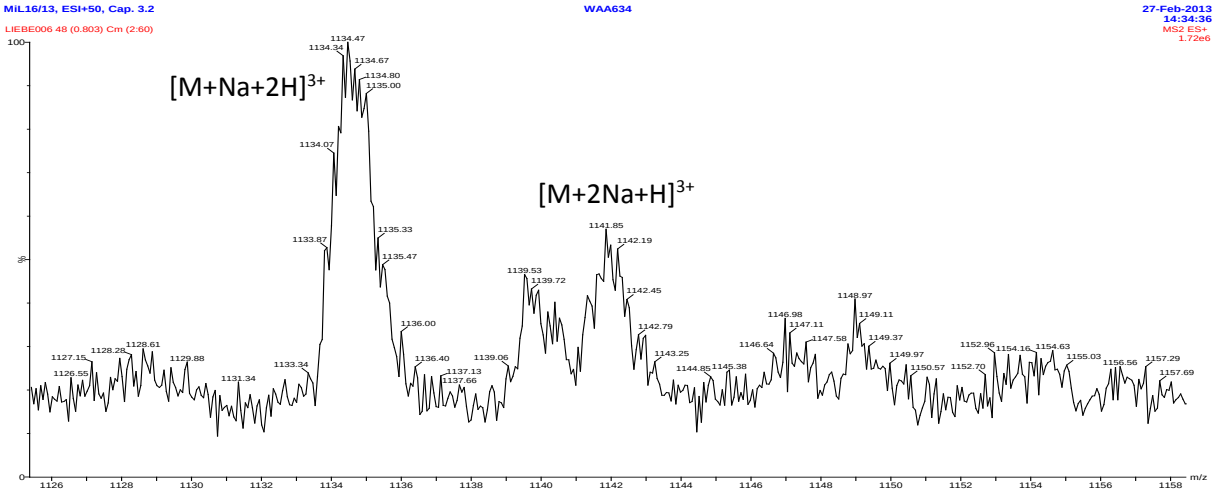
MiL16/13, ESI+50, Cap. 3.2
LIEBE006 48 (0.803) Cm (2:60)
WAA634
27-Feb-2013
14:34:36
MS2 ES+
1.72e6
[M+Na+2H]3+
[M+2Na+H]3+
m/z

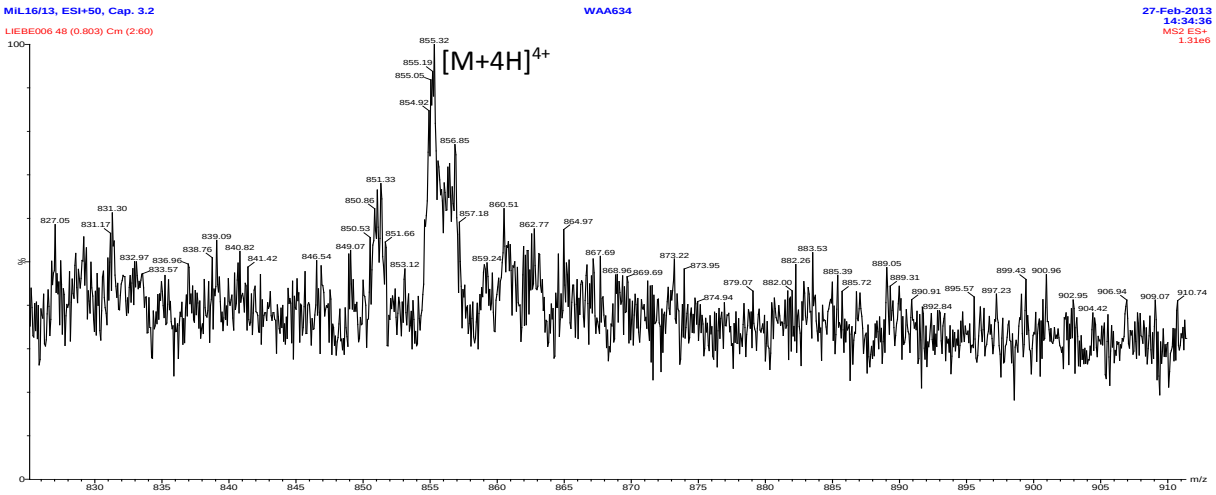
MiL16/13, ESI+50, Cap. 3.2
LIEBE006 48 (0.803) Cm (2:60)
WAA634
27-Feb-2013
14:34:36
MS2 ES+
1.31e6
[M+4H]4+
m/z